On the Ability of Error in Measured Head Kinematics to Explain Strain Errors in a Brain Finite Element Model: A Regression Study Using the Simulated Injury Monitor

by

Manju Baarkavi Sivam

A thesis submitted in partial fulfillment of the requirements for the degree of

Master of Science

Department of Mechanical Engineering
University of Alberta

ABSTRACT

In on-field studies considering impact to athletes, biomechanical parameters are measured to quantify the severity of a head impact and in some cases estimate the risk of head and brain injury. Wearable sensors play an important role in such studies because they are devices that measure head kinematics. Kinematics can be used as inputs to numerical models of the head-brain that estimate tissue strain. These strains have been proposed as metrics on which risk and severity of brain injury can be inferred. Kinematics from wearable sensors have systematic and random errors – they measure head motions that differ from the actual motion of the athlete's head. Kinematic errors will undoubtedly lead to brain strain estimates that differ from strains estimated based on the actual motions of the head. The difference in strains estimated from wearable sensor kinematics, and the kinematics describing the actual head motion, can be considered as strain error. It is not known which kinematic errors explain strain errors best. Knowledge of which kinematic errors explain strain errors is important because:

(1) This knowledge could inform the ongoing improvement of wearable sensors; specifically wearable sensors could be refined to minimize the kinematic errors that lead to strain errors; and

(2) This knowledge could inform researchers conducting on-field studies; specifically by quantifying the extent of strain errors that result from imperfect wearable sensors.

While brain injury researchers are relying more and more on finite element brain models, it is essential to try and understand which kinematic errors lead to strain errors.

Football helmet impacts were simulated in laboratory-based experiments using the Hybrid III head and GforceTracker (GFT) mounted football helmets. Impact kinematics from both the

Hybrid III and the GFT sensor were collected and used in a finite element brain model (the Simulated Injury Monitor (SIMon)) to calculate the corresponding brain strain response. Errors in brain strain response between the Hybrid III and the GFT data were compared with corresponding input kinematic errors using regression analysis to determine the input error that has the highest coefficient of determination (R^2) with the output error. Maximum principal strain (MPS) from both rotationally transformed, and linear and rotationally transformed GFT kinematics to the Hybrid III reference frame were also compared to determine the effect on brain strain calculation. In addition, the distribution of strains predicted by Hybrid III and GFT was examined.

The overarching findings from this study were: (1) errors in resultant angular velocity are most explanatory of strain errors; and (2) errors in component directions of angular velocity affect the magnitude and the spatial distribution of strains throughout the brain. The results of this study also suggest that linear accelerations do not contribute to SIMon predicted brain strains. Therefore, the complex kinematic transforms that re-express linear accelerations measured on the helmet to a co-ordinate system with the origin at the head center, may be unneeded. Also, through regression of MPS with 99.9%, 99% and 95%-ile strains, it was found that variations in any of the 95%, 99%, and 99.9%-ile strains could explain over 96% of the variations in MPS.

The primary interpretation of these findings is that the accurate measurement of both resultant and component rotational velocity is neccesary to obtain accurate estimates of strain magnitude and strain distribution.

ACKNOWLEDGEMENTS

I would first like to thank my supervisor Dr. Christopher Dennison for the knowledge he offered in the field of biomechanics and in academic writing. He had patiently guided me through this research and steered me towards a substantial target.

I would also like to thank my co-supervisor Dr. Gunter Siegmund for his valuable insights and constructive feedbacks that helped me shape this research better.

I extend my thanks to the members of the Biomedical Instrumentation Lab for sharing my workload in running hundreds of finite element simulations and their assistance in experiments and thesis reviews. A special mention to Lowell McAllister for his enthusiastic assistance in processing and analyzing a massive amount of 3D finite element data.

And finally, I would like to express my humble thanks to my in-laws for their endless encouragements and blessings. I cannot find enough words to thank Kannan for being my critic, catalyst and haven. His love and care had helped me turn around any tough day with ease.

TABLE OF CONTENTS

LIST OF TABLES

LIST OF FIGURES

NOMENCLATURE

a	Linear acceleration (g)
v	Linear velocity (m/sec)
ω	Angular velocity (rad/sec)
α	Angular acceleration (rad/sec^2)
K	Kinematics
Δ	Error
a_x, v_x, ω_x, α_x	x-axis kinematics
a_y, v_y, ω_y, α_y	y-axis kinematics
a_z, v_z, ω_z, α_z	z-axis kinematics
ΔK	Error in Kinematics (GFT – Hybrid III)
MPS	Maximum Principal Strain or 100%ile strain
Vol	Volume
R^2	Coefficient of determination
CI	Confidence Interval
SE	Standard Error
Top 1% strains	FE brain model elements with strain magnitude greater than 99%ile strain
Top 5% strains	FE brain model elements with strain magnitude greater than 95%ile strain
Category X	Impacts with maximum rotation about the x-axis
Category Y	Impacts with the maximum rotation about the y-axis
Category Z	Impacts with maximum rotation about the z-axis

95th percentile strain	Strains of 95% of the elements in the FE brain model falls below this strain magnitude.
99th percentile strain	Strains of 99% of the elements in the FE brain model falls below this strain magnitude.
99.9th percentile strain	Strains of 99.9% of the elements in the FE brain model falls below this strain magnitude.
Full transformation	Rotational transformation and linear transformation of GFT axis to Hybrid III head COG
Partial transformation	Only rotational transformation of GFT axis directions to match with that of Hybrid III axis directions. The origin of GFT kinematics still located at the center of the device.

1. Introduction

This chapter discusses brain trauma in sports and corresponding epidemiological studies, the role of wearable sensors in these studies and why the investigation of the errors in these wearable sensor measurements is necessary.

1.1 Repetitive brain trauma in sports

The likelihood of repetitive brain trauma in sports has been a concern since the 1920s, during which the 'punch drunk' condition was common in boxing. Martland examined the relation between punch drunk to post-traumatic encephalitis and stated that a single or repeated blow to the head or jaw could result in a definite brain injury [1]. His study shed light on the potential brain damage associated with impacts that were considered minor merely based on external damage. Brain trauma in other contact sports garnered attention after Omalu et al. published a report associating Chronic Traumatic Encephalopathy (CTE) to the neuropsychiatric history of a former National Football League (NFL) player who had no known brain trauma outside professional football [2]. Approximately 300,000 sport-related injuries were estimated to occur annually in the United States [3]. Repetitive head injuries that have an increased probability of brain damage form a considerable percentage of the estimated count. Due to the increased pathological evidence of CTE in deceased football players [4]– [6] and high exposure of impacts per player [7]– [10], traumatic brain injury in football has gained major attention among researchers. A cohort study conducted by the National Collegiate Athletic Association (NCAA) on 2905 collegiate football players reported 6.3% had a concussion and 6.5% of them had repeat concussion within the same season [11]. Of the football players in the 1997 season Canadian Football League (CFL) 44.8% of players experienced symptoms of a concussion and 69.6% of all concussed players experienced repetitive concussions [12]. A study by Crisco et al. on 188 collegiate football players during 2007 fall season reported that an individual player could receive up to 1400 head impacts during a single season [9] with a median value of 14.3 impacts per game. The high risk of exposure to head impacts in the game of football demanded prompt improvement in player safety.

1.2 Early steps towards traumatic brain injury prevention

To reduce the risk of repetitive brain trauma, both changes to the rules of football and improvements to the testing and certification of protective gear like helmets are needed. Though current football helmets have successfully prevented most fatal focal injuries [13], [14], their ability to limit diffuse brain injury that results in Mild Traumatic Brain Injury (MTBI) is not proven [15]. In response to the safety concerns in football, the MTBI committee formed by NFL identified two areas that require attention. The first was to monitor the frequency of the MTBIs in NFL through clinical symptoms and the second was to define concussion biomechanics in professional football [16]. The earliest study to quantify the concussion biomechanics was conducted by Pellman et al. through video reconstruction of NFL league games in laboratory tests using Hybrid III test dummies [17]. As an initial step, Pellman's study focused on obtaining kinematic thresholds relating to a concussion as impact kinematics have been causally linked to diffuse brain injuries since the 1940s [17], [18]. Despite this and other efforts to characterize thresholds for concussion [19] [21], the kinematic thresholds for MTBI are yet to be confirmed.

1.3 Wearable sensors in traumatic brain injury research

Early studies on brain injury in football players estimated head kinematics through a complicated process beginning with video analysis. Based on those video analyses, impacts were recreated in a laboratory. While the methods applied were rigorous in their design, an arguably more direct method to ascertain athlete head kinematics could be wearable sensors that measure kinematics of the athlete. Early systems included helmet-based accelerometers [18], [19], and more recent sensors include skin-mounted [20], [21]and mouth-guard systems [22]. Specific to helmet-based (sometimes referred to as helmet-mounted) systems, most of the available literature that examines the accuracy of kinematic measurements details both systematic and random errors. The general tendency is that helmet-mounted systems over-estimate head kinematics [15], [18], [23]. One commonly identified error source in wearable sensors is poor contact of the wearable sensor with respect to the head [23]. Despite the known kinematic inaccuracies in the wearable sensors, there is little research on how the kinematics from a wearable sensor translates to tissue level injury in the brain. A limited number of articles

[24]– [26]document kinematics measurements from athletes and the use of these kinematics as inputs to numerical models of the head-brain. The overarching goal of these past studies is to use kinematics to compute stress and strain in brain tissue using finite element (FE) approximations, and from these stresses and strains attempt to ascertain threshold limits on head kinematics that could be used to estimate injury in athletes. Currently, brain strain computation using FE models are predominantly studied in laboratory-based experiments using reference sensors and anthropometric head models. To identify real-time in-vivo brain injuries, researchers are now more and more using wearable sensors [9], [10], [21]. Brain models are also now commonplace in sports brain injury research. If wearable kinematics is to be used as inputs to brain models, then a clear understanding of how kinematic errors can alter strain predictions is needed. This thesis aims to contribute to the understanding of kinematic errors that lead to altered strain predictions.

1.4 Problem statement

Impact kinematics are essential for continued research to better understand head kinematic parameters and traumatic brain injury in sports. Though wearable sensors are a better option compared to laboratory based reconstruction techniques in collecting real-time impact data, their inaccuracies are a major concern as they could lead to wrong brain injury predictions. The objective of this thesis is to determine the kinematic error sources from a wearable sensor that are most explanatory of brain strain errors using a simple linear regression model. This thesis will also examine the extent to which kinematic errors can lead to errors in the distribution of strain from a skull-brain FE model.

1.5 Contributions

Upon a detailed comparative study of the FE brain model response from the wearable head impact sensor kinematics and reference sensor kinematics, this thesis will provide the following contributions:

- The kinematic errors that are most explanatory of strain error.
- The extent to which misalignment in wearable sensor component axes relative to reference axes, affects strain error magnitude.

- A quantitative analysis of MPS and several percentiles of principal strain that suggests any of MPS, 99.9%ile, 99%ile or 95%ile could be used in statistical analyses.
- The extent to which kinematic errors affect the distribution of strains in the brain.
- Data suggesting that a simplified kinematic transform of wearable sensor kinematics could suffice to yield accurate predictions of brain strain.

1.6 Thesis organization

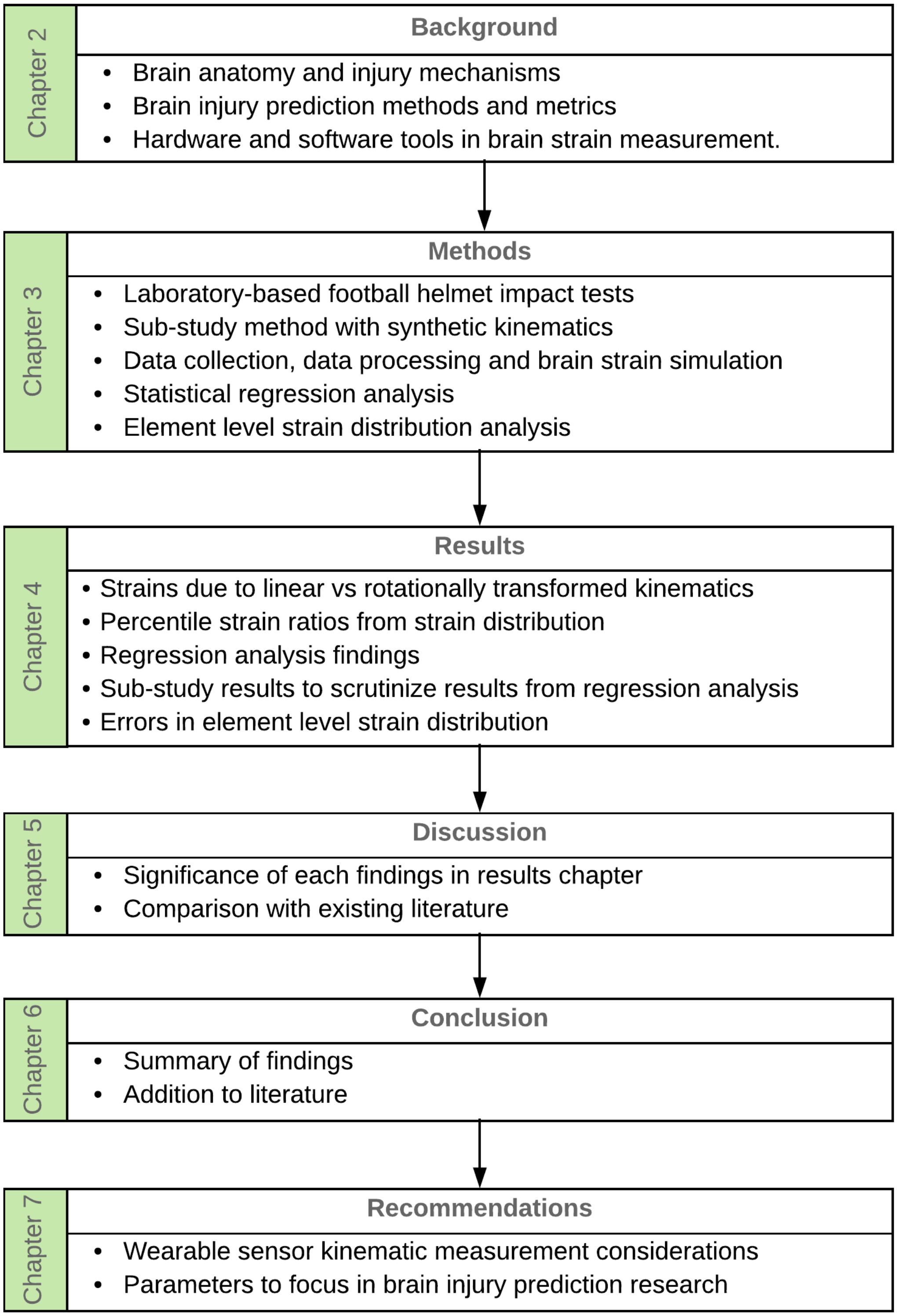

Figure 1.1 Thesis organization

2. Background

This chapter provides fundamental information related to brain injury research including brain anatomy, mechanisms of brain injury, research approaches used in predicting the risk of brain injuries and the common tools used by brain injury assessment researchers.

2.1 Brain injury mechanics

To understand head injury mechanics, it is essential to understand the structure and the composition of the brain. The brain is a complex organ and research is still in progress to understand it completely. The brain has mostly uniform density with an average of 1.081 g/mm^3, slightly more than water and suspended in the cerebrospinal fluid within the skull. It is highly incompressible similar to water and has a very low modulus of rigidity [27]. The brain is protected by meninges which are formed by three layers - dura mater, arachnoid mater and pia mater (**Figure *2.1***).

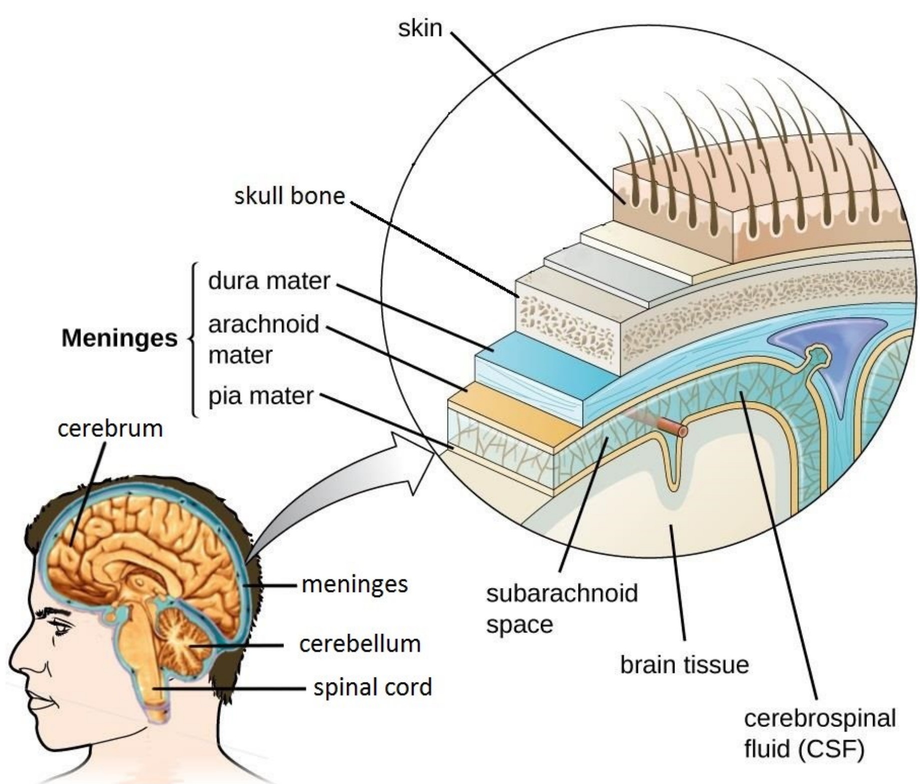

Figure 2.1: Layers of the brain *[28]*

This image is modified from OpenStax College. (2014). "Microbiology" and is licensed under the Creative Commons Attribution 3.0 Unported license.

The dura mater is attached to the skull relatively firmer than the other two layers [29]. The middle arachnoid mater is fibrous and has tubular structures that merge with the pia mater. The cerebrospinal fluid (CSF) circulates in this region between the arachnoid mater and the pia mater. Unlike other layers, only the pia mater follows the contours of the brain.

Injuries to the brain are often classified as i) focal injury and ii) diffuse injury [30]. Focal injuries are a result of direct loading to the brain that may lead to localized skull deformation or skull fracture at the location of impact ('coup') or at the location opposite to the impact ('contrecoup') [28]. Focal injuries include contusions, epidural, subdural and intracerebral hematomas. A contusion is hemorrhagic necrosis of brain tissue due to the impact of the brain with the inside of the skull and is frequently associated with a skull fracture. The dural hematomas are laceration of the veins or arteries due to the shear stress caused by relative motion of the meningeal layers in the brain during an impact. Intracerebral hematomas are homogeneous collections of blood within cerebral parenchyma due to sudden acceleration, deceleration or penetrating wounds [28]. Focal injuries hence are often fatal.

Diffuse injuries involve a spectrum of injuries ranging from mild concussion to diffuse white matter injuries [30]. One mechanism that can lead to diffuse injury is the sudden rotational motion of the head [29] caused by the direct or indirect impact to the head. In general, sliding motion of the brain along the intracranial wall is induced by blunt impacts resulting in shear stress between the meningeal layers. This shear stress, as opposed to volume change in the brain tissue, is due to the brain having relatively much lower shear modulus than bulk modulus. The shear motion of the brain also causes cerebrospinal fluid displacement that increases the intracranial pressure which could lead to laceration of vessels in deeper parts of the brain. The laceration of the vessel due to intracranial pressure was explained by Cassasa (1924) as an event caused by sudden overfilling of spaces surrounding the nerve and blood vessels with CSF [29]. Diffuse axonal injury (DAI) is one type of diffuse injury that involves damage to the axons. Contrary to focal injuries that occur mostly at the outer brain layer, DAI can extend below the midbrain and into the brain stem. The severity of the DAI varies from mild traumatic brain injuries (MTBI) to fatal injuries. The mild diffuse injuries can be either due to a single impact or multiple traumatic impacts to the brain. Repeated low-grade injuries are believed to cause delayed post traumatic changes due to the biochemical cascades induced by cumulative effects of the blows [2].

In contact sports, the incidence of focal injuries was significantly reduced due to the adoption of improved helmet designs [13], [31]. By 1980, there was a 51% reduction of fatal head injuries in youth football [2]. But the risk of MTBI is still a concern as the symptoms of neurodegeneration related to mild traumatic brain injuries are not immediate, some of which can only be diagnosed under microscopic examination [2], [30]. Due to this and because of the reluctance of athletes in reporting head injuries, most MTBI cases are not detected at an early stage. All these factors increased the need to monitor impact biomechanics in contact sports to predict brain injuries.

Translational and angular kinematics of head impact have been traditionally studied to explain head injuries since the 1940s [29]. Linear acceleration was commonly related to focal injuries and skull fracture and less related to diffuse injuries. A widely accepted theory is that the strains produced by linear acceleration forces are small compared to those produced by rotational kinematics [25], [29], [32]. Holbourn in 1943, was the first to explain this theory with a gelatin brain model suspended in water and by applying rotational forces. The resulting shear strains in the brain model matched with hemorrhage locations noted in autopsies. The same has been proved in later studies that used primates instead of gel brain model. The velocity of head rotation has been shown to correlate with concussion, contusion and sub-dural hematoma in adult rhesus monkeys with and without direct impact to the head [33], [34]. A study by Gennarelli et al., [35] related angular acceleration of monkey heads to concussion and reported agreement with clinical findings. Denny-Brown and Ritchie Russel on their experiments to study cerebral concussion using cats noted that concussions were difficult to create when the head is fixed, and rotational movement of the head resulting from a blow is essential to create concussion in the brain [36] which confirms that rotational forces are major contributors in concussion. However, the consideration of linear acceleration in brain injury prediction is not entirely dismissed due to its role in intracranial pressure and severe focal injuries [32]. In the case of diffuse injuries, the role of angular acceleration, as opposed to angular velocity on brain strain, was discussed extensively in earlier literature [35], [37]. While researchers agree that angular acceleration might be explanatory for long duration impacts [17], [35], [39], the angular velocity is still a better mechanism for brain strain for the impact durations in football [25], [38], [40].

2.2 Brain injury metrics

Because head kinematics during an impact is a convenient and effective measure that correlates with head injuries, several researchers have focused on quantifying head injury using impact kinematics. A fundamental method in kinematic brain metric was to use peak linear acceleration (PLA) or peak rotational velocity (PRV) [41]. The earliest head injury prediction method using kinematics was proposed by Gurdjian et al. [30] which was later termed as Wayne State tolerance curve (WSTC). The curve was developed by studying linear accelerations that caused skull fracture in cadavers and concussive effects of varying pressure pulses in animal experiments [42], [43]. The WSTC curve relates the probability of head injury to the duration of linear acceleration pulse. Gadd Severity Index (GSI) (Equation 2.1) was later proposed by Gadd which is an extension of WSTC curve [42] with an approximation factor (n = 0.25), acceleration (a) and time (t).

$$SI = \int [a(t)]^n dt \tag{2.1}$$

GSI was adopted by the National Operating Committee on Standards for Athletic Equipment (NOCSAE) as a standard helmet testing measure and is used to date. But the index was not considered valid by researchers for longer duration impacts [42].

Considering the ineffectiveness of GSI in longer duration impacts, Versace proposed the Head Injury Criterion (HIC) by combining impact duration data to linear acceleration measurements [44] which was later adopted by NHTSA. HIC (Equation 2.2) is the most commonly used metric in head injury assessments. However, HIC as an injury criterion lead to concerns, as it is based on a single parameter and disregarded rotational influences.

$$\mathrm{HIC} = (\mathrm{t}_2 - \mathrm{t}_1) \left[(\mathrm{t}_2 - \mathrm{t}_1)^{-1} \int_{\mathrm{t}_1}^{\mathrm{t}_2} \mathrm{a(t)dt} \right]_{\mathrm{Max}}^{2.5} \tag{2.2}$$

GAMBIT (Generalized Acceleration Model for Brain Injury Threshold) proposed by Newman in 1986 was one of the earliest metrics to consider both linear and angular kinematics. This method assumed the relationship between linear and angular acceleration analogous to normal and shear strain in the brain [41]. GAMBIT was followed by other metrics that considered both linear and angular kinematics to quantify head injuries. One such metric, Kleiven's Linear combination (KLC) combined peak change in angular velocity with HIC(Equation 2.3) that resulted in high correlation (R^2=0.98) with brain strain [32].

$$\mathrm{KLC} = \beta 1\, \omega_{\max} + \beta 2\ \mathrm{HIC} \tag{2.3}$$

Other metrics that modified HIC by including rotational parameters were PRHIC (Power Rotational Head Injury Criterion) and RIC (Rotational Injury Criterion) [45].

Takhounts et al. developed a metric that was purely based on rotational kinematics [25]. The study used Simulated Injury Monitor (SIMon), a FE head model to calculate brain strain using real-time impact kinematics obtained from collegiate football players. Brain Injury Criterion (BRIC) was then formulated (Equation 2.4) to correlate with the calculated brain strain.

$$BRIC = \frac{\omega_{max}}{\omega_{cr}} + \frac{\alpha_{max}}{\alpha_{cr}} \tag{2.4}$$

Maximum angular velocity and angular acceleration are denoted as ω_{max} and α_{max} respectively and corresponding critical values are denoted as ω_{cr} and α_{cr}. Takhounts et al. later updated the BRIC [46] to contain only angular velocity components after finding that angular velocities are sufficient for brain strain predictions. The updated BRIC (Equation 2.5) considered directional components of angular velocity instead of resultant value.

$$BrIC = \sqrt{\left(\frac{\omega_x}{\omega_{xcr}}\right)^2 + \left(\frac{\omega_y}{\omega_{ycr}}\right)^2 + \left(\frac{\omega_z}{\omega_{zcr}}\right)^2} \tag{2.5}$$

Where ω_x, ω_y, ω_z, are maximum angular velocities in x, y and z directions and ω_{xcr}, ω_{ycr}, ω_{zcr} are corresponding critical angular velocities. Similar to the BRIC, the RVCI (Rotational Velocity Change Index) by Yanaoka et al. [47] used directional velocity components in predicting the brain strain. RVCI used a theoretical consideration that the response of brain element is similar to a simple mass-spring.

$$RVCI = \sqrt{R_x\left(\int_{t_1}^{t_2} \alpha_x dt\right)^2 + R_y\left(\int_{t_1}^{t_2} \alpha_y dt\right)^2 + R_z\left(\int_{t_1}^{t_2} \alpha_z dt\right)^2} \tag{2.6}$$

The α_x, α_y, α_z in the RVCI equation corresponds to directional angular accelerations and R_x, R_y and R_z are corresponding weighing factors. The weighing factors were calculated from the average ratio of tissue level predictors obtained by applying sine curve inputs to each axis of the Global Human Body Models Consortium (GHBMC) FE model. Gabler et al. compared 15 injury metrics and concluded that metrics based on rotational kinematics predict brain injury better than other kinematic-based metrics [41]. The study also found that BRIC and RVCI had the highest correlation with brain strains calculated using FE brain models.

Though the kinematic brain injury predictors were shown to predict brain injury risk, the predictors do not quantify brain strain. Quantifying the brain injury was made viable by FE brain models that calculate tissue level brain strain response from impact kinematics. Of late researchers are relying more on numerical brain models to calculate the mechanical response of the brain due to an impact. Commonly used strain based injury risk assessment metrics are MPS (Maximum Principal Strain) and CSDM (Cumulative Strain Damage Measure). Strain has been related to cell death through multiple studies [48], [49] and large strain region has been reported to coincide with the highest incidence of injury [37]. The MPS provides the highest strain predicted through the FE brain models. CSDM is the cumulative volume of a given percentage of the brain model that exceeds a certain strain level [50]. Damage in single axon does not reflect diffuse injury. Increasing levels of axonal damage result in increasing pathological changes [50]. Hence, CSDM was used to define the severity of the brain strain by considering strain over a minimal volume of the FE brain model to define diffuse brain injury.

2.3 FE head models in head injury risk assessment

For decades research on brain injury often involved cadaver and animal experiments which are experimentally complex and involved ethical concerns. FE brain models allowed researchers to estimate the mechanical response of the brain to impact and created possibilities to explore the tissue-level response of the brain to impact kinematics. Early brain FE models mostly considered the head-brain complex as a fluid-filled spherical shell [42]. A notable study by Hardy et al. provided the much-needed data on the relationship between kinetic input and corresponding head injury [51]. Thirty-five impact tests were conducted by the team using eight human cadavers, neutral density targets (NDT), bi-planar and high-speed x-rays. The documented kinematics, intracranial pressure, and NDT data showing relative motion between the brain and skull corresponding to each impact were intended to be used in validation of FE brain models. Complex FE models evolved with access to information on the brain from magnetic resonance imaging (MRI), computer tomography (CT) and NDT experimental data available from the cadaveric experiments. A few of the FE brain models are the Wayne State University Brain Injury Model (WSUBIM) developed by Zhang et al. [52], Simulated Injury Monitor (SIMon) by Takhounts et al. [50], Atlas Based Model (ABM) [53], Global Human Body Models Consortium (GHBMC) head model [54] and Kungliga Tekniska Högskolan (KTH) model [55]. More numerical brain models in addition to the listed exist that vary in the number of distinct parts in the brain, material properties, and mesh size.

SIMon was developed by the National Highway Traffic Safety Administration (NHTSA) for automotive crash tests [50]. The topology of SIMon was primarily based on CT scans of a single male individual and scaled uniformly to a total mass of 4.5kg analogous to the 50th percentile male. SIMon was modelled with distinct parts for cerebrum, cerebellum, skull, brainstem, ventricles, CSF and Pia-arachnoid layer combined, falx-tentorium and parasagittal blood vessels (**Figure 2.2**). The initial SIMon model (released in 2003) was constructed with 10,475 nodes and 7,852 elements. A later version of SIMon released in 2008 had geometrically detailed parts with 42,500 nodes and 45,875 elements. The material properties were tuned to match real impact data, by measuring the shear stress of material models from literature and comparing it with cadaver experiment neutral density targets and animal injury data [50], [56].

FE brain models designed for high-resolution brain injury prediction includes the Atlas Based Model (ABM, Miller et al.,2016), Global Human Body Models Consortium (GHBMS) head model (Mao et al.,2013) and Wayne State University Brain Injury Model (WSUBIM). Brain response curves of these FE models are however shown to be similar though their resultant magnitudes vary [26], [57]. L.E.Miller et al. conducted a study comparing 6 brain FE models including ABM, SIMon, and GHBMC with experimental data over a range of impact severities and directions. The displacements predicted by the models were evaluated using CORelation and Analysis (CORA) which compares the error in shape, magnitude, and phase between two curves. SIMon was ranked second in this study following ABM in predicting the brain displacements [58]. It is to be noted that ABM and WSUBIM models are developed with an aim to create a high resolution, anatomically accurate head model that mimics human head as close as possible, with finer mesh sizes and distinguished brain regions and parts. The WSUBIM underwent continuous changes since its first version at 1993. The latest version of WSUBIM by Zhang et al. has 281,800 nodes and 314,500 elements [52]. The ABM is constructed with 2 million nodes and elements [53].

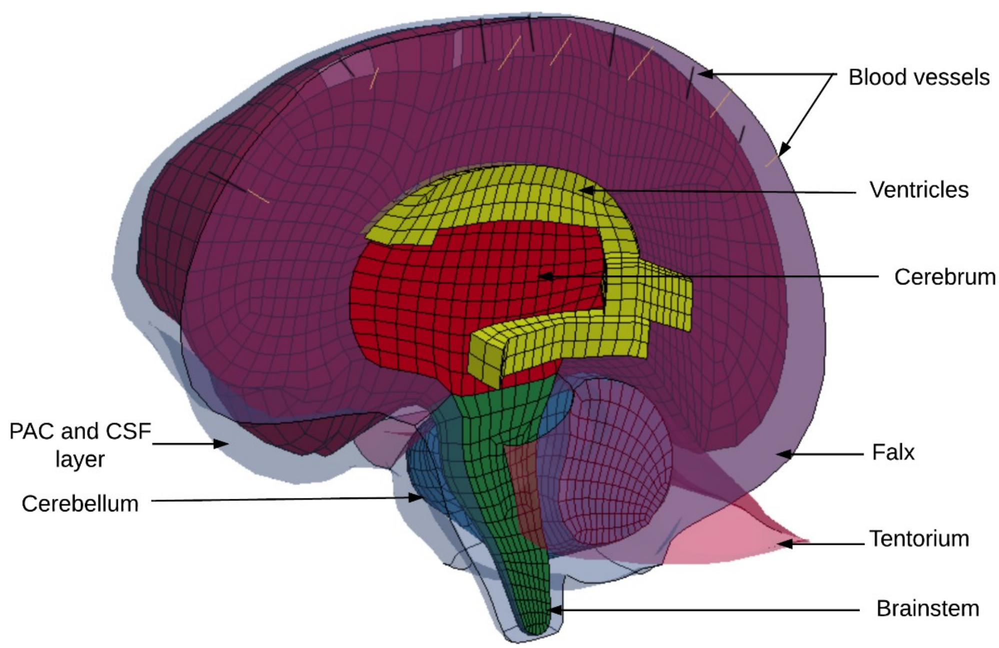

Figure 2.2: The improved Simulated Injury Monitor brain finite element components
(Image rendered using Ls-PrePost)

The SIMon model contrarily gives priority to the simulation time to make brain strain prediction viable. The complexity of the FE model was hence limited in SIMon, to be able to simulate the brain response to an impact event of up to 150 milliseconds within 2 hours on a high-end PC. The brain strain response generated by the model was also comparable to high-resolution models [26], [58]. SIMon uses three different injury metrics- Cumulative Strain Damage Measure (CSDM), DDM (Dilation Damage Measure) and RMDM (Relative Motion Damage Measure) as correlates to diffuse axonal injury, contusions, and acute subdural hematoma respectively, since the mechanisms that cause these injuries are different. The critical values for each injury metric are determined by data from animal experiments which was then scaled to human head response. The model's response was validated against both cadaver and animal experiment data. For the earlier validation method, all of Hardy et al. neutral density target displacement-time history data was used to compare with SIMon model response. Animal injury data was used to validate the model by scaling kinematic loading conditions to corresponding stress/velocity scale between the particular test animal and human brain [56].

Tissue level strains in the brain are often associated with diffuse axonal injury. As the intensity of the strains to the axons increase, a series of pathological changes occur which could lead to axonal swelling and loss of axonal transport. The loss of axonal transport is observed at a strain level of 15 and 18 percent by a few studies [59], [60]. Hence, CSDM was introduced to specifically predict DAI by monitoring the accumulation of strain greater than specified strain levels [50]. Like CSDM, MPS has been proposed as a correlate to brain injury risk. SIMon simulation calculates the MPS experienced by every element in the brain model and reports the maximum MPS which is the strain magnitude experienced by a single, maximally deformed element.

2.4 Test devices to simulate head injury biomechanics

To measure the kinematic response of the human head to impacts, the anthropomorphic test device (ATD) referred as dummy that mimics the biofidelity of a human head is often used. One such dummy head model adopted in head injury research is that of the Hybrid III head which was primarily developed for automotive crash testing. The Hybrid III head is an updated model of multiple earlier versions used in crash testing to achieve the biofidelity it has today. The first crash test dummy was Sierra Sam developed in 1949 for ejection seat tests by US air force [61]. 1n 1972, GM developed a mid-size adult male dummy called Hybrid II to mimic the 50th percentile human male [61]. It was the first dummy specified in Federal Motor Vehicle Safety Standards for compliance testing of vehicles with passive restraint. The limitations of the Hybrid II family of dummies is they were sparsely instrumented and lacked humanlike response stiffness for head, neck, thorax, and knees. The Hybrid III midsize male developed in 1976, overcame the above-mentioned limitations and had excellent biofidelity compared to Hybrid II. Hence in 1977, NHTSA replaced Hybrid II with Hybrid III making it the only midsize adult male dummy specified for regulatory frontal restraint evaluation throughout the world. Hybrid III dummy is specified in worldwide regulation and approved by various regulatory bodies. It is instrumented with 3-2-2-2 array of the accelerometer, tri-axial force, and moment sensors to measure the 3-dimensional response of the head during an impact [61].

Another commonly used ATD is Hodgson-WSU head model developed specifically for helmet testing by National Operating Committee on Standards for Athletic Equipment (NOCSAE) [62]. This model was more human-like with a gel-filled cavity for brain and nylon based human-like material for the skull and is fitted with a triaxial accelerometer. One main disadvantage of the Hybrid III is it does not extend down far enough to fit the padding at the back of the helmets. The NOCSAE headform is designed to fit the helmet better and has the upper part of the neck [62]. The profile view of the two headforms is illustrated in **Figure *2.3***. The Hybrid III has narrower jaw and chin which makes it anatomically less perfect for helmet testing compared to NOCSAE [56]. The larger gap between the helmet and Hybrid III head at the base of skull, jaw, and chin allows for increased relative rotation between head and helmet which is not desirable for a helmet impact study. But, when it comes to the instrumentation of these headforms, the NOCSAE headform has a shaft from the underside of the chin designed to allow only a triaxial accelerometer and does not include a 3-2-2-2 accelerometer array system as in Hybrid III [63]. To implement 6 DOF instrumentation, the model demands the use of external sensors or accelerometer packages [63]. Also, a study by Kendall et al. has shown that Hybrid III generates linear acceleration peaks closer to cadaver data than Hodgson-WSU model, though their dynamic responses are similar [62], [64]. In addition, there are fewer documents that are available on NOCSAE instrumentation and validation of its measured kinematics. Despite the anatomical disadvantage of Hybrid III, it is standardized globally and its instrumentation is validated by multiple studies [64], [65].

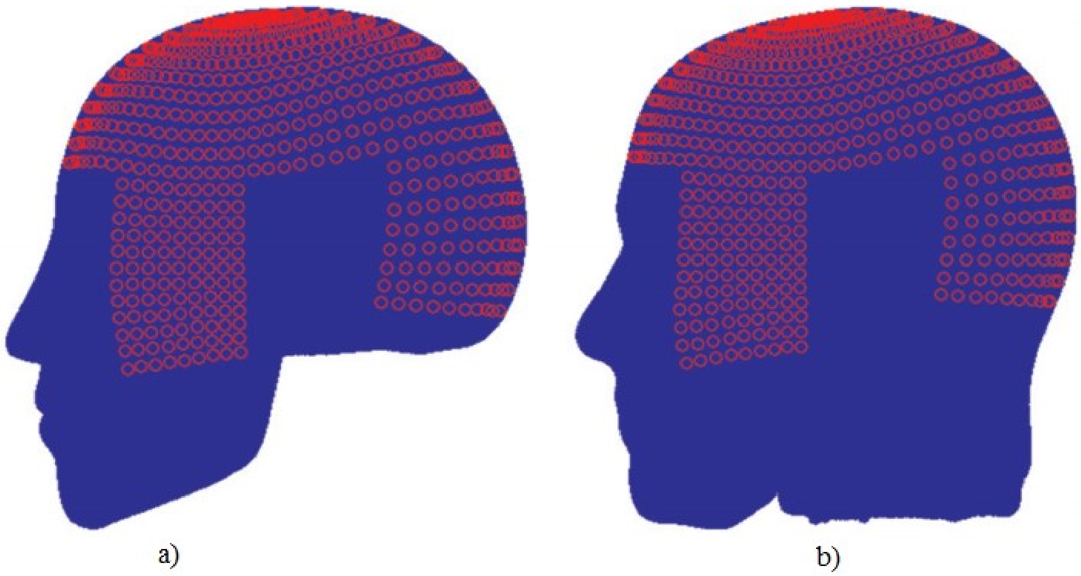

Figure 2.3: Profile view of the a) Hybrid III and b) NOCSAE headforms *[66]*

Used with permission from "Proceedings of the Institution of Mechanical Engineers".

2.5 Head impact sensors

Head impact data of players during the game are valuable additions for on-field studies. Laboratory-based impact experiments using ATDs, however, cannot replicate all the environmental factors in real-world such as the different head size of players and helmet fit. Thus, wearable sensors are preferred in collecting real-time impact data of the players. Wearable impact sensors measure kinematics during impact, the most common kinematics are linear acceleration and rotational velocity. These systems can either measure kinematics about a coordinate system that is centered at the center of gravity of the head[67], [68], or about a coordinate system that is centered at the location of the wearable sensor [69] (i.e. at a location on the helmet). When using measures from wearable sensors for estimation of head injury risk (and indeed with brain models), many researchers presume that wearable kinematics must be expressed relative to the head center of gravity [67], [70], ostensibly because kinematics based head injury assessment functions (e.g. BRIC) use kinematics expressed about the head center. Interestingly, many of these assessment functions rely upon rotational velocity which can be measured anywhere on the head, and through principles of rigid body mechanics shown to be the same at the head center of gravity. Therefore it is unclear whether or not measures from wearable sensors require transformation to be expressed at the head center and indeed this question has not been examined in the research literature.

HITS or Head Impact Telemetry System introduced in 2003 by Simbex marked itself as a pioneer for in situ measurement of head impacts in sports. HITS uses a 6 accelerometer array to measure the linear acceleration at a sampling rate of 1000 Hz and 40 ms time window [10]. Multiple inventions followed HITS in the wearable sensor market thus contributing to new design changes and testing methods. GForceTracker© (GFT) is a wearable sensor that can be mounted on the helmet. It uses both accelerometers and gyroscopes to record linear acceleration at 3,000 Hz (low-pass filtered at 300 Hz) and angular velocity at 800 Hz (low-pass filtered at 100 Hz) [24]. X2 Biosystems (Seattle, WA) designed mouthguard sensor system (X2 mouthguard) and skin patch sensors (Xpatch) to measure impact kinematics using linear accelerometers and angular rate sensors and recorded 100ms traces for an impact[20], [67]. Few other wearable sensors include Shockbox (i1 Biometrics, Kirkland, WA) and mouthguard sensors by Stanford researchers and Cleveland clinic.

Validation studies on most of these wearable sensors have reported a high incidence of false positives or overestimation of head impact kinematics. In a study by Cortes et al., skin patch sensor was used to measure the head impact on girls' lacrosse participants, and the GFTs were deployed in boys' lacrosse helmets. The impacts were verified by a video recording of the game time-synchronized with sensors. In the results, 38% of boys and 65% of girls head impacts recorded by the sensors suggested false positive impacts [15]. Duma et al. collected a total of 3312 impacts from 38 players on a 2003 football season where players were instrumented with the HITS system. The study observed that most of the impacts that exceeded the tolerance level for concussion did not result in any reported concussion [10]. Another experiment with the HITS system also reports 55% of the peak linear acceleration data with errors in excess of 15%. This error magnitude could lead to a concussed player being missed or non-concussed player being falsely removed from the game [23]. In a study comparing mouthguard, skin patch and skull cap with mouthguard as a reference, skin patch and skull cap are reported to overpredict linear acceleration up to a maximum of 22g and 81g respectively. Angular acceleration of the sensors also had high errors [21]. Mouthguards were tested to report linear acceleration and angular velocity in better correlation with ATDs. However, the errors were high when it came to facemask impacts [22]. Siegmund et al. conducted helmeted impact tests using HITS and X2 mouthguards at 12 impact sites and 5 speeds and found that neither system accurately estimated the direction and magnitude for all the impact sites and speeds[67]. Brain strain estimation with wearable sensor kinematics using FE brain models was shown to overestimate brain injury risk up to 40% for impacts with peak kinematic errors less than 10% [24]. Given the overwhelming evidence in the literature on the inaccuracies in wearable sensor kinematic measurements, it is worth considering how these kinematics errors could lead to inaccurate strain prediction (inaccurate relative to strains resulting from correct kinematics of the athlete head) when used on the field, on athletes.

2.6 Open questions in the area

The resultant linear and rotational kinematics are used by MTBI tolerance estimates to predict the presence or absence of a concussion [10]. Research that validates wearable sensor have also focused on peak resultant kinematic errors [24], [70]. However, if correcting the peak resultant kinematic errors measured by wearable sensors will result in approximate brain injury prediction using FE brain models is unknown. Additionally, in research comparing impact kinematics to numerically calculated brain strain, there is a gap in literature regarding the reference axis of the impact kinematics recorded and the choice of MPS. Research recommends that sensors measure impact kinematics with respect to head COG [70]. However, whether the strain varies between the kinematics measured at the head surface (coordinate axis of wearable sensor) and the head center is unknown. Also, the MPS (100^{th}%ile strain) in brain strain analysis is questioned in few studies as it corresponds to the strain of a single element in the FE brain model and hence 95^{th} percentile MPS is used [45], [71]. The choice of 95^{th} percentile MPS over the 100^{th} percentile MPS is not justified in literature. These facts and unanswered questions combine into the following list of open questions:

- Will the outcome of a regression analysis vary between the choice of MPS and other percentiles of strain (e.g. 95%ile)?
- Are coordinate transforms of kinematics from a wearable sensor to head COG essential to reduce strain errors?
- Will kinematic errors lead to significant strain error in FE brain strain calculation?
- If so, error in which kinematic variable best explains or influences the strain error?

2.7 Objectives

The overarching objective of this thesis is to identify the error sources in wearable sensor measurements that contribute towards an error in brain strain calculation using FE brain models. Towards the fulfillment of the objective this thesis is structured to answer the open questions in the area through the steps mentioned below

- Determine the appropriate strain level (MPS or percentile-ranked MPS) to be used in regression analysis.
- Determine if the wearable sensor kinematic inputs to the FE brain models should be linearly transformed to the head center of gravity (Details and rationale related to transformation will be supplied subsequently).
- Identify the kinematic error that best explains the strain error.
- Determine if limiting the identified kinematic error will limit the strain errors in FE brain model calculations.

3. Methods

The overall methods used in this thesis include experimental football helmet impacts, FE brain model simulation, and statistical analysis, towards the goal of comparing the brain strain response corresponding to the kinematics from a reference sensor and wearable sensor. The experimental football helmet impacts use a Hybrid III head sensor system as the reference sensor and a GforceTracker (GFT) for the wearable sensor. Impact kinematics were obtained from laboratory drop tower experiments using these sensors. The simulation section employs a FE brain model to calculate the brain strain response from the kinematics recorded by both the Hybrid III and the GFT. Error in input kinematics and brain strain response were then used in regression analysis to identify which kinematic error has the highest coefficient of determination with the output strain error. **Figure** ***3.1*** provides an overview of the methods used in this study. In addition to analysis using experimental data, this thesis also conducts a sub-study with synthetic kinematics, to understand the effect of different kinematic data on brain strain calculation.

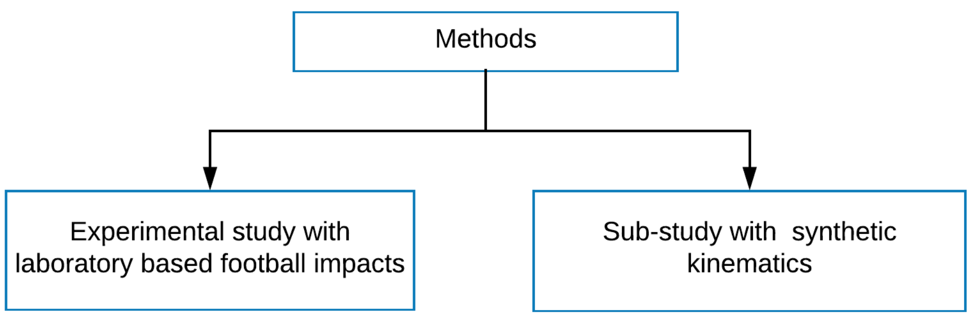

Figure 3.1: Methods used in the study

The experimental study comprised of simulated laboratory impacts to football helmets on the Hybrid III head and the data generated from these laboratory impacts (kinematics measured from the Hybrid III and GFT), were input to SIMon to allow estimation of strain (***Figure 3.2)***. The kinematics and strains were then used in the regression analysis structured to determine which kinematic errors explain strain errors.

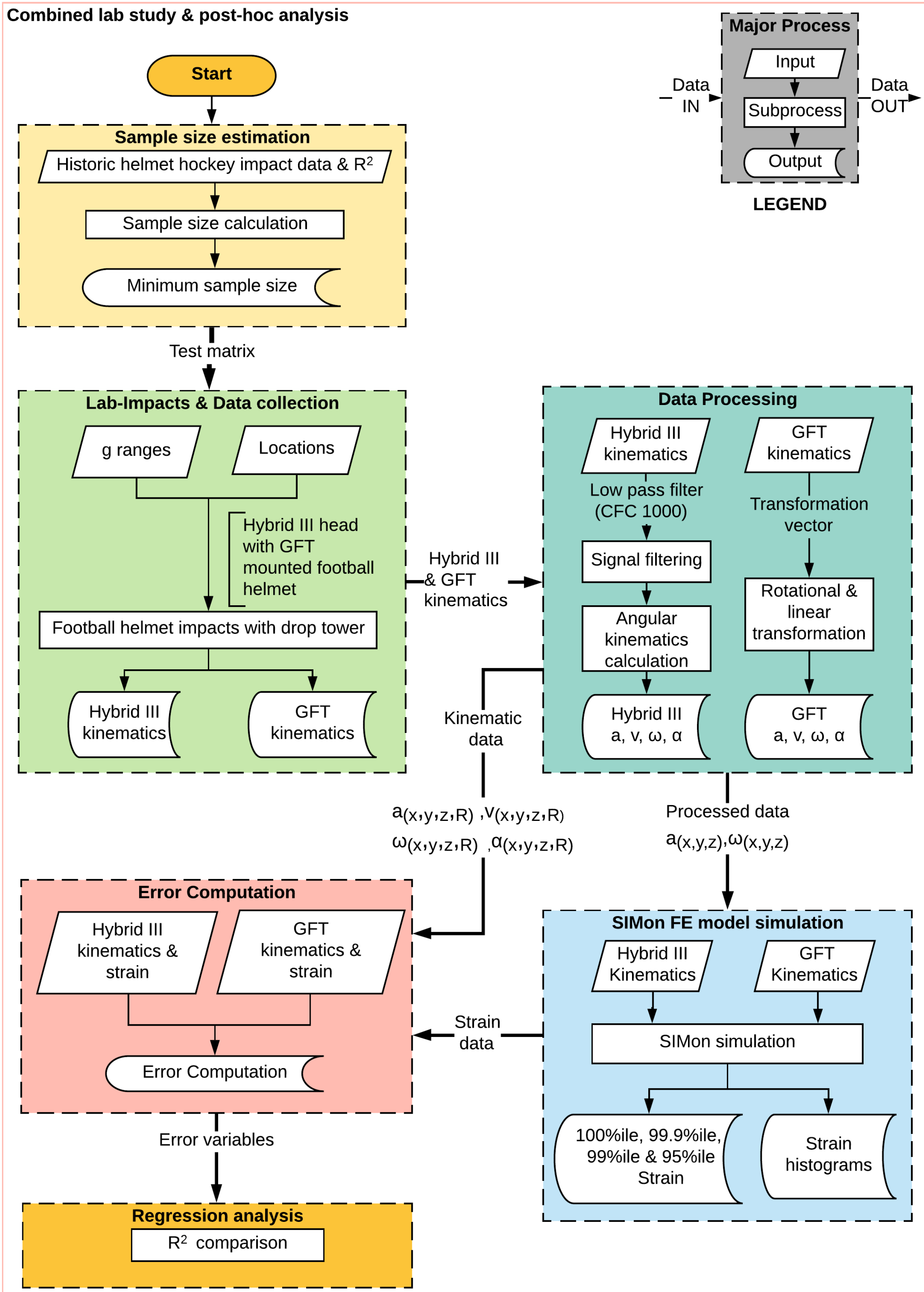

Figure 3.2: Overview of the experimental method

The sub-study used both laboratory impact data, and synthesized kinematics to understand effects of each input kinematic and kinematic transform (rotational) on SIMon-predicted strain (***Figure 3.3***).

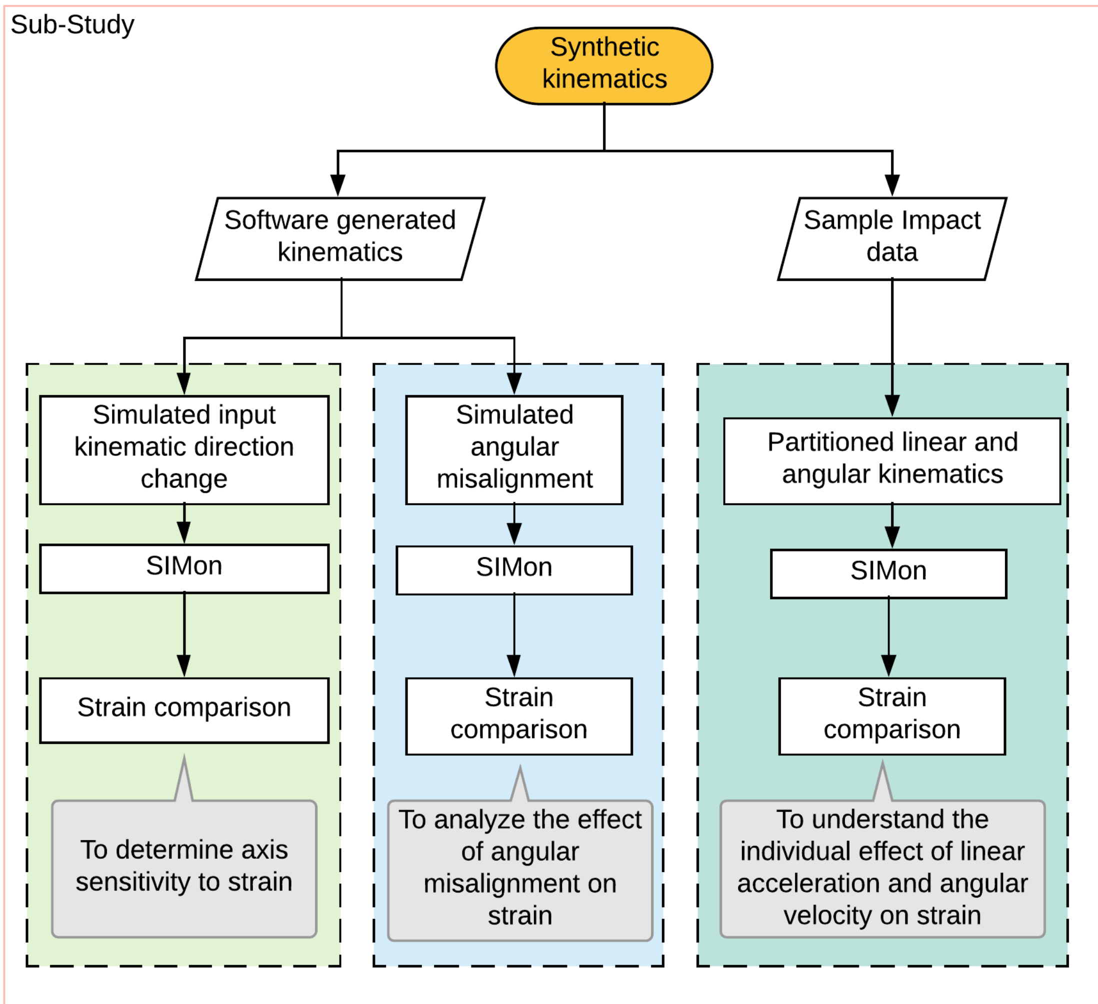

Figure 3.3: Overview of sub-study

3.1 Experimental setup

The overall experimental setup including the Hybrid III head with GFT mounted football helmet on a drop tower assembly is as shown in **Figure** *3.4*. Flat anvil and angled anvil (inclination 30˚) were used as impact surfaces for different experimental categories.

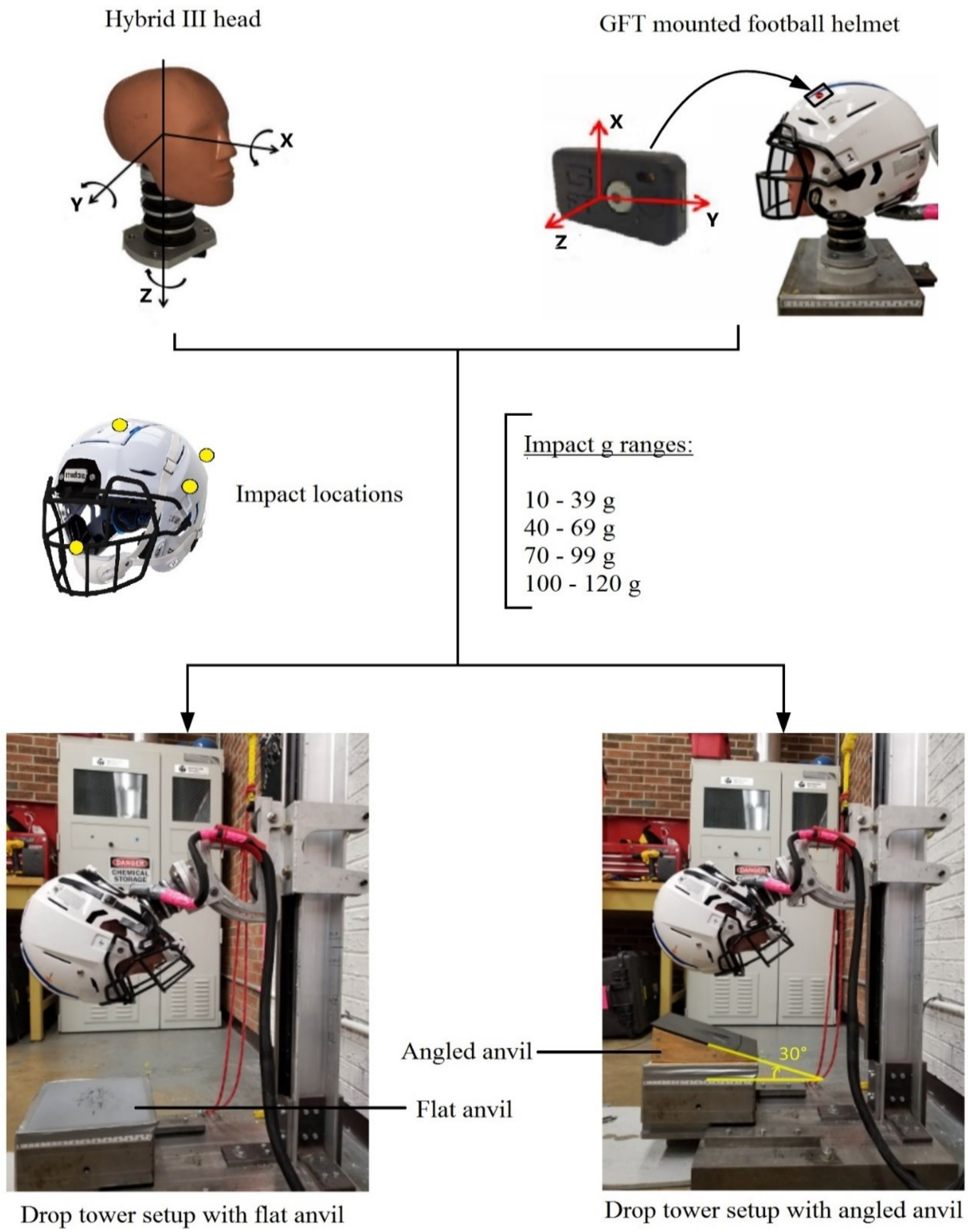

Figure 3.4 Overview of the experimental setup for football impacts

3.1.1 Drop tower assembly and Hybrid III

The 50th percentile male crash test standard dummy Hybrid III head was used as the test subject in this experiment. Football helmet impacts were conducted in the laboratory-based setup with a guided rail drop tower assembly that allows for repeatable drop impacts. The drop tower consists of a vertical rail with an anvil at the bottom of the test-bed. A gimbal is attached to the vertical rail, using a rail mount and grooved wheels to allow guided free fall of the Hybrid III head mounted on the gimbal. The gimbal design allows the Hybrid III head and neck to be positioned at different angles or to be rotated about the axis of the neck, providing the flexibility to create impacts at different locations of the Hybrid III head. A velocity gate attached near the bottom of the rail structure measures impact speed and triggers the data acquisition from the Hybrid III instrumentation system [72]. The impacts were conducted with a flat anvil and an angled anvil to create both centric and oblique impacts respectively. The anvils were fit with a hard plastic (ABS) surface to replicate helmet to helmet impact. The angled anvil was custom made with layers of plywood and with an inclination angle of 30°. The inclination of the angled anvil was chosen based on literature that achieved sufficient increase in angular kinematics with anvil inclinations up to 30° [73], [74].

The Hybrid III head and neck have a combined mass of 6.08 kg and is equipped with 9 uniaxial accelerometers (Measurement Specialties Inc. Hampton VA, model 64C-2000-360) in a 3-2-2-2 array to allow measurement of linear accelerations about the COG of the head. Three accelerometers are mounted on the head center of gravity, and the additional 6 accelerometers are located at the left side (A), the front (B) and at the crown(C) as shown in **Figure 3.5**. Acquisition of the impact kinematics was made using National Instruments hardware and software (PXI 6251 and LabVIEW v8.5, Austin TX) at a rate of 100 kHz. The signals were filtered with a low-pass cut-off frequency of 1650 Hz as per Channel Frequency Class (CFC) 1000 [2]. Though few researchers have considered lower cut-off frequencies (300 Hz – 1000 Hz) [76]– [78] to eliminate noise, it is a known fact that lower cut-off frequencies attenuate peak magnitudes of

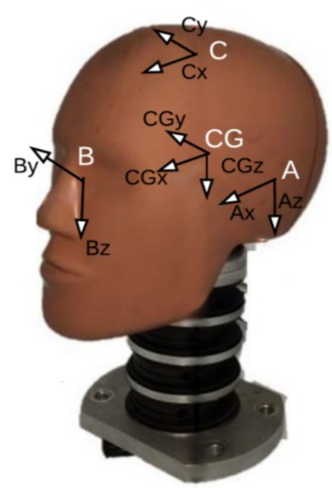

Figure 3.5 Hybrid III uniaxial accelerometers position and alignment

acceleration as well as the injury severity measure [78], [79]. Wu et al. estimated the bandwidths required for head impact sensors by measuring the attenuation of injury criterion with different bandwidths [79]. The study concluded that most rotation-based injury criterions required a minimum of 1650 Hz bandwidth of angular acceleration to achieve less than 10% attenuation. The cut-off frequency of 1650Hz was thus selected to filter Hybrid III kinematics. Butterworth filter in Matlab was used for software filtering the acceleration signals. Angular kinematics were calculated from the linear accelerations using the method proposed by Padgoankar [80]. The laboratory impacts were conducted using a Hybrid III head model that was tested for polarity conformance as per instrumentation standards [75] and accelerometer compatibility [24]. The polarity conformance is recommended by instrumentation standards to validate that the sensors correctly report the negative and positive directions of the component kinematics. This was achieved through test drops where the polarity of the component kinematics is validated against the impact direction. For example, during a front impact, the linear acceleration about the x-axis is expected to be negative, corresponding to the backward motion of the head. The test was repeated with trial drops for different impact directions and polarities were confirmed.

3.1.2 **Wearable sensor setup**

A GFT is a wearable sensor designed to be mounted on sports helmets to measure the helmet kinematics during an impact. The device weighs approximately 20 grams and has dimensions of 52 mm x 28 mm x 10 mm. It is instrumented with a triaxial accelerometer that measures linear acceleration at a rate of 3000 Hz and a gyroscope measuring angular velocity at an 800 Hz frequency. The GFT records impact data for a 40 ms time span. However, it continues to collect consecutive 40 ms data until the impact acceleration falls below the minimum threshold (10 g) [70]. The device was fitted to the inside of the helmet to the left side as shown in **Figure *3.6.b***. The location of the device on the helmet was chosen based on the recommendations in GFT user manual [81]. Double sided tape (3M) was used to secure the GFT to the helmet. The Hybrid III head was fit with NOCSAE certified football helmets (Schutt F7, Size: Large) over an unmodified scalp surface of the Hybrid III. A vertical distance of one inch from the brow to the helmet rim was ensured for consistent helmet fitting. Schutt chin straps were used to secure the helmet tightly to the Hybrid III head to minimize the head helmet relative movement. The tightness of the fit was not measured. Prior to recording any impact kinematics, the GFT software application requires the device to be calibrated after fitting it on the helmet. GFT calibration procedure was hence performed every time the sensor is changed, or a new helmet is used. Four helmets were used in total. In the software calibration procedure of the GFT, the location of the GFT device is first logged (inside or outside the helmet). The calibration procedure then instructs the user step by step to place the helmet on its three different sides (upright, left and back). With this procedure, the software predicts the location of the GFT in the helmet and uses the information to re-orient the axis of the device. GFT software calibration system then transforms the GFT kinematics from the axis orientation of the device to the axis orientation of the head as shown in **Figure *3.6.a***. The calibration system ensures that the impact directional kinematics reported by all GFT devices corresponds to the same direction irrespective of the location of the sensor in the helmet. However, it is to be noted that the GFT axis orientation does not agree with the axis orientation of the Hybrid III (**Figure *3.6.b***). This mismatch of axis directions could potentially affect the brain strain response calculation since the SIMon FE model uses a coordinate system in agreement with Hybrid III head axis directions.

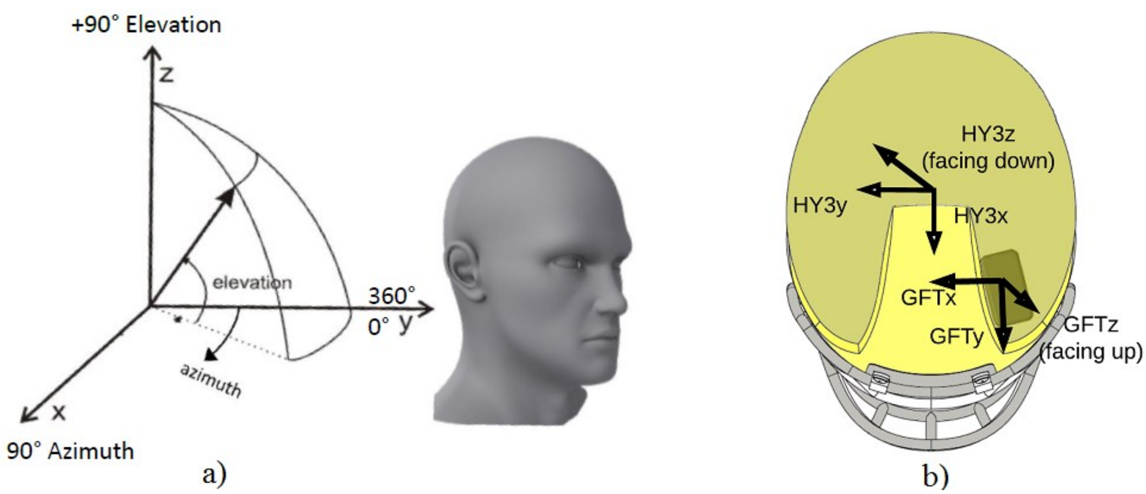

Figure 3.6: Direction of GFT kinematics after software calibration where the GFT coordinate directions are shown with respect to a) head and b) Hybrid III axis

Correction algorithms were designed to match the GFT kinematic directions with the Hybrid III head. Linear transformation of wearable sensor's kinematics to the Hybrid III head COG was practiced in studies validating the kinematics of a wearable sensor [21], [22], [82]. However, for strain calculations using wearable sensor kinematics, there is no existing research that studied the necessity of a linear transformation. Hence, to fill the gap in existing literature, the correction algorithms were designed to calculate brain strain response with and without linear transformation of GFT kinematics. The two methods used to process the GFT kinematics are discussed below.

i) Rotational or partial transformation of GFT kinematics

Though the GFT calibration system aligns the component kinematics to a consistent orientation as given by **Figure *3.6.a***, the direction of the component axes does not align with the Hybrid III axes. To correct the direction mismatch, Matlab codes were prepared to swap GFT x-axis and y-axis kinematic data and reverse z-axis kinematics. This method was validated against a computational rotation transformation using a rotation matrix (180˚ rotation about the y-axis and 90˚ rotation about the z-axis). The resultant angular velocity magnitudes were confirmed to be unaltered with the rotational transformation. **Figure 3.7** illustrates the expected GFT axes position and orientation after applying the rotational transformation to the GFT kinematics in its calibrated orientation (**Figure *3.6.b***). To validate if the corrected GFT kinematics matched with the Hybrid III kinematic directions, LS-PrePost simulations of Hybrid III and GFT impacts were analyzed. LS-PrePost is a free post processing software for FE results. An example of the motion of the head due to a facemask impact at different timeframes is shown in **Figure *3.8***. It is to be noted that the direction of the head movement simulated from GFT kinematics is comparable with that of Hybrid III. This method was repeated to compare the brain displacements due to impacts at the front, back, left and right side of the head. After comparing the FE brain model's displacement directions for multiple impacts, it was confirmed that both the Hybrid III and the GFT kinematics resulted in a similar motion of the head for each impact, which suggested that the corrected GFT kinematics was in agreement with the Hybrid III axes directions. In summary, the rotational transform results in kinematics that are expressed relative to the GFT coordinate system shown in **Figure 3.7**. In

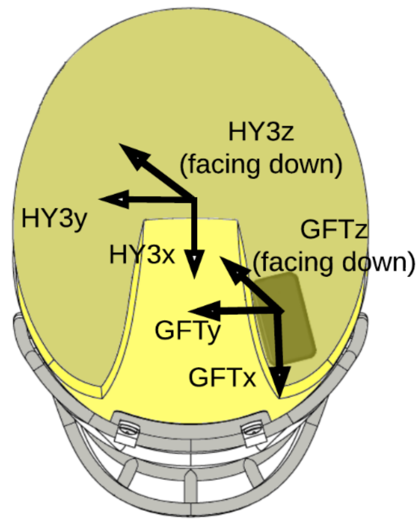

Figure 3.7 GFT axis orientation after rotational transformation

this orientation the component axes are parallel to the Hybrid III system, but not coincident with the Hybrid III system.

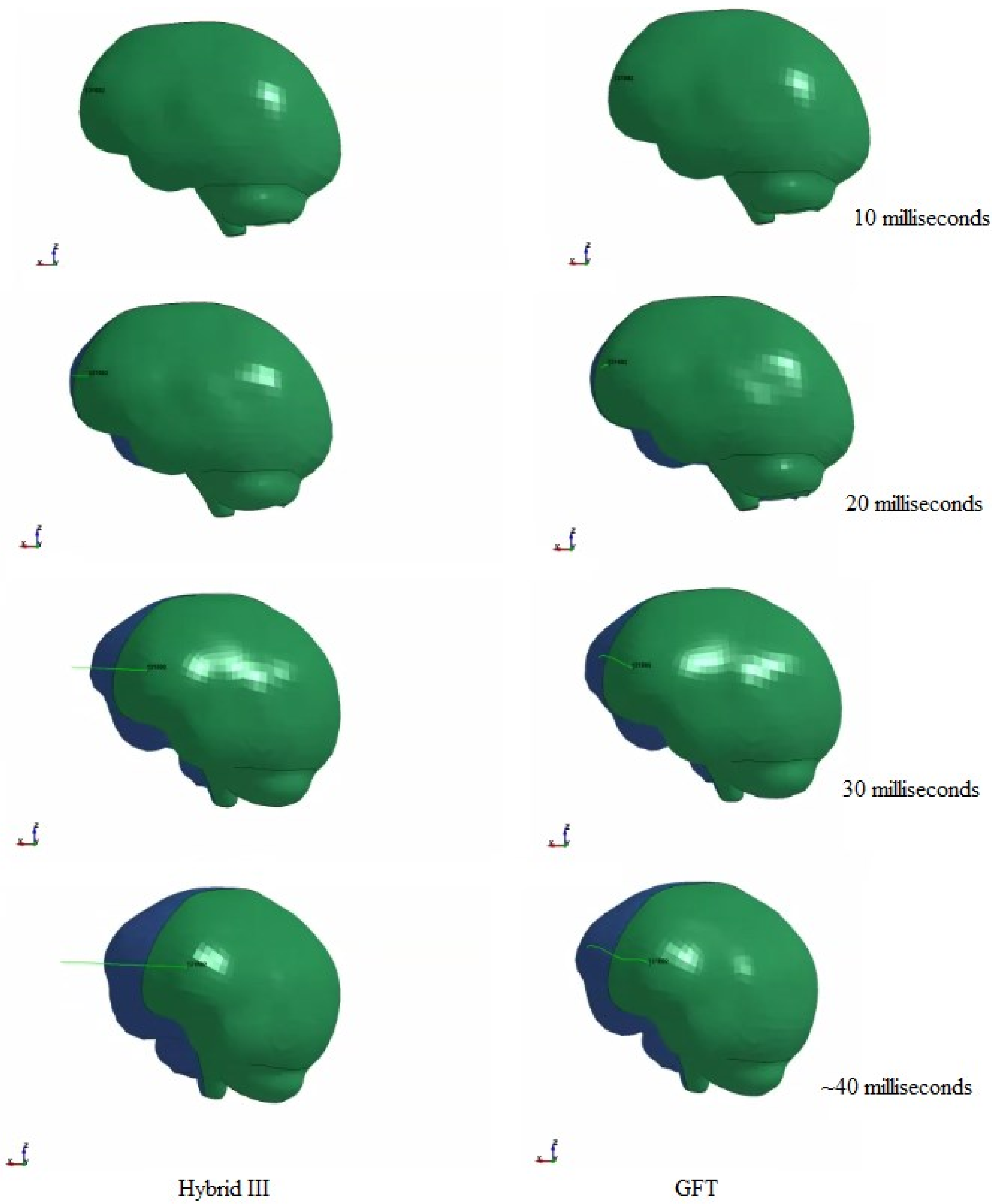

Figure 3.8: Example of FE brain model displacement from Hybrid III and GFT data for a facemask impact, with the displacement path of a node

For some analyses in this thesis, it was necessary to transform GFT kinematics to be expressed relative to a coordinate system that matched the Hybrid III system (i.e. the component axes are parallel and coincident), and this was achieved through a linear transformation (as described below).

ii) Linear or full transformation of GFT kinematics

Linear transformation of the kinematics from GFT coordinate system origin to the Hybrid III head center of gravity requires a position vector to be determined between the two reference frames. This was achieved by marking the approximate position of GFT origin on the outside of the football helmet (B). Pictures of the GFT mounted football helmet fit over Hybrid III head were then taken from different directions. A pixel/inch scale was used to measure the distance between B and Hybrid III head boundaries as x_{ref} and z_{ref} (**Figure 3.9**). z_{ref} was adjusted for the distance between B and GFT center (at the inside of the helmet). The point A in **Figure 3.9** refers to Hybrid III center of gravity. The distance between the helmet's center (along the coronal plane) and B was measured as y_{ref} distance. The position of GFT center with reference to Hybrid III head outer dimensions being gathered, $r_{A/B}$ was then defined as a position vector that documents the straight-line path (i.e. position vector defining the GFT location relative to the Hybrid III head center of gravity) between the GFT coordinate system origin and Hybrid III head center of gravity. Note that the location of the Hybrid III head center of gravity is determined from publicly available Hybrid III engineering drawings [83]. Matlab code was then generated using the position vectors to apply linear transformation [61, p.523] to the GFT kinematics using Equation 3.1.

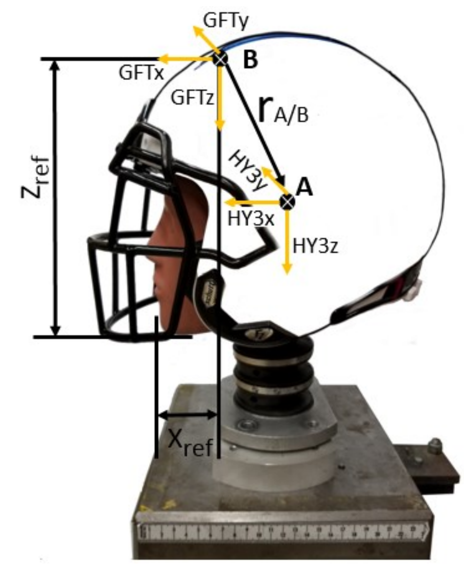

Figure 3.9 Position vector measurement of GFT COG w.r.t Hybrid III COG

$$a_{CG} = a_{GFT} + \alpha_{GFT}\, X\, r_{A/B} + \omega_{GFT}\, X\, (\omega_{GFT}\, X\, r_{A/B}) \quad (3.1)$$

Where a_{CG} refers to linear acceleration at the center of the Hybrid III head. The GFT angular acceleration (α_{GFT}) was calculated using five point stencil method [85]. Equation 3.1 is a vector equation that transforms linear accelerations expressed relative to the GFT coordinate system to linear accelerations expressed at the Hybrid III coordinate system.

3.1.3 **Football helmet impacts**

A test matrix for the football impacts was created to generate impacts up to 120 g. In a study by Pellman et al. that used reconstructed NFL game data [86], the average linear acceleration for concussive impacts in different location did not exceed 117g. An upper boundary of 120g for the impact ranges targeted in test matrix was set based on this data. The test matrix of most research on the helmet impacts also recommends impacts to be conducted at different locations of the head such as front, back, side and crown to replicate real-time impact scenarios [22], [70], [82]. Multiple impacts sites were also considered in this thesis; however, they are chosen based on corresponding kinematic directions. Kinematics being the physical quantity used to measure an impact, the impact direction categorization can be translated to kinematic direction categorization. For example, an impact to the front of the head will create higher linear acceleration in the x-axis of the Hybrid III head and greater rotation about the y-axis. This will simplify the category from several impact directions to three (corresponding to x, y, z directions) and further help in better understanding of the relationship between kinematics and brain strain response. Though both linear acceleration and angular velocity are used in brain strain response calculation, an overwhelming number of studies have shown angular kinematics to be a mechanism for diffuse brain injuries [24], [25], [29], [87]. Hence rotation about the x, y and z axes was chosen for the kinematic direction categorization. To obtain impact kinematics over a range of values, impacts were repeated at every 10 g increments. The impact directions were selected such that the crown and the back impacts were expected to have maximum rotation about the y-axis, the side impacts create maximum rotation about the x-axis, and the facemask impacts were designed to create maximum rotation about the z-axis. **Table *3.1*** shows the football test matrix with the count of impacts obtained in each g range from the drop test considering different impact locations and anvil types.

The direction of rotation was not always as anticipated and drop tests tend to create more rotation about the y-axis. The facemask drop impacts created more y-axis rotations, and impact with maximum z-axis rotations were challenging to achieve with the drop test setup. Hence, to create impacts with maximum rotation about the z-axis, the Hybrid III head was suspended at a 1.3 meter height from the ground with facemask facing roof and slightly tilted towards the left (**Figure *3.10***). Impacts were created manually by hitting the helmet facemask with another helmet. These impacts created mostly rotational head motion and corresponding linear accelerations were much lower compared to other drop impacts. Due to these reasons, the repeatability in terms of g-ranges was not plausible for the facemask impacts, though angular velocities were achieved up to a range of 50 rad/sec.

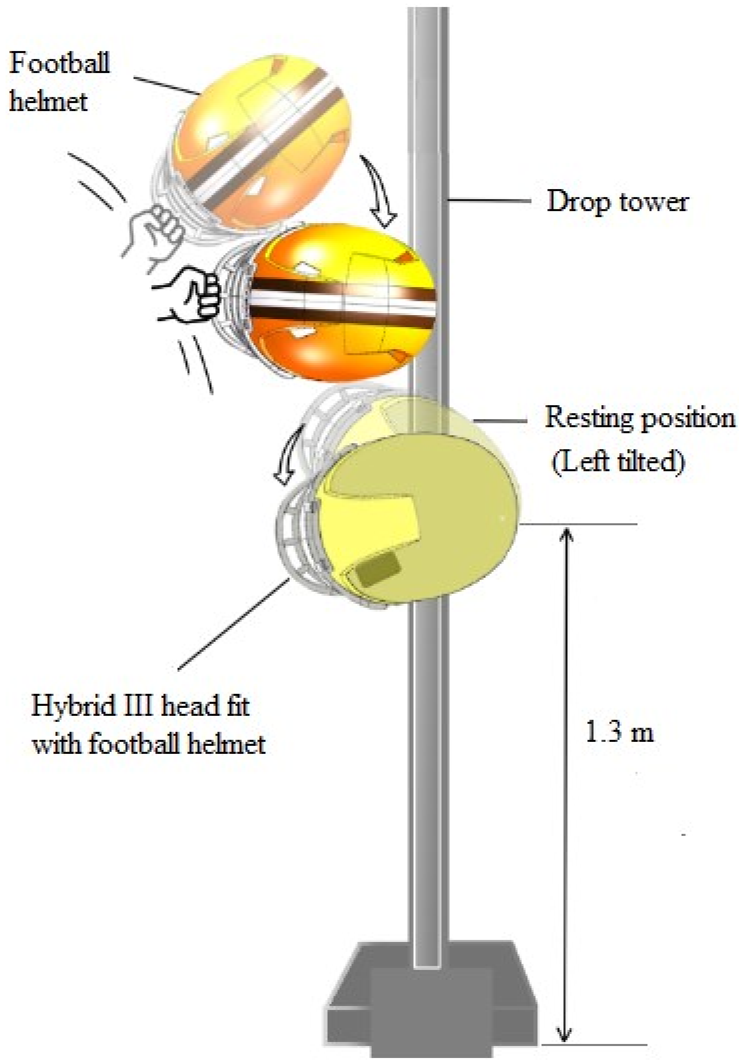

Figure 3.10: Illustration of test setup for manual impacts to generate Hybrid III head rotation about the z-axis

Table 3.1: Football impact test matrix: Count of impacts obtained in each g range from the drop tests conducted on different impact location and with two anvil types

Impact Location Vs g range	<40 g			40-69 g			70-99 g			>100 g			Total Impacts
	10g	20g	30g	40g	50g	60g	70g	80g	90g	100g	110g	> 120g	
						Flat Anvil							
Crown	-	-	-	-	-	-	-	3	1	4	4	11	23
Back	-	1	9	3	10	5	3	-	6	4	1	11	53
Left	3	6	7	4	4	1	4	2	4	2	6	3	46
						Angled Anvil							
Crown	-	-	5	8	1	7	8	5	3	3	1	-	41
Left	7	16	6	2	6	10	4	1	-	-	-	-	52
Facemask	3	12	2	3	4	4	-	-	-	-	-	-	28
Facemask (Helmet-helmet impact)		20			12			1		-	-	-	33
Total impacts		97			84			45			50		276

In the case of the drop tests, higher g range impacts with angled anvil were limited due to the below reasons,

1. For crown impacts, the linear acceleration did not increase with the increase of the drop height after 90g. This was believed to be due to the increased engagement of the helmet cushions at higher drop heights.
2. For the facemask and left impacts, the Hybrid III neck flexing was greater which posed a risk of damaging the Hybrid III neck and instrumentation.

The impacts were repeated with both flat anvil and angled anvil. A total of 276 impacts were achieved over a range of peak magnitudes in both linear acceleration and angular velocity as given in **Figure *3.11***. Few impacts with low g-ranges (<30g) in crown impacts were removed from the test due to errors in the GFT signals because of loosely adhered GFT device to the helmet surface. Though high g-ranges could not be achieved in few impact categories, sufficient sample size of these g ranges in other categories restricted any skewed distribution of impact kinematics in the overall experimental data. Of the 276 samples, 91 impacts had maximum angular velocity about the x-axis, 131 impacts had maximum angular velocity about the y-axis, and 54 impacts had maximum angular velocity about the z-axis (considering Hybrid

III kinematic magnitudes). Though the targeted peak range was only up to 120g, few impacts with higher drop heights (> 2 meter) resulted in linear accelerations greater than 120g. The peak magnitudes in **Figure *3.11*** correspond to the Hybrid III impact kinematics recorded from the drop tests and the impacts with peak magnitudes that did not fall within 10g -120g were not removed.

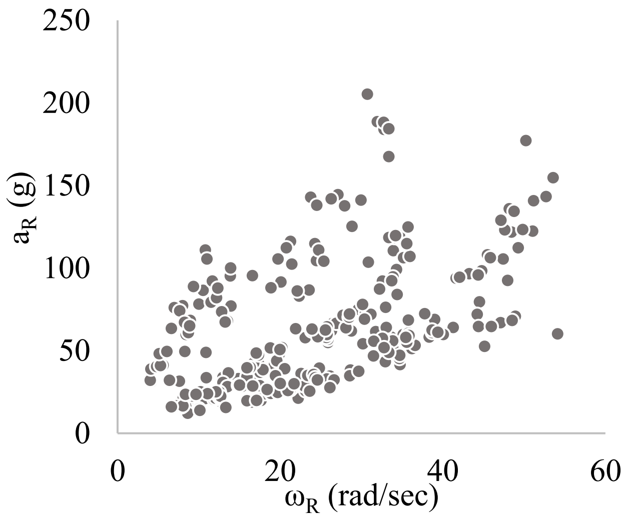

Figure 3.11 Peak resultant angular velocity (ω_R) vs. peak resultant linear acceleration (a_R) of all impacts conducted, showing peak impact kinematics achieved in all g ranges and angular velocities in drop impacts

3.1.4 Sample size estimation

When using regression analysis for prediction purposes, it is often necessary to determine the sample size large enough to obtain a useful prediction. Hence for the football impacts tests conducted for this thesis, a sample size estimation formula (Equation 3.2) proposed by Sande Milton [88] for multiple regression studies was used. Though this thesis will mostly work on simple regression models, a multiple regression model was used for sample size estimation.

$$n = k + 1 + \frac{t^2(1-R^2)}{\Delta r^2} \tag{3.2}$$

Where n refers to sample size, R^2 is the anticipated coefficient of determination, k is the number of variables used in the final regression model for which the input kinematics to SIMon that are used to calculate strain was considered. The variable t is the desired t-statistic value, and Δr^2 could be elaborated as the addition to R^2 when a new variable is entered at last to the regression prediction. It could also be stated that when a variable added at last to a regression analysis contributes an addition to R^2 by the specified value (Δr^2), the sample size calculated will assure the desired confidence level (or t-level) [88]. To allow detection of changes in R^2 of 5%, or in other words to detect 5% increase/decrease in the ability of a model to explain error, Δr^2 was set at 0.05. The desired t-value of 2 was set to assure a statistically significant regression coefficient of $p < 0.05$ from the sample size [88]. Anticipated values for R^2 were determined from data collected previously collected in our laboratory by Knowles et al. [24] in a similar experiment that compared GFT and Hybrid III brain strain response using hockey helmets. This previous work by Knowles et al. examined a hypothesis that differed from those posed in the present thesis. The hockey helmet impact experiments conducted by Knowles et al. used the same experimental setup including the drop tower, Hybrid III head and the FE brain model that was utilized in this thesis. A total of 109 impacts from the hockey helmet impact database were used to calculate the R^2 between input parameter errors and output strain error. Two sets of data were used to calculate the sample size. One with the k value set to 8 including component and resultant kinematic errors of both linear acceleration and angular velocity. Though resultant is a function of component kinematics, it was decided to treat the resultant separately. The historic R^2 value obtained from the multiple regression considering 8 independent variables and MPS error (dependent variable) was 0.58. For the second set of data, only resultant angular velocity errors were considered (k=1) for the independent variable. The linear regression between $\Delta\omega_R$ and strain errors yielded an R^2 of 0.55. The sample size for football helmet impact experiments was thus calculated with

i) $R^2=0.58$, k=8, t=2 and $\Delta r^2=0.05$ which yielded n=43. And,

ii) $R^2=0.55$, k=1, t=2 and $\Delta r^2=0.05$ which yielded n=38.

Though for a simple linear regression with one predictor (k=1), a sample size of 38 might be sufficient as per the above result, a higher number was chosen to have a sample size larger than what is required. Thus, a minimum sample size of 43 was targeted in each category of impact direction and impact speed ranges of the football impact test matrix to have sufficient data in category (Category X, Y and Z) based statistical analysis.

3.1.5 Brain Finite Element Model

The handling of SIMon brain FE model output data that was used in further regression analysis is discussed in this section. **Figure** ***3.12*** provides an overview of the types of data that were retrieved from SIMon.

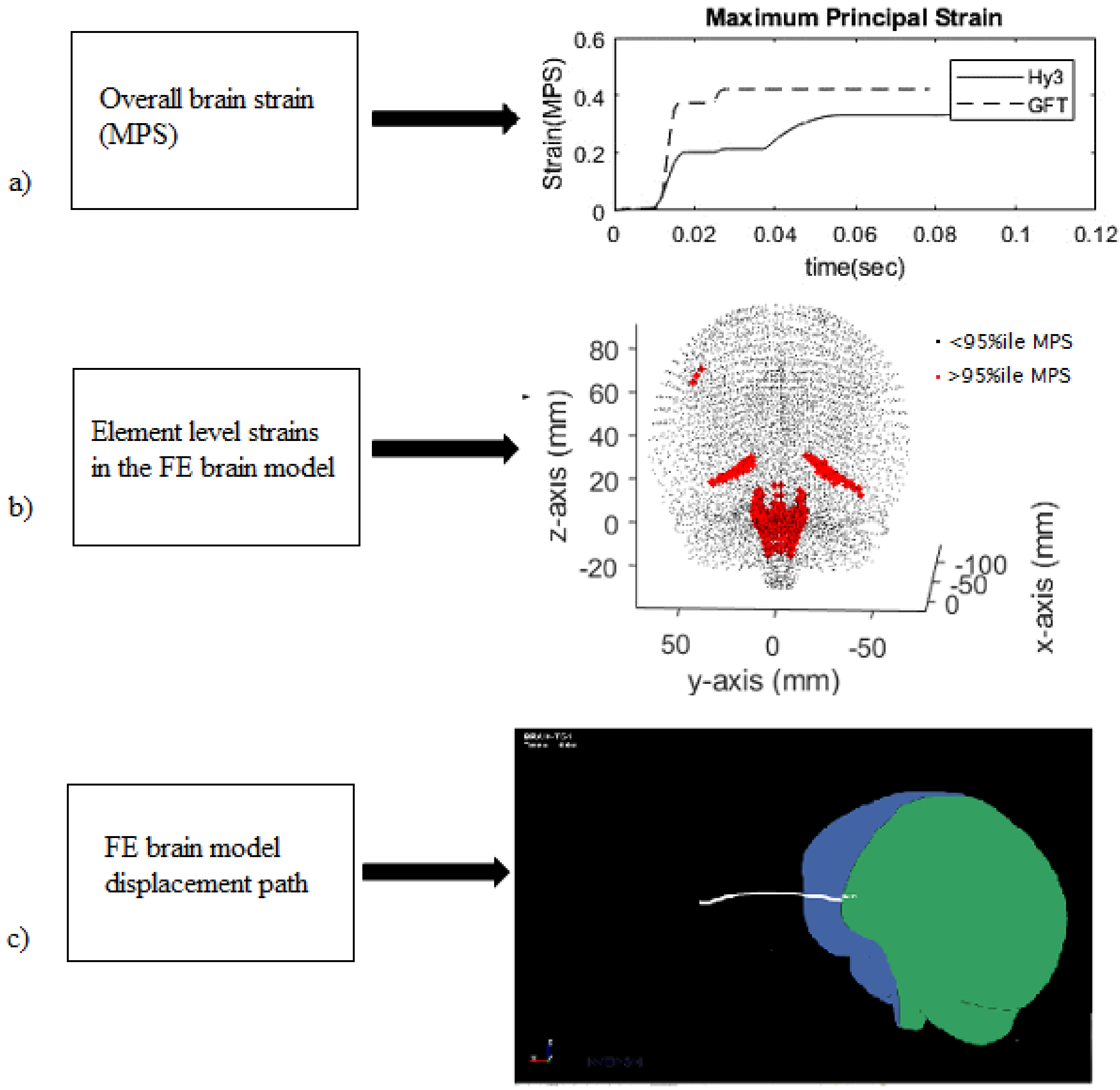

Figure 3.12: Overview of outputs from simulation using SIMon brain model including a) the MPS output for both Hybrid III and GFT in time domain b) 3D brain plot with red dots showing top 5% strains obtained from element level strain data and c) the displacement path of the 3D brain model due to an impact

The SIMon includes major parts of the brain such as cerebrum, cerebellum, brain stem, ventricles, parasagittal blood vessels, falx tentorium, cerebrospinal fluid, foramen magnum and skull. The material properties for these parts were based on Kelvin-Maxwell model after comparing the brain model response with several other material models [56]. The Kelvin-Maxwell material model was used in SIMon for its softest stress response as well as numerical stability in LS-Dyna environment [56]. The model with its material properties was also validated against the NDTs displacement-time histories and pressure-time histories [56]. The material properties used for different parts of the model is given in **Table 3.2**.

Table 3.2: Material properties of SIMon FE brain model parts

Material properties	Cerebrum/ Cerebellum/ Brain stem	Ventricles	Blood vessels	Falx-tentorium	CSF	Foramen - magnum
Type	Kelvin-Maxwell Viscoelastic	Elastic Fluid	Cable Discrete Beam	Elastic	Kelvin-Maxwell Viscoelastic	Elastic
Density, ρ (kg/m^3)	1040	1000	5000	1130	1050	1050
Bulk Modulus, K	558.47	2100	-	-	4.97	-
Short time shear modulus, G_0 (MPa)	0.00166	-	-	-	0.1	-
Long time shear modulus, G_l (MPa)	9.28E-04	-	-	-	0.02	-
Decay Constant	16.95	-	-	-	0.01	-
Young's modulus, E	-	0	0.275	31.5	-	6933.3
Poisson's ration, υ	-	0.5	-	0.45	-	0.45
Viscosity coefficient, VC	-	0.2	-	-	-	-
* The data in the table is adapted from *[56]*						

The SIMon brain model calculates the brain strain response using linear acceleration (a_x, a_y, and a_z) and angular velocity (ω_x, ω_y, and ω_z) data generated during an impact. To obtain angular kinematics for Hybrid III, the method proposed by Padgoankar [80] was used to calculate angular accelerations α_x, α_y and α_z from the linear acceleration data obtained by the nine acceleration sensors. The calculated angular acceleration was then integrated to generate angular velocities. Hundred milliseconds of Hybrid III impact data were extracted for each impact. With GFT, for impacts that had more than one 40 ms data, first two sets were combined to create an 80 ms data file. Of the 276 GFT kinematic files, 112 of these comprised two, 40 ms duration, kinematics files in succession. For 76 of the 112, the two consecutive 40 ms files were required so that the strain magnitude for these impacts reached a stable maximum. In addition, for 16 of the 112 impacts the strain magnitude did not reach a stable maximum value even at 80 ms. 164 GFT kinematic files were 40 ms duration. As specified earlier the GFT kinematics are filtered with 300Hz low pass filter for linear acceleration and 100Hz filter for angular velocity [15], [24]. Hence no further filtering was applied to the GFT kinematics.

The maximum principal strain (MPS) of the brain model is obtained as a direct output of the SIMon simulation (**Figure *3.12.a***). MPS is the largest principal strain computed for any element in the brain model over the entire time-duration of the simulation. Therefore, MPS represents the biggest tensile strain experienced over the impact simulation. Further information from the simulation including brain displacement due to an impact and strain data for each element in the brain model were obtained using LS-PrePost, an advanced pre and post-processor delivered by LS-Dyna. The three-dimensional displacement of the brain model can be simulated with LS-PrePost using the output files from SIMon. The brain model displacement was used to verify that the brain motions simulated with corrected GFT directional kinematics matches with brain motions obtained from Hybrid III data. The strain data of each element in the brain model were used in percentile MPS calculation (detailed subsequently) and to compare the location and volume of the highest strains predicted by the Hybrid III and the GFT kinematics.

3.2 Sub-study: Test methods using synthetic kinematics and sample impacts

A sub-study involving three different methods was designed to understand how each input to SIMon affects the brain strain magnitude individually. The kinematic inputs (a_x, a_y, a_z, ω_x, ω_y, ω_z) to the SIMon brain model are treated as vectors of Hybrid III Cartesian coordinate system. A wearable sensor's coordinate system, however, may not perfectly align with Hybrid III like in GFT, where the sensor's coordinate system is both rotationally and linearly misaligned. This section was hence aimed at studying the errors in brain strain magnitude calculation due to possible angular misalignment between the Hybrid III and the wearable sensor. This was achieved by using computationally generated kinematics and by simulating angular errors in Hybrid III impact data. Two methods were designed to study the effect of axis direction mismatch and rotational misalignment of angular kinematics respectively. Only angular kinematics was considered in this first two methods based on earlier literature that states rotational kinematics a better predictor for brain strain than translational kinematics [25], [40]. However, a third test method was designed to compare the brain strain response of linear acceleration and angular velocity when treated individually.

Simulated angular velocity curves were generated using Matlab code for the input files used in the method I and method II. Angular velocity data was obtained by integrating the angular acceleration curve with an acceleration peak (P_α) and a deceleration peak as illustrated in **Figure *3.13***. Angular velocity curves with different peak velocities were obtained by varying the acceleration peak P_α value. Null kinematics was applied to all linear acceleration input files in method I and method II.

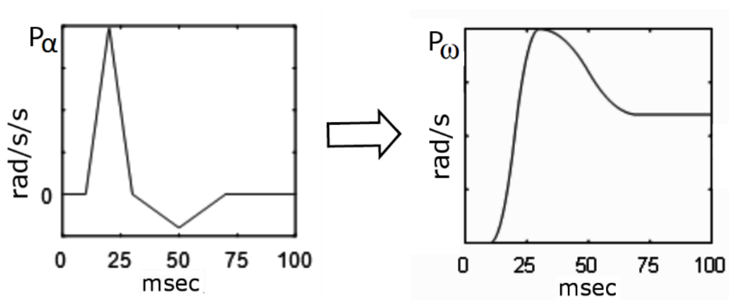

Figure 3.13: Angular velocity curve generated from angular acceleration curve

In the **method I**, 15 SIMon datasets were designed in total with a set of five angular velocity input files with peak magnitudes (P_ω) of 6, 10, 20, 30 and 40 rad/s. This method was designed to analyze the sensitivity of strain to each of the x, y and z axes. Each angular velocity input file generated was applied to one axis (x or y or z axis) at a time, and null kinematics was applied to the rest of the axes as shown in **Figure *3.14***.

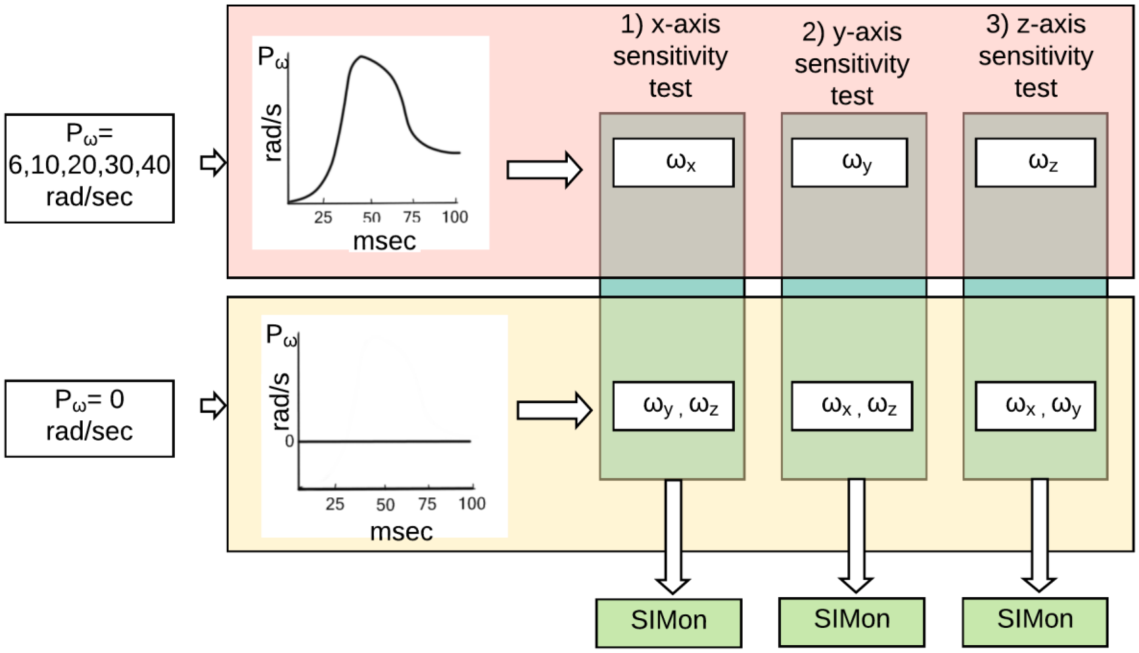

Figure 3.14: Method I sub-study: Input dataset design with software generated files

Method II had 18 datasets in total with angular rotation errors of 15˚, 30˚, 45˚, 60˚, 75˚ and 90˚ at each axis as in **Figure *3.15***. Software generated velocity curve with a peak magnitude of 30 rad/sec was applied in an axis other than the rotating axis. A rotational transformation was then applied to the angular velocity data using rotation matrix R as given in equation 3.3.

$$\omega' = R.\omega \tag{3.3}$$

$$Rx = \begin{bmatrix} 1 & 0 & 0 \\ 0 & \cos\theta & -\sin\theta \\ 0 & \sin\theta & \cos\theta \end{bmatrix},\ Ry = \begin{bmatrix} \cos\theta & 0 & \sin\theta \\ 0 & 1 & 0 \\ -\sin\theta & 0 & \cos\theta \end{bmatrix},\ Rz = \begin{bmatrix} \cos\theta & -\sin\theta & 0 \\ \sin\theta & \cos\theta & 0 \\ 0 & 0 & 1 \end{bmatrix}$$

Where Rx, Ry, and Rz are rotation matrix for a rotation about the x-axis, y-axis and z-axis respectively. The datasets were created by repeating rotational transformation with each of the above R matrix with six different angles (θ).

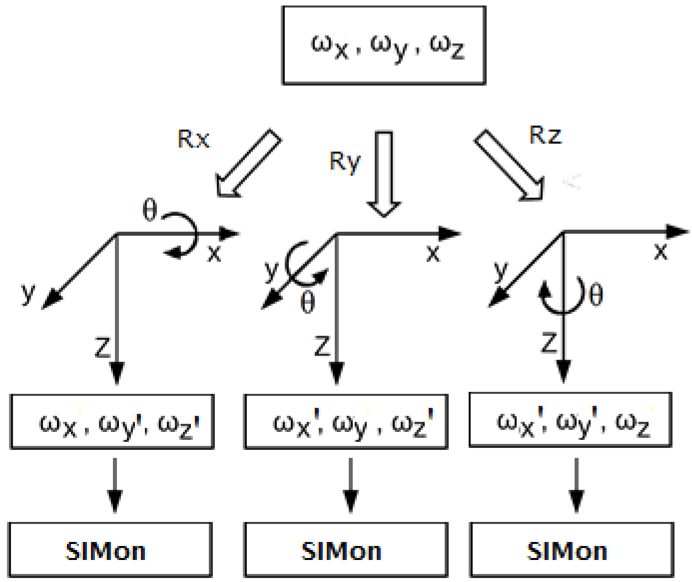

Figure 3.15 Method II sub-study: Generation of SIMon input files with rotational error applied to the component axes. ω_x, ω_y, and ω_z are component angular velocities and ω_x', ω_y' and ω_z' are angular velocities after rotational error. θ – Error angle

For the test **method III**, a set of 5 impacts were chosen from the GFT football impact data with high linear acceleration magnitude (110 g to 250g). The sample impact chosen include two facemask impacts, a side impact, a back impact, and a crown impact. Each impact data was split into three datasets, one with only linear acceleration inputs, the second with only angular velocity inputs and third dataset with both linear acceleration and angular velocity inputs.Brain strain response (MPS) was calculated for all the datasets created in the above three methods using SIMon. The resulting brain strains in each method were compared to study the effect of individual input kinematics of SIMon.

3.3 Statistics

The three major steps followed towards statistical analysis conducted in this thesis are described in **Figure *3.16***. First, percentile strain values of the distribution of the strain in the FE brain model was calculated for each impact from element level strain data. Second, the error between Hybrid III and GFT was calculated for each of the input and the output parameter. Third, the calculated error variables were used in the regression analysis to obtain the R^2 values to determine which input error is most explanatory of the strain error.

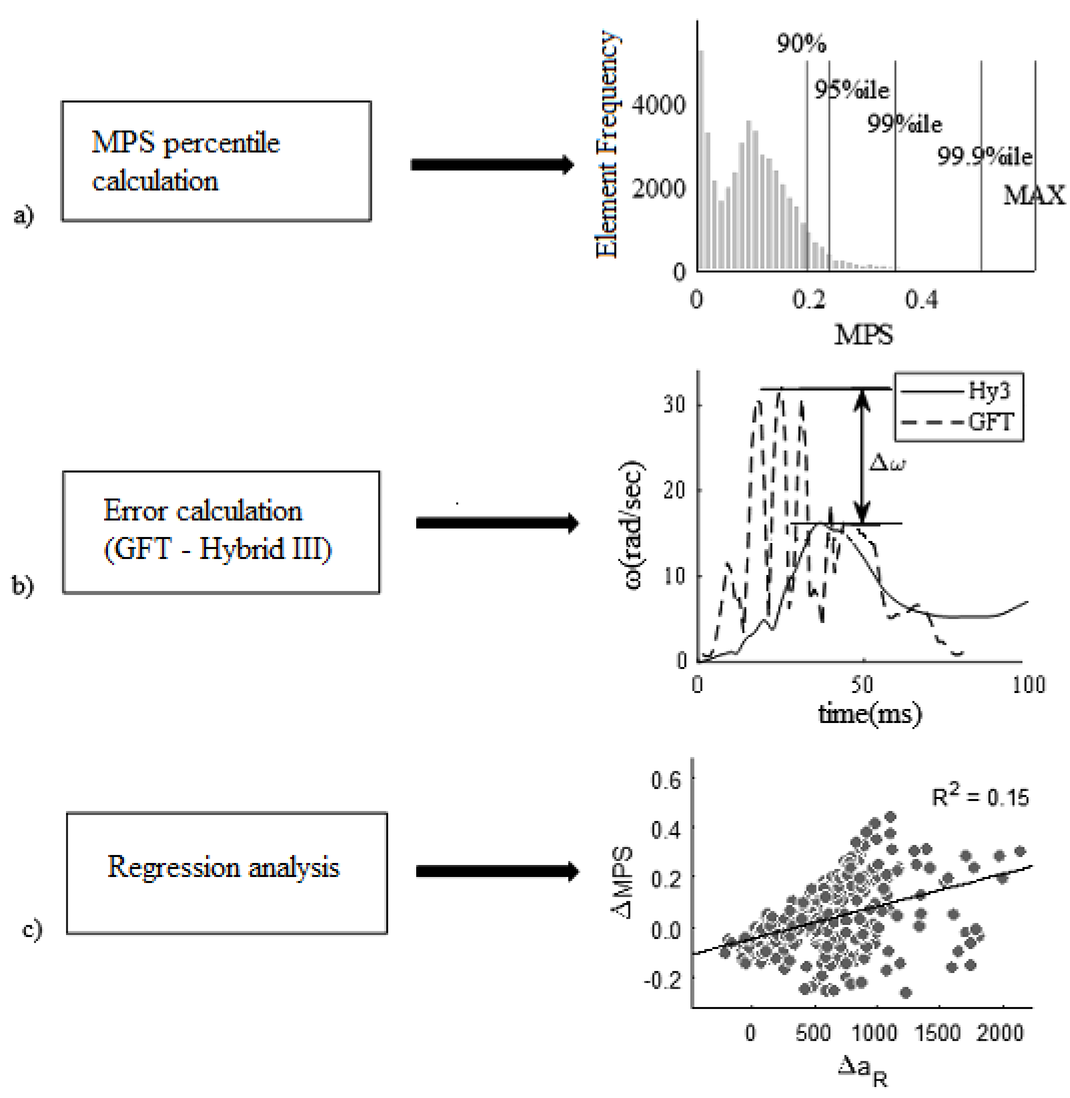

Figure 3.16 Overview of statistical analysis where the histogram a) at the top shows percentiles calculated from strain distribution of the elements, the kinematic comparison plot b) illustrates error (Δ) determination between two sensor variables and regression analysis c) explains regression (R^2) between two error variables

3.3.1 MPS percentile calculation

The use of MPS calculated by the FE brain models as a metric on which to infer the likelihood of brain injury is currently under debate in the biomechanics community, because it is based on the output of a single element in the FE model[71]. To clarify why this is a source of debate, one should consider that it is possible (in any FE model) that some elements (due to poor mesh quality or other factors) calculate strains that are not representative of the strains in adjacent elements and therefore could calculate strain magnitudes that are considered spurious [39], [41]. In brain FE models, if such spurious elements calculate strains that are greater than adjacent elements, and if the strain is used to infer injury risk, then inferences on injury could be argued as poorly motivated because they are based on high (spurious) strain levels. One approach that has been proposed and applied by researchers to prevent the influence of spurious strain on their studies is to use strain magnitudes that are lesser than the maximum principal, typically the 99%ile or 95%ile in principal strains. The rationale is that by disregarding the greatest 1% or 5% of strains, respectively, then the influence of spurious strains is eliminated. However, a full justification explaining the choice of 95%ile strain, as opposed to another percentile, is absent in the literature. In this thesis, we examined regressions between MPS (or 100%ile principal strain) and other percentiles to examine whether or not the findings of this thesis would be specific to a choice of a certain percentile.

The distribution of the maximum strains of all the 45,875 elements in the SIMon brain model was compared to decide on the appropriate percentile value of MPS to be used in this research. The strain data of all the elements were extracted using LS-PrePost for all 276 impact data (GFT & Hybrid III). Matlab code was then used to obtain the maximum strain of each element. The strain magnitude of 95th, 99th, 99.9th, and 100th percentiles were then calculated for each of the 276 impacts. The 99th and 99.9th percentiles were calculated for additional information on how the magnitudes of these percentile data compare with the 100th percentile and to understand the distribution of the strain magnitudes across percentiles (***Figure 3.16.a).***

3.3.2 Error calculation

After input kinematics and the output brain strain response data were collected, the error between both the sensor data was calculated. Literature and brain strain metrics comparing brain strain to impact kinematics have predominantly focused on peak magnitudes of the impact kinematic data [24], [41], [67], [70], [86]. While an error in peak kinematics is time independent, another possible error definition could be a time domain error between impact kinematics from the two sensors. Because there is no agreed upon definition of error in kinematic measures, both errors based on peak magnitudes and maximum difference in time series kinematics were considered. Errors based on peak magnitudes were calculated because the literature suggests brain strain correlates well to peaks [38], [56]. Time series error was calculated to consider the differences in kinematics that vary in time. However, a time domain kinematic error calculation in this study has the following challenges:

i) The Hybrid III and the GFT are two independent systems operating at different frequencies (100 kHz and 3 kHz, respectively) and time synchronization between such systems was therefore not possible without employing down-sampling of Hybrid III data, and perhaps more importantly;

ii) The GFT that records the helmet kinematics might record impact data earlier than the Hybrid III (which records the head kinematics). Thus any synchronization of the impact kinematics based on the kinematic profiles may not be accurate.

Despite the known challenges in a time-domain analysis, a simple time domain error definition was formulated to analyze its ability to explain the strain errors. In addition, error in peak kinematics was compared against strain error because peak head impact kinematics are good predictors of brain strain.

Time-domain kinematic error definition: One of the approaches to quantify kinematic error, used in this thesis, is based on computing the numerical difference in kinematics for all time in the impact data, and choosing the maximum difference as the error. A time-domain comparison of a closely aligned kinematics of Hybrid III and GFT is given in **Figure *3.17***. The Hybrid III kinematics were down sampled to the frequency of the GFT kinematics (linear acceleration: 3000Hz, angular velocity: 800 Hz) for this time domain comparison. In the plot comparing the angular velocities, the maximum difference in magnitude between the two angular velocity curves was driven by a valley in the GFT signal. This influence of the valleys in the signals in time domain difference was noticed in more than 50% of the impacts conducted in this thesis. A time-domain analysis was however made by comparing the maximum difference in the Hybrid III and the GFT kinematics against the maximum strain error. With time-domain kinematic errors, using signs in the error variables resulted in equal scatter of data on all quadrants and hence no relationship could be obtained. Thus, only absolute differences (|ΔK | & |ΔMPS|) were considered in this method. Both component kinematics errors and resultant kinematic errors were calculated using equation 3.4. Strain errors were calculated using equation 3.5.

$$|\Delta K| = \max |K_{GFT} - K_{Hybrid\ III}| \tag{3.4}$$

$$|\Delta MPS| = |\max K_{GFT} - \max K_{Hybrid\ III}| \tag{3.5}$$

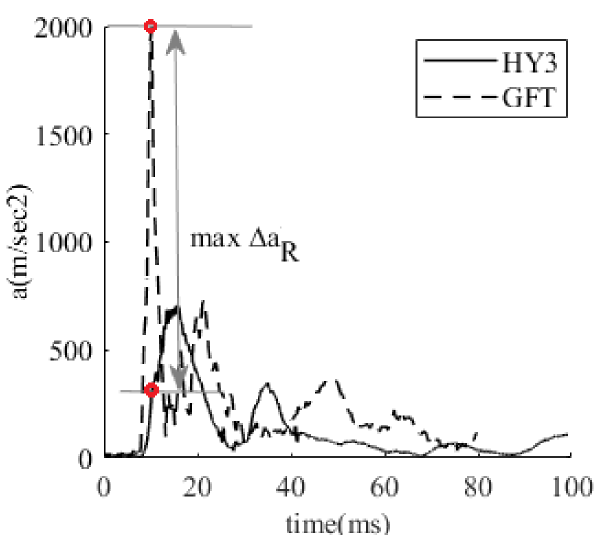

Figure 3.17: Time-domain error between Hybrid III and GFT resultant kinematics

Peak kinematic error definition: This thesis also considered kinematic errors that were computed based on the magnitudes of peak kinematics measured by the GFT and Hybrid III, considering both resultants in measurements and component kinematics. The kinematic peaks for GFT were chosen within a window of 40ms or 80ms if simultaneous two 40ms files were available for an impact. For Hybrid III data, the peaks were chosen within a window period of

80ms. The kinematic peaks were chosen irrespective of the time and the Hybrid III and GFT kinematics were not time synchronized.

Different methods of error calculation were employed to treat the peak differences of resultant kinematics, component kinematics and the volumetric data differently. All error variables in this thesis are denoted by a prefix delta (Δ).

1. **Resultant Error:** Since resultant kinematics is always positive, it is treated as a scalar quantity in this error calculation. Error calculation for the resultant kinematics was done using simple mathematical subtraction GFT – Hybrid III. In a regression plot, this means that
    i. Error variable is positive (positive quadrant) if $VAR_{GFT} > VAR_{Hybrid\ III}$.
    ii. Error variable is negative (negative quadrant) if $VAR_{GFT} < VAR_{Hybrid\ III}$.

   Where VAR_{GFT} and $VAR_{Hybrid\ III}$ are GFT variable and Hybrid III variable respectively.

2. **Component error:** Peak component kinematics measured by the GFT and Hybrid III can be both positive and negative valued, and therefore it is an open question on how best to define errors. For completeness, two different types of errors were thus defined for the component kinematics based on the choice of the GFT peak.

   Component error type I: This error definition considers GFT component kinematic peak that has the highest absolute magnitude irrespective of the polarity of Hybrid III peak (**Figure** ***3.18***.a).

   Component error type II: This error definition considers the polarity of the Hybrid III in choosing the GFT peak. In **Figure 3.19.a** the GFT peak with the highest absolute magnitude is in the opposite direction of the Hybrid III peak. However, there is another GFT peak in the same direction as the Hybrid III peak. This error type was defined to ignore the negative peaks in GFT. **Figure** ***3.19.b*** shows another example of an impact's kinematics where the GFT peak in the direction of the Hybrid III peak is chosen. However, in this case the GFT peak with highest absolute magnitude is also the peak in the direction of the Hybrid III peak.

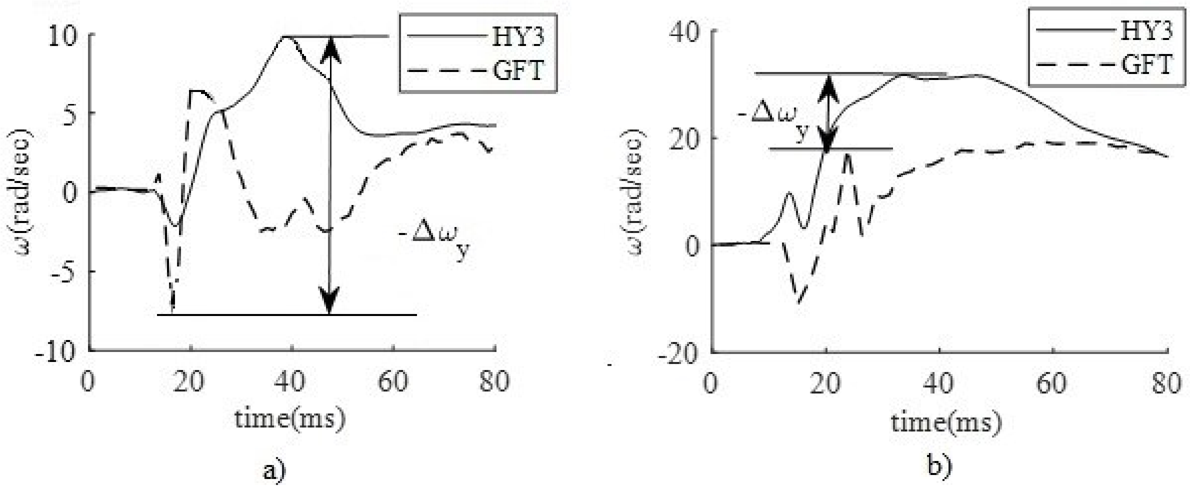

Figure 3.18: Examples of choice of peaks to calculate the error. In both a) and b) GFT peaks are chosen based on the magnitude irrespective of the polarity of the Hybrid III peak

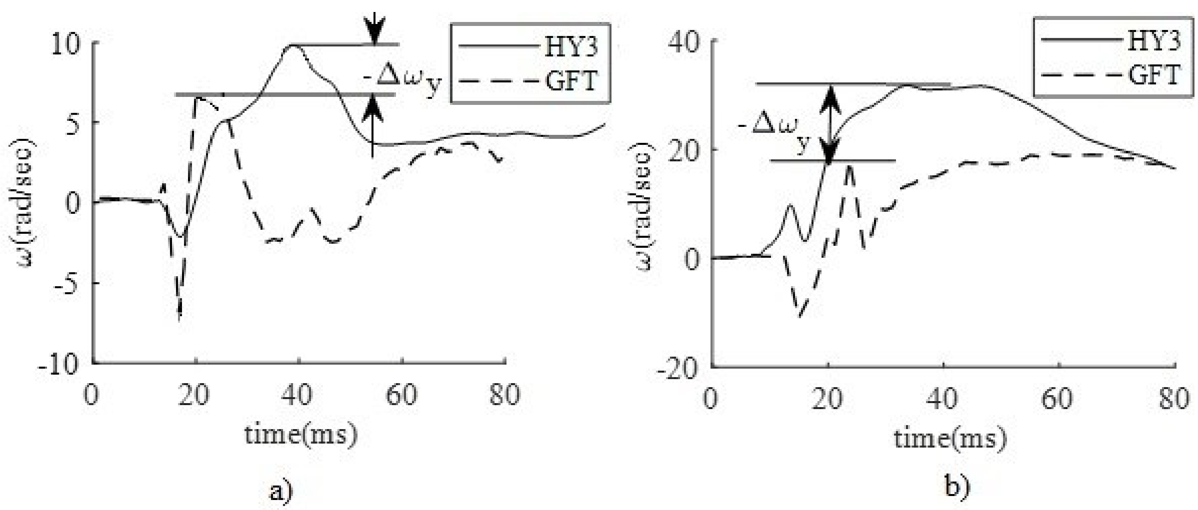

Figure 3.19: Examples of choice of peaks to calculate the error. In both a) and b) GFT peaks are chosen based on the polarity of the Hybrid III. The maximum GFT angular velocity in the direction of the Hybrid III peak is selected for error calculation

The component kinematics are not treated as scalar and the positive and negative directions of the kinematics are considered in error magnitude calculation. The error magnitude for the component kinematic vectors was obtained by mathematical subtraction of GFT and Hybrid III peak variables. The sign of the error variable was however assigned as per condition in **Figure *3.20***.

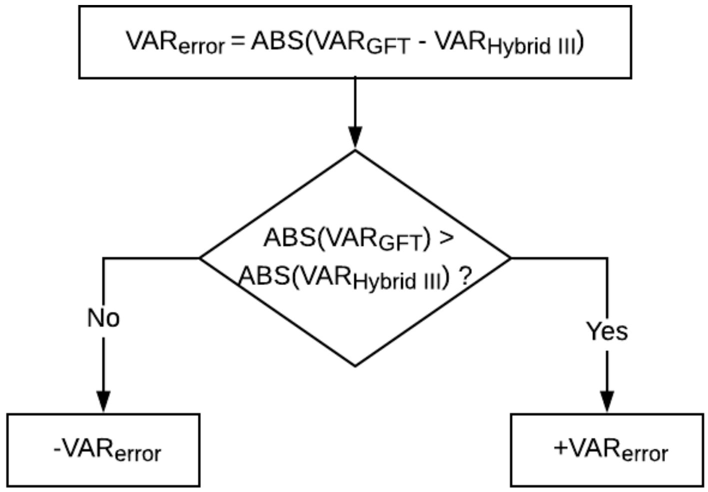

Figure 3.20: Condition for the error variable sign assignment

The error variable would take a positive sign if the absolute value of the GFT variable was greater than the corresponding absolute Hybrid III variable else the error variable is assigned a negative sign. This was done to ensure that the direction of the error variable is not driven by the polarity of the higher component kinematic peak but rather conveys which sensor kinematic data is higher (similar to resultant kinematic error variable). In both **Figure *3.18*** and **Figure *3.19*** the Hybrid III peak is greater than the GFT peaks and hence the error variable is assigned a negative sign.

3. **Strain error:** Strain error was calculated using simple mathematical calculation (MPS_{GFT} – $MPS_{Hybrid\ III}$) similar to resultant peak kinematic error calculation.

4. **Strain volume error:** Strain volume error is the volume of error in strain distribution predicted by GFT kinematics. To quantify the strain volume error between GFT and Hybrid III, elements were sorted by descending the strain magnitude, and the first 459 (1%) and 2294 (5%) elements and their corresponding volumes were extracted from each impact data. **Figure *3.21.a*** shows the top 5% of elements with the highest strain predicted by Hybrid III, GFT and both. The volumes A, B and C are calculated by summation of the volume of elements represented by ‘o’, ‘Δ’, ‘x’ in **Figure *3.21.a*** respectively. The error volume is calculated as a percentage of volume error predicted by GFT which is given by the equation 3.6.

$$\Delta Vol\% = \left(\frac{B-C}{B}\right) * 100 \tag{3.6}$$

Where ΔVol is the error volume percentage. B is the volume of elements with maximum strain(1% and 5%) predicted by GFT and C represents the volume of elements among B that are predicted in agreement with Hybrid III respectively as explained in the **Figure *3.21***.

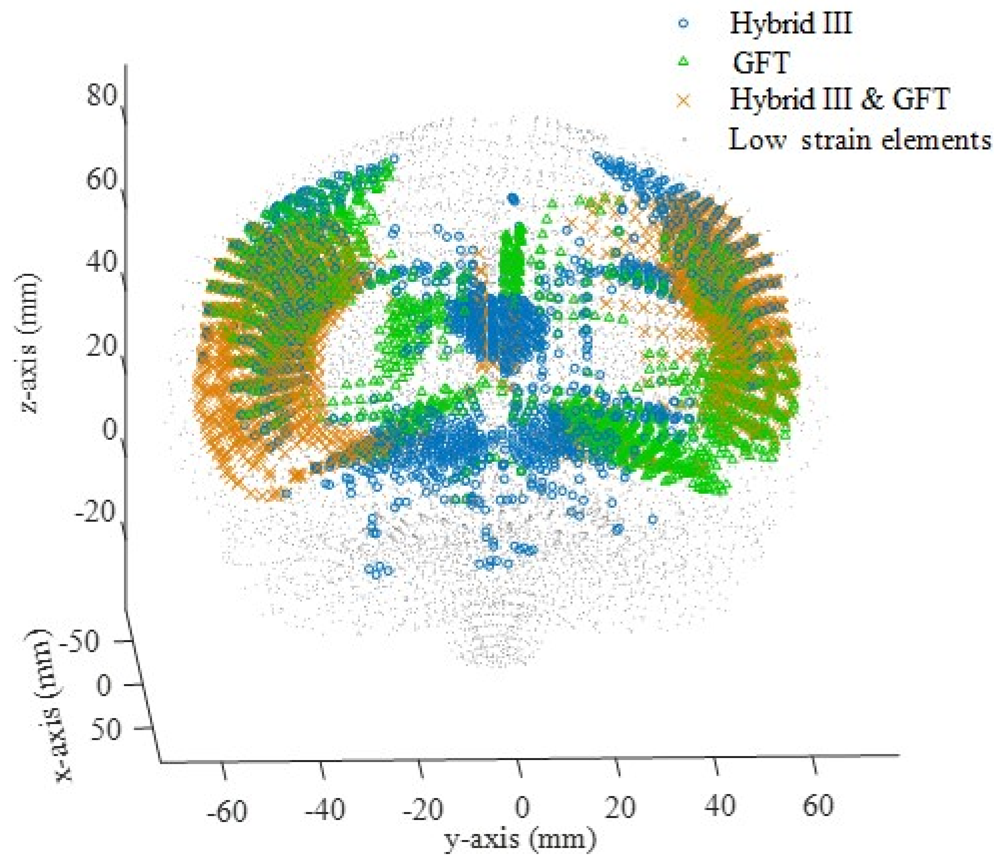

a)

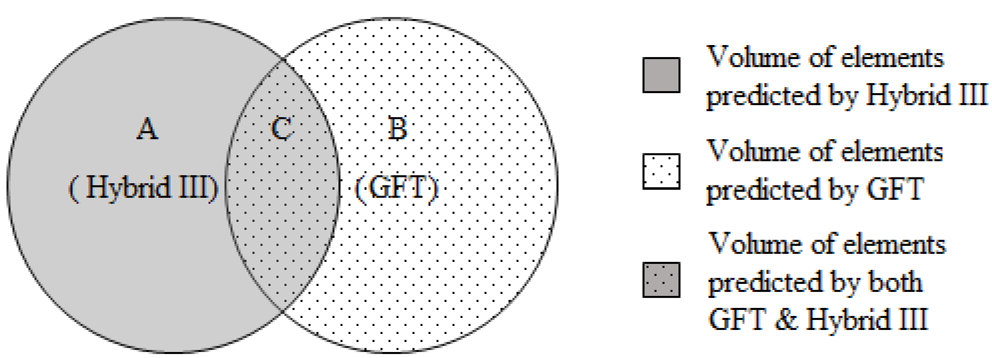

b)

Figure 3.21: Strain distribution error where a) 3D brain plot displaying 5% elements with highest strain predicted by Hybrid III, GFT and both and b)Venn diagram to explain the error strain volume equation 3.6

3.3.3 **Regression analysis**

All the error variables were compared using simple linear regression analysis to determine the R^2 between the input and output errors. To determine the input kinematic error that best predicts the output brain strain error, the MPS error was regressed on all the kinematic error variables. In addition to regression analysis including all impacts in a single dataset, the process was repeated for impact subsets based on kinematic directions categorized as follows.

i. Category X – Impacts with maximum rotational head motion about the x-axis.
ii. Category Y– Impacts with maximum rotational head motion about the y-axis.
iii. Category Z – Impacts with maximum rotational head motion about the z-axis.

The regression analysis based on kinematic directions were to determine the effect of the directional kinematic error on brain strain. The R^2 of all the regressions were compared to determine the predictor that is most explanatory of the MPS errors with wearable sensor kinematics.

As discussed in the earlier section, for error definition with peak kinematics, it was ensured in error calculation that both the resultant and component error variables convey the same message where the positive error variable denotes higher VAR_{GFT} magnitude and negative error variable denotes a higher $VAR_{Hybrid\ III}$ magnitude. This method allowed decomposition of scatter plot into four quadrants, each conveying a different association as shown in **Figure *3.22***.

For the volumetric analysis where GFT volume error was calculated as a percentage, the data was scalar and hence comparing it against the error variables with direction will not provide a meaningful regression. Hence for the volumetric analysis, absolute error variables ($|\Delta MPS|$ or $|\Delta K|$) was used against the volumetric error for the regression comparison and the scatter plot is not decomposed into quadrants.

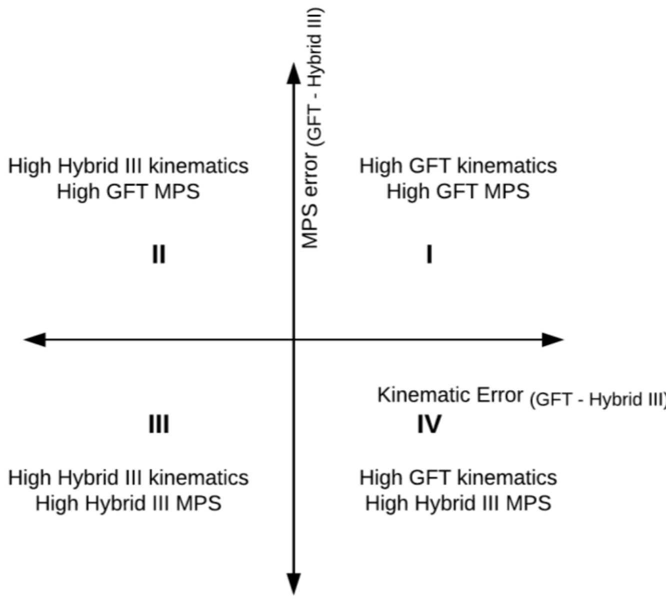

Figure 3.22: Interpretation of quadrant formed by the scatter plot of independent kinematic error variables against dependent brain strain error variable

The confidence intervals for one standard deviation of the R^2 variables were calculated using the equation 3.7 [89] The confidence intervals and the standard error (Equation 3.8) were calculated to construct the error bars for the regression analysis.

$$CI = R^2 \pm SE \tag{3.7}$$

$$\mathrm{SE} = \sqrt{\frac{4R^2(1-R^2)^2(n-k-1)^2}{(n^2-1)(n+3)}} \tag{3.8}$$

Where CI is the confidence interval, SE is the standard error, n is the sample size and k is the number of independent variables in the regression analysis. Statistical significance for R^2 was not inferred in this thesis. SE was used to convey only the standard deviation in R^2 and not as a basis to determine statistical significance for R^2.

4. Results

Because this chapter documents a large number of findings, the below list attempts to help the reader by offering a concise summary of key results. The results from the limited laboratory study and post hoc simulation and statistical analysis suggest:

1. Variations in 95%ile, 99%ile, 99.9%ile and 100%ile strain can explain the variation of one another.

2. Linear and rotational transformation of GFT kinematics to head COG did not result in an appreciable change in strains when compared to the strains predicted from kinematics that were rotationally transformed.

3. Angular velocity errors are most explanatory of strain errors.

4. Error in both the direction and magnitude of kinematics create strain errors.

5. When errors in strain are relatively small in magnitude, the percentage volume of the error in strain distribution, can be large.

An overview of the parameters compared in each section and results, the key findings and how the results from the section contribute to the thesis findings is provided in **Figure *4.1***. To aid the reader, **Figure *4.1*** conveys the key logical relationships between results, in hopes that the order of results presentation is clarified.

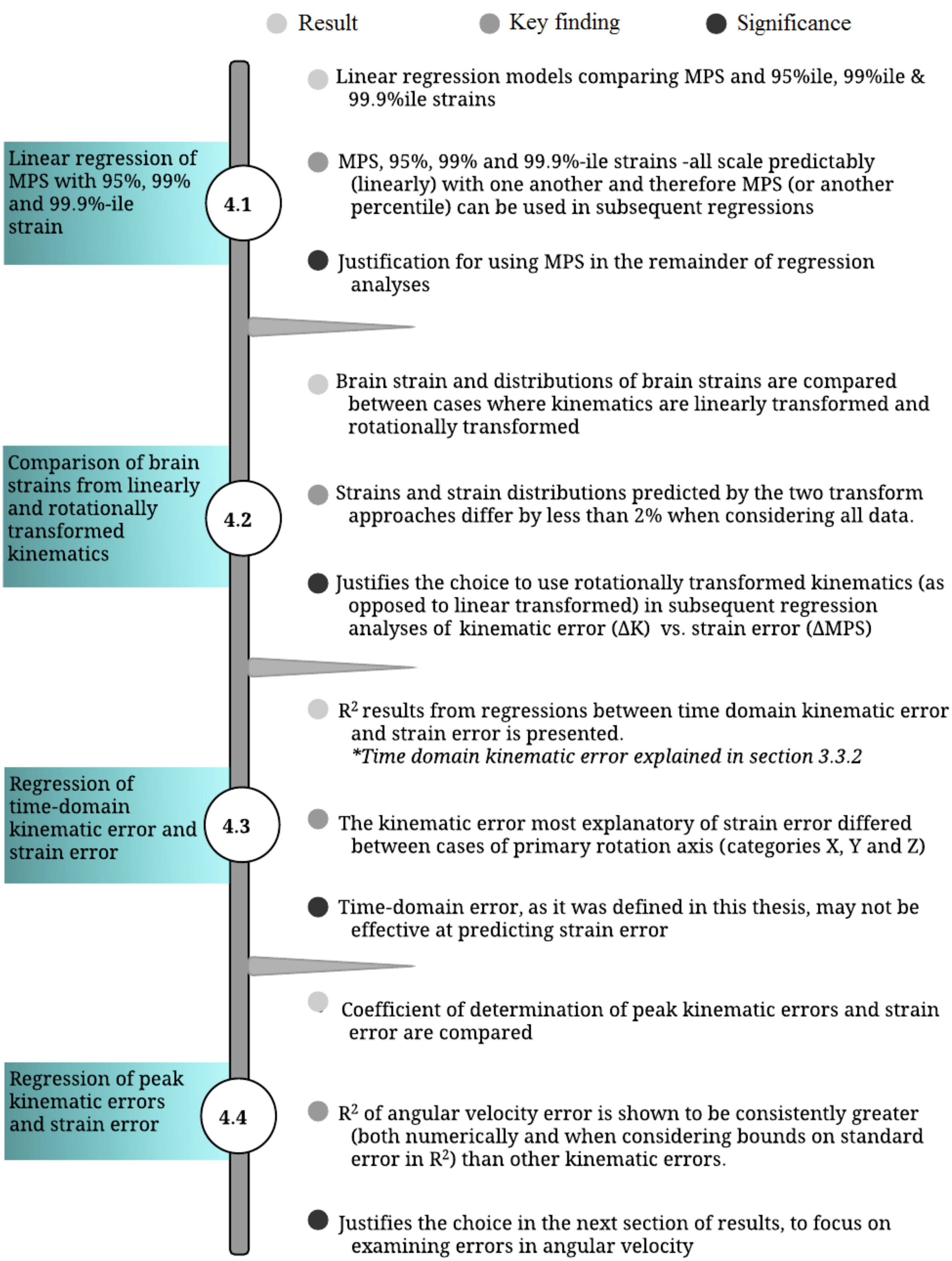
Result
Key finding
Significance
Linear regression of MPS with 95%, 99% and 99.9%-ile strain
4.1
Linear regression models comparing MPS and 95%ile, 99%ile & 99.9%ile strains
MPS, 95%, 99% and 99.9%-ile strains -all scale predictably (linearly) with one another and therefore MPS (or another percentile) can be used in subsequent regressions
Justification for using MPS in the remainder of regression analyses
Comparison of brain strains from linearly and rotationally transformed kinematics
4.2
Brain strain and distributions of brain strains are compared between cases where kinematics are linearly transformed and rotationally transformed
Strains and strain distributions predicted by the two transform approaches differ by less than 2% when considering all data.
Justifies the choice to use rotationally transformed kinematics (as opposed to linear transformed) in subsequent regression analyses of kinematic error (ΔK) vs. strain error (ΔMPS)
Regression of time-domain kinematic error and strain error
4.3
R2 results from regressions between time domain kinematic error and strain error is presented.
*Time domain kinematic error explained in section 3.3.2
The kinematic error most explanatory of strain error differed between cases of primary rotation axis (categories X, Y and Z)
Time-domain error, as it was defined in this thesis, may not be effective at predicting strain error
Regression of peak kinematic errors and strain error
4.4
Coefficient of determination of peak kinematic errors and strain error are compared
R2 of angular velocity error is shown to be consistently greater (both numerically and when considering bounds on standard error in R2) than other kinematic errors.
Justifies the choice in the next section of results, to focus on examining errors in angular velocity

a)

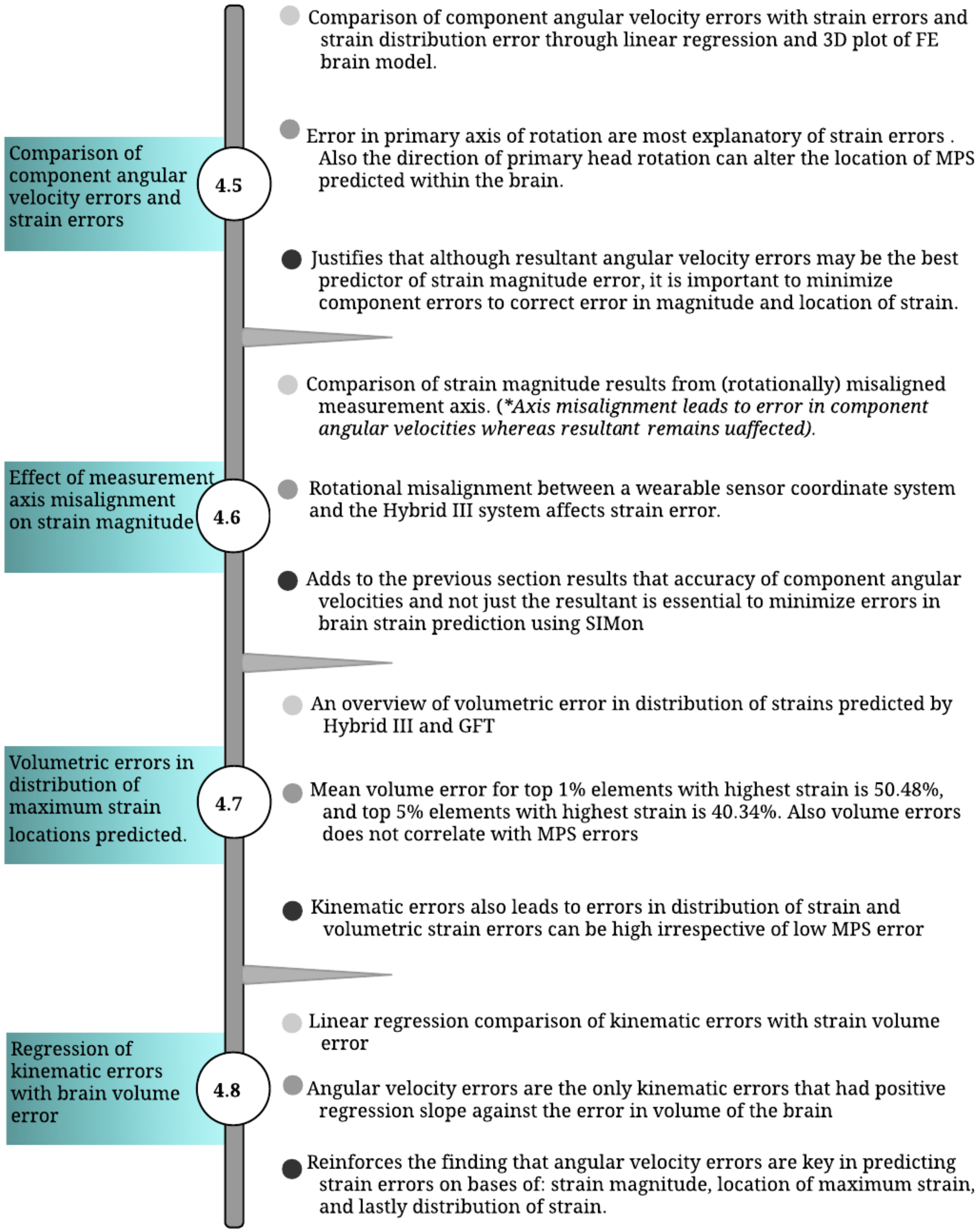

b)

Figure 4.1: Overview of each section in the results chapter. a) Contain sections 4.1 to 4.4 and b) contain sections 4.5 to 4.8

4.1 Linear regression of MPS with 95%ile, 99%ile and 99.9%ile strain

As implied by the three scatter plots of 95%ile, 99%ile and 99.9%ile strain with MPS (**Figure *4.2***), at least 96% of the variation in MPS can be explained by the three percentiles plotted. The 95%ile, 99%ile and 99.9%ile regression comparison against the 100^{th} percentile MPS result in $R^2 > 0.96$. ***Figure 4.2*** shows the plots comparing the percentile strain magnitudes of all 276 impact data used for regression analysis. Strain is a quantity that has units of length change per unit reference length, therefore it can be written absent a unit system, as it is in this thesis. The regression comparison of percentile strains suggests that using different percentiles may not alter the outcome of a regression analysis. Hence, the regression analysis comparing input kinematic errors with strain errors in this thesis was performed using only MPS.

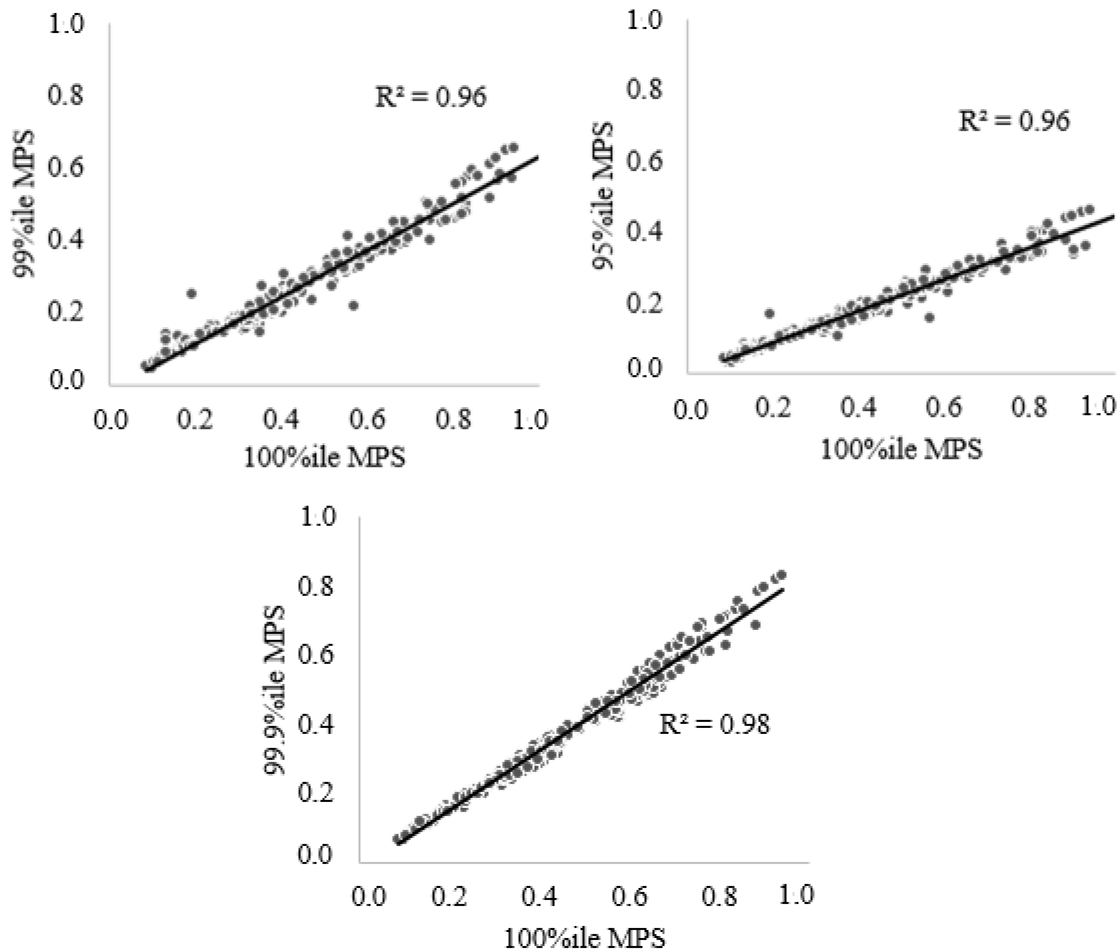

Figure 4.2: MPS plotted against 95%ile, 99%ile, and 99.9%ile strain

The choice of the percentile strain used can further be explored by looking into the histograms of the strain distribution in the FE brain model. The element level strain data obtained from both the Hybrid III and the GFT data show a similar distribution with a bimodal trend (***Figure 4.3***). The first peak of the bimodal curve is near zero indicating the maximum density of elements having strains closer to zero and the second curve is right-skewed.

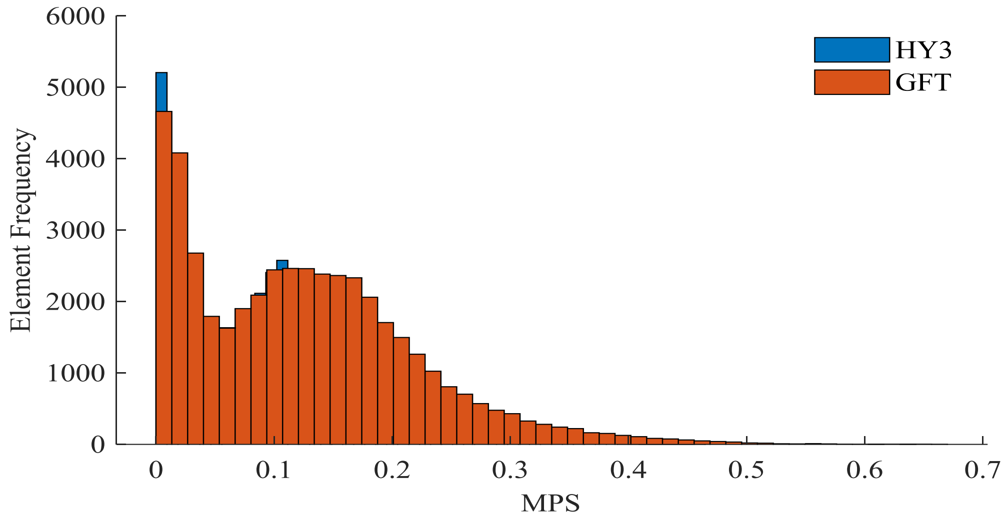

Figure 4.3: An example MPS histogram plot with strain distribution calculated from Hybrid III and GFT kinematics for the same impact

Magnitude comparison of percentile strain data of all the impacts collected in this experiment shows that the 95th percentile strain was less than half of the MPS. After 95th percentile, there was an exponential increase in strain difference between each percentile strain values as in **Figure *4.4*** due to the right-skewed distribution. The amplified value of the MPS compared to 95th percentile strain can be explained as an outcome of the right skewness.

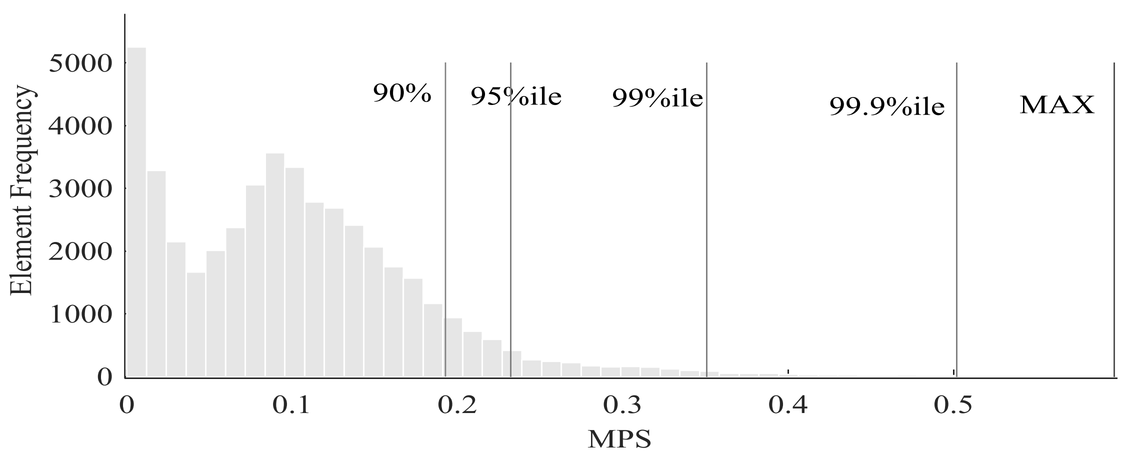

Figure 4.4: An example MPS histogram plot with percentile distribution

The scaling of the MPS with other percentile strains (**Figure** ***4.2***) also suggests that all the impacts in the experiment follow similar strain distribution. Thus, the choice of MPS in this thesis for regression analysis will not affect the outcome of the analysis.

4.2 Comparison of brain strains from fully and partially transformed kinematics

MPS predicted by fully transformed kinematics differed by less than 1% from MPS predicted from partially transformed kinematics, when considering all data in this thesis (**Figure** ***4.5***). GFT strain data from kinematics that were fully transformed to Hybrid III head COG compared with strains from partially transformed GFT kinematics is shown in ***Figure 4.5***. The scatter plot exhibits that the strains from fully transformed and partially transformed data can explain the variation of one another ($R^2 > 0.99$) which implies that linear transformation does not affect the MPS magnitude.

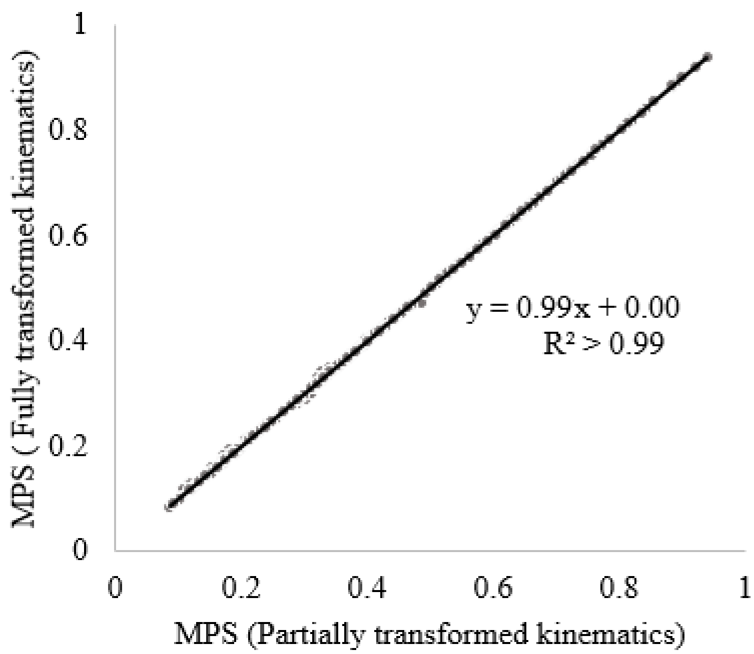

Figure 4.5: MPS (100th percentile strain) obtained from GFT kinematics that was fully transformed to head COG vs MPS from GFT kinematics that were not linearly transformed to head COG

The volume of the brain elements considered to be in error, between cases where kinematics were linearly and rotationally transformed, differ by only 2% (from the equation on the slope in **Figure** ***4.6***). Error in strain distribution observed with linearly transformed GFT data and rotationally transformed GFT data is compared in **Figure** ***4.6***. The volume of elements with strain distribution error from the fully transformed and the partially transformed data are similar except, full transformation improves the volume strain error by ~2%. Also, the minimal residual errors in the regression comparison support the conclusion that rotational transformation is sufficed in brain strain calculations. Hence the regression analysis between kinematic errors and strain errors in this thesis will focus on the partially transformed GFT kinematics.

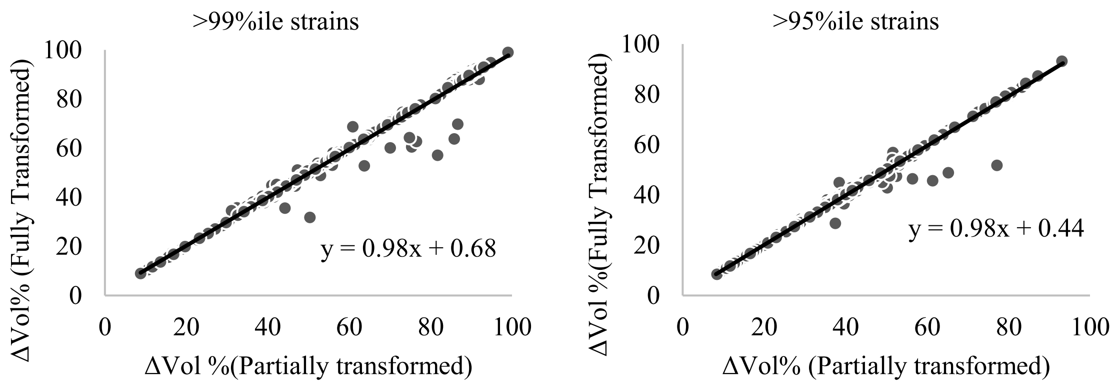

Figure 4.6: Comparison of errors in maximum strain volumes predicted by GFT fully transformed and partially transformed data. The error in the volume of a) top 1% elements with maximum strains predicted and b) top 5% elements with maximum strains predicted are compared

4.3 Regression of time domain kinematic error and strain error

Coefficients of determination for kinematic errors regressed against strain errors indicated that the best kinematic error predictor varied based upon the primary axis about which the head rotated (**Figure *4.7***). The coefficients of determination obtained from regression analysis of all the impacts' maximum time domain kinematic errors and MPS errors was less than 0.3 (**Figure *4.7***). No single kinematic error was consistently the better predictor of strain error across the different categories. A single kinematic error could not be found as the obvious best predictor of strain error in this method which suggests that the maximum kinematic error in time series may not be the best error definition towards predicting the strain error.

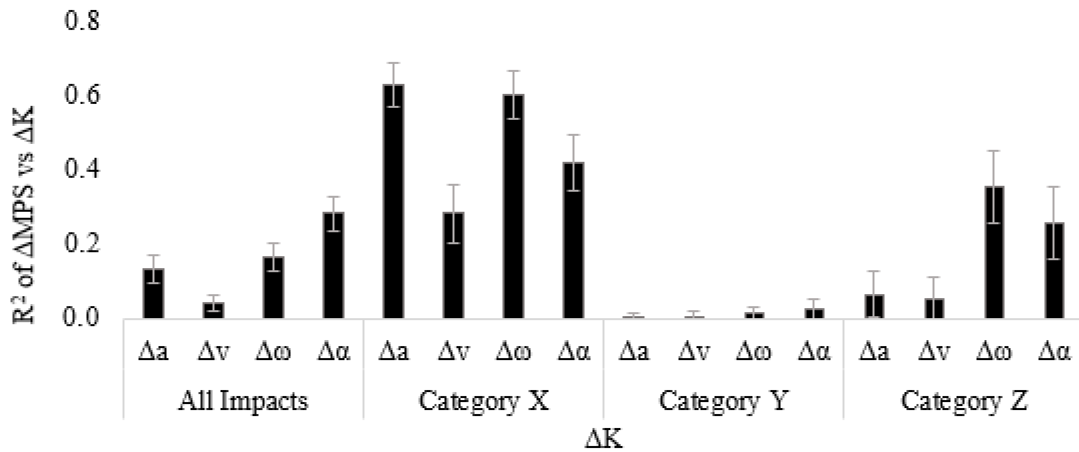

Figure 4.7: R^2 of ΔMPS vs time domain kinematic resultant error under different categories

4.4 Regression of peak kinematic errors and strain errors

Regression analysis results comparing all the resultant kinematics errors with the corresponding MPS errors show resultant angular velocity errors having higher R^2 with MPS errors (**Figure *4.8***). R^2 for angular velocity error (Δω) vs. MPS error (ΔMPS) is greatest for the entire dataset as well as in each category, outside the bounds of one standard error. The regression results suggest that the peak resultant angular velocity errors could predict the strain errors best compared to other kinematics errors. The Δα has the second high R^2 following Δω except for the impacts in category X. However, the confidence interval (for one standard deviation) of R^2 for Δω vs ΔMPS does not overlap with R^2 from other kinematic errors which suggest that angular velocity errors are best explanatory of the strain errors.

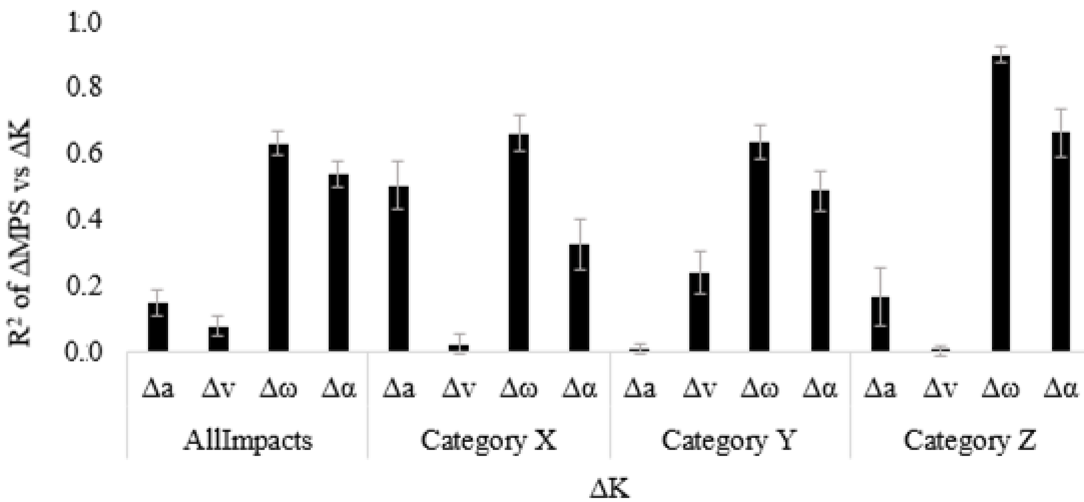

Figure 4.8: R^2 of ΔMPS vs peak resultant kinematic error under different categories

The coefficient of determination of Δa in category X differs largely compared to results from other categories where Δa has a low R^2 (<0.2). This behavior is explained by inspecting the kinematics specific to Category X for both Hybrid III and GFT. The resultant peak linear acceleration exhibits high R^2 with MPS under conditions when linear acceleration regressed against angular velocity have high R^2. In categories where the variation in linear acceleration did not explain the variation in angular velocity, linear acceleration and linear acceleration error had poor R^2 in regressions against strain and strain error respectively. This trend can be observed in ***Table 4.1***.

Table 4.1 : Results of regression comparison showing high R^2 of linear acceleration with MPS is driven by its relationship with angular velocity

	Hybrid III		**GFT**		**Error (GFT – Hybrid III)**	
Regression variables	a_R vs ω_R	a_R vs MPS	a_R vs ω_R	a_R vs MPS	Δa_R vs $\Delta\omega_R$	Δa_R vs ΔMPS
All Impacts	0.28	0.21	0.56	0.68	0.04	0.15
Category X	0.80	0.73	0.77	0.80	0.30	0.50
Category Y	0.14	0.27	0.22	0.47	0.08	0.01
Category Z	0.15	0.15	0.85	0.83	0.15	0.17

The strains from purely linear acceleration kinematics simulated on SIMon showed that linear accelerations with magnitudes as high as 249 g did not have an appreciable effect on strain compared to the effect of angular velocity (**Figure** ***4.9***). SIMon simulations using only angular velocity kinematics were able to generate MPS magnitudes equal to the MPS generated using both linear and angular kinematics.

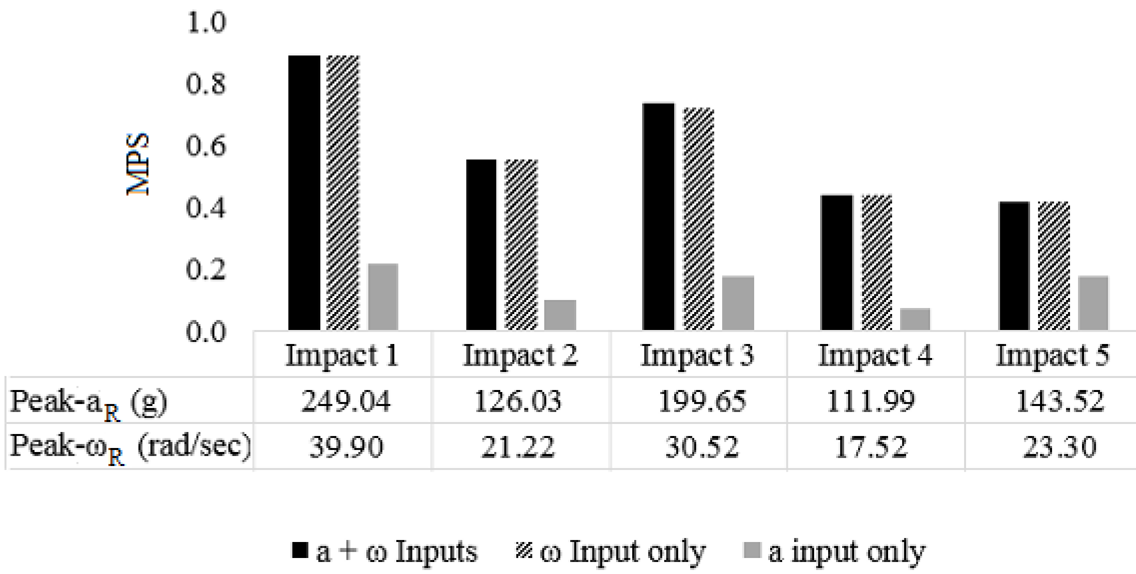

Figure 4.9: Comparison of MPS magnitude calculated with GFT linear acceleration (a input only) and angular velocity (ω input only) separately, with MPS magnitude obtained by using both kinematics (a + ω input)

The linear acceleration ranges tested in the sub-study were chosen to determine the strain response of the highest possible linear acceleration. The impacts with 199g and 249g are exaggerated by the GFT (corresponding Hybrid III measurements are 143g and 64g respectively), and such magnitudes may not occur in real game impacts.

4.5 Comparison of component angular velocity errors and strain error

Since the resultant angular velocity errors resulted in highest R^2 with strain errors, the angular velocity errors were focused for further component kinematic error analysis. The R^2 of ΔMPS regressed with each angular velocity component kinematic errors (from both error type I and error type II) are compared in **Figure** ***4.10***. Error in the primary axes of rotation had higher R^2 with MPS errors compared to the other two axes, indicating that MPS error is influenced by directional errors. For example, for impacts with primary axis of rotation about the z-axis, the z-axis errors were most explanatory of MPS errors compared to other two axis (excluding resultant), outside the bounds of one standard error. Since resultant is a vector sum of component kinematics, the resultant error consistently explained the strain errors best. However, it is also necessary to identify which angular velocity error (resultant or component) influences the strain error most and if it is sufficient to address only the resultant angular velocity error to minimize the strain errors.

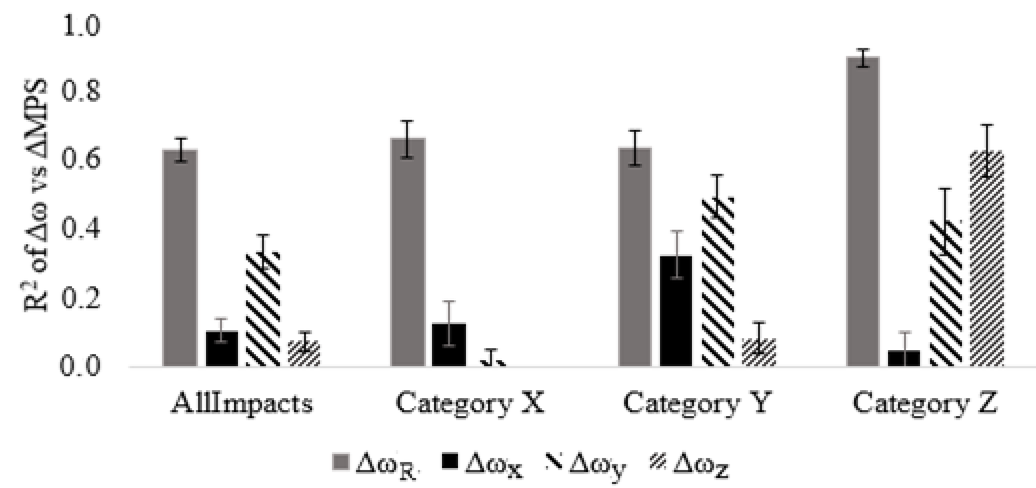

a)

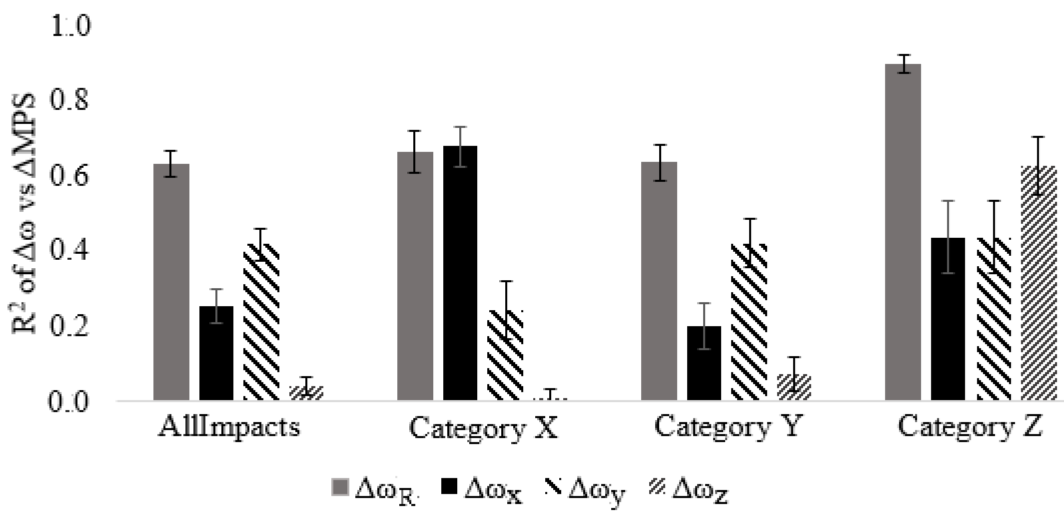

b)

Figure 4.10: Regression results between MPS errors and component angular velocity errors from a) component error type I and b) component error type II

The effect of resultant and component angular velocities on strain distribution is compared by using data of 3 impacts with approximately same resultant magnitude (~33.4 rad/sec) but with the maximum peak value in different axes components as given in ***Table 4.2***. The impacts chosen correspond to a crown impact (CR) with primary rotation about the y-axis, facemask impact (FM) with high ω_z and left impact (LE) with high ω_x. In addition to exhibiting different maximum principal strains, the difference in the distribution of strains could also be noted between these impacts as shown in ***Figure 4.11***. In the localized strain distribution (> 95%ile strain) of these impacts (***Figure 4.11.a***) , the strains due to the facemask impact could be seen extending to cerebellum whereas the crown impact with same resultant angular velocity creates major strains in the cerebrum. Though the left impact and facemask impact appear to create similar strain distribution, a closer view on the location of the maximum strain (100%ile strain) reveals that the left impact (with high ω_x) comparatively creates strain in a deeper part of the cerebrum (**Figure *4.11.b***).

Table 4.2: Example impact data that was chosen to compare the effect of resultant and component angular velocities on the strain

Impacts	Peak ω_R (rad/sec)	Peak ω_x (rad/sec)	Peak ω_y (rad/sec)	Peak ω_z (rad/sec)	MPS
CR	33.38	7.12	32.22	-7.40	0.51
FM	33.38	-9.87	5.72	-31.93	0.73
LE	33.36	30.26	12.92	-21.89	0.44

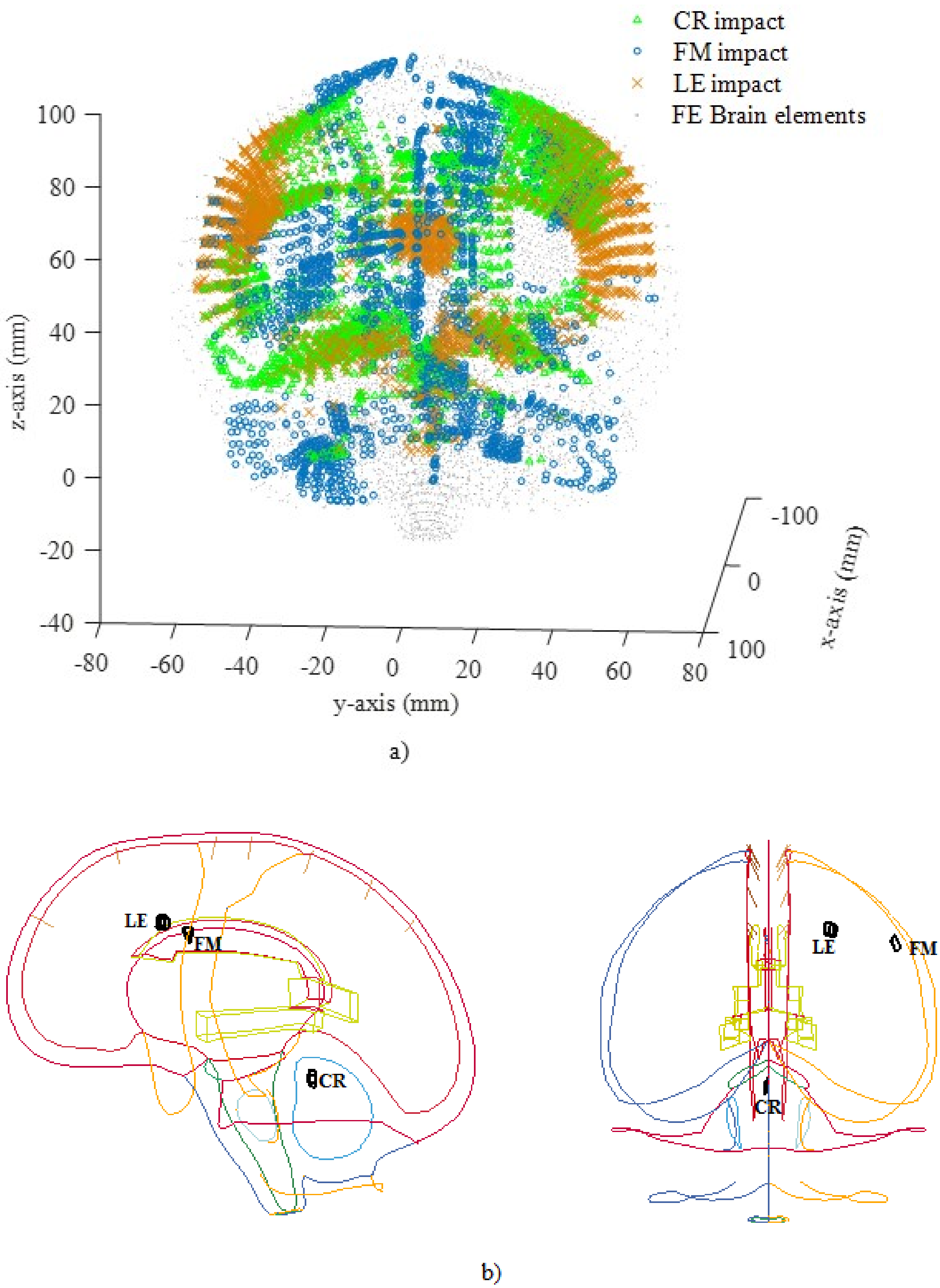

Figure 4.11: Strain distribution corresponding to a) >95%ile strain and b) MPS in the crown impact (CR), facemask impact (FM) and left impact (LE) from Table 4.2

Despite similar resultant angular velocity, the high difference in the distribution of the strains when the magnitude of the directional angular velocities change convey that between resultant and component angular velocities, the latter might have higher influence over the strain and the strain errors.

4.6 Effect of measurement axis misalignment on strain magnitude

Misalignment in axes between the GFT and Hybrid III head will lead to errors in component kinematic measures that will in turn lead to strain errors. When analyzed separately, each axis in the SIMon brain model subjected to the same angular velocity (sub-study method I) resulted in different MPS values as given in **Figure *4.12***. For example, a 40 rad/sec angular velocity, applied about the x-axis generated a strain of magnitude 0.53 whereas the same angular velocity about the z-axis produced a maximum strain of 0.76. A similar trend was observed for different magnitudes of input angular velocity where the x-axis exhibited the least sensitivity and the z-axis exhibited the highest sensitivity to strain. This suggests that directional velocity has an influence over strain magnitudes and measuring only resultant error may neglect the underlying directional velocity errors, which could eventually lead to error in strain prediction using the impact kinematics.

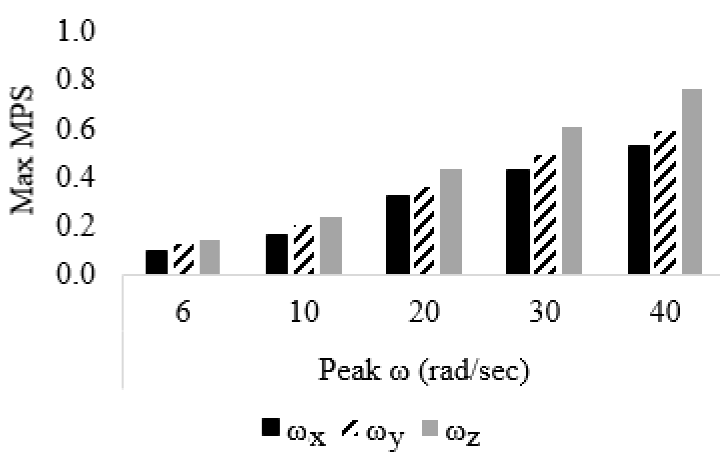

Figure 4.12: MPS results of angular velocity inputs in different axis directions

Sub-study Method II (determining the MPS errors due to angular misalignment) demonstrated that up to 15% error occurred in calculated strains in the presence of angular misalignments of 30˚ (about y-axis). MPS errors due to simulated angular misalignment about each axis from 30˚ to 180˚ are given in **Figure *4.13***. From these results, it is evident that a rotational error about an axis could alter the strain calculated from the wearable sensor kinematics. The output strain errors corresponding to rotational error about each axis is explored using **Figure** ***4.14***.

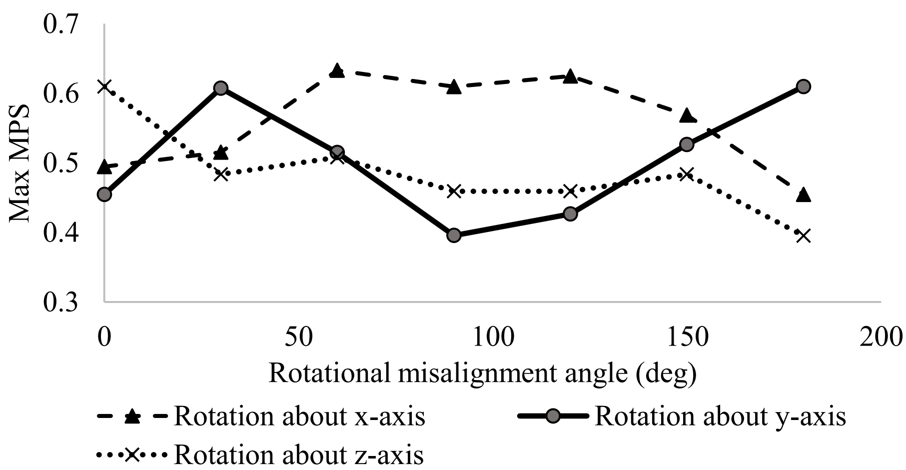

Figure 4.13: Change in MPS observed with simulated rotation error about each individual axis

Errors in MPS due to rotation about each axis were examined by comparing the MPS with input data at each rotation step. The rotational errors redistributed the component angular velocity magnitudes, altering the corresponding MPS value. As the y-axis and z-axis input magnitudes increased due to the rotation, there was an increase in the strain value. When the input values in these axes decreased, an eventual decrease in the MPS occurred. The positive and negative direction of the angular velocity magnitude also affected the resulting MPS differently which could be observed in the 0˚ and 180˚ data points of **Figure** ***4.14***. At these data points only one component axis has a non-zero angular velocity in each plot with the same magnitude, but the direction reversed between 0˚ and 180˚. The resulting strains were however different despite the identical input angular velocity magnitude at the same axis. MPS error of up to 20% was noticed in this test method, though the resultant angular velocity was constant for the entire dataset used. Comparing the results from **Figure** ***4.12*** and **Figure** ***4.14***, it can be stated that rotational data about z-axis has the highest sensitivity followed by y-axis rotational data. The rotation about the z-axis created higher strains and rotational error altering the data corresponding to the z-axis displayed high strain errors.

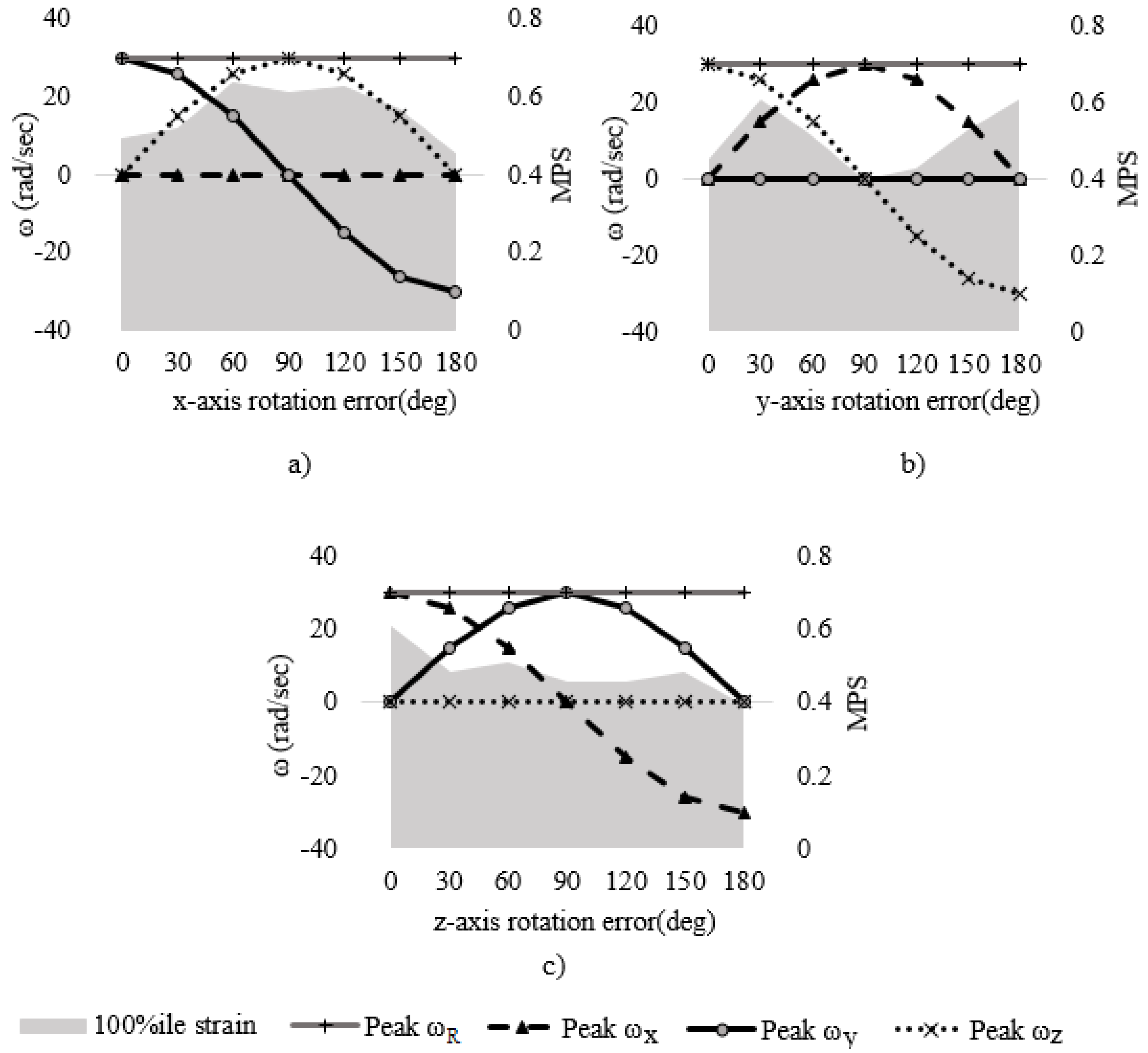

Figure 4.14: Plots comparing the change in component angular velocity magnitude and the corresponding change in strain due to rotational error about a) x-axis, b) y-axis and c) z-axis

Experimental data was used to determine how errors in all the 3 axes create strain errors. ***Figure 4.15*** compares the R^2 results of GFT angular velocity vs. corresponding MPS with average component velocities under each category. R^2 was highest between MPS and whichever axes had the highest average angular velocity in each category. In category X and category Y, though the ω_y average was greater than ω_z average, the z-axis component had high R^2 with MPS. This can be explained due to the higher sensitivity of z-axis data to MPS as determined in an earlier paragraph. When x-axis average velocity was significantly higher than z-axis (category X), ω_x gave a better coefficient of determination. Under other condition (category

Y), ω_z resulted in higher R^2 with MPS than ω_y. This suggests that MPS is determined by the magnitude of component angular velocities combined with the strain sensitivity of each axis.

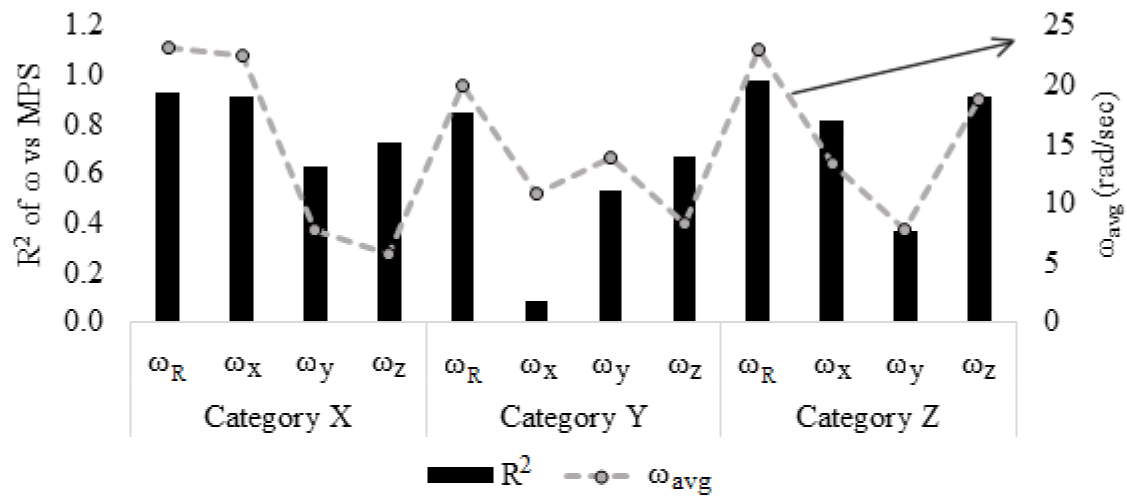

Figure 4.15: Regression results of GFT peak angular velocities and corresponding MPS along with the average of the peak angular velocities in each regression

The results in this section show that MPS is an outcome of directional kinematics and therefore sensitive to errors in directional kinematics. From these findings, it can be understood that the alignment of the wearable sensor kinematic direction to that of the reference sensor axis is crucial in brain strain prediction using these sensor measurements. Also, attention towards axes kinematics, as opposed to absolute resultant kinematics, will benefit in achieving brain strain prediction with limited errors.

4.7 Volumetric errors in the distribution of maximum strain locations predicted

Nearly half of the impacts exhibit more than 50.48% volume error in the top 1% strains predicted, and there are 23 impacts with more than 90% volume error in the same category. For strains greater than 95%ile (top 5%) the mean volume error is 40.34%. Error in the distribution of strain also result in the wrong part of the brain being predicted to have a maximum strain. An example of the case where a different part of the brain was predicted by Hybrid III and GFT is given in **Figure *4.16***. In this example, most elements with maximum strain predicted by Hybrid III is seen in cerebrum whereas GFT predicts most of the elements in the brain stem. In an ideal condition where GFT predicts the strain distribution exactly the same as Hybrid III, the **Figure *4.16*** will not have the blue and the red data points and all the elements with maximum strain (top 5%) will be in green.

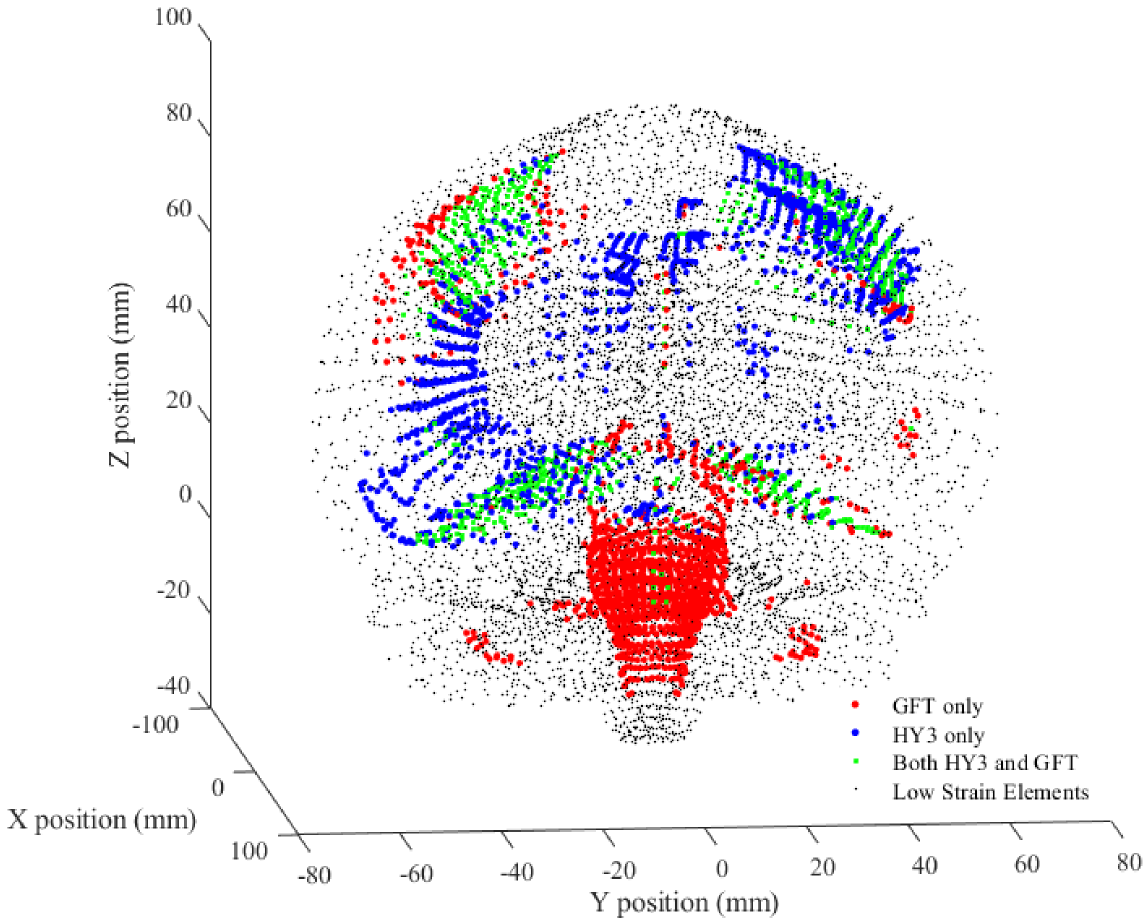

Figure 4.16: An example plot showing the location of top 5% brain strains predicted by Hybrid III and rotationally transformed GFT for the same impact

Impacts with strain errors less than 0.1 (10%) still had error in maximum strain volume predicted, where the error percentage was noticed up to 93% (top 5%) and 99% (top 1%). Comparison of strain error vs. error volume in the top 5% and top 1% elements with maximum strain (**Figure *4.17***) found no relationship between strain errors and corresponding volume errors. A considerable number of samples with low MPS errors had volume error greater than 80%.

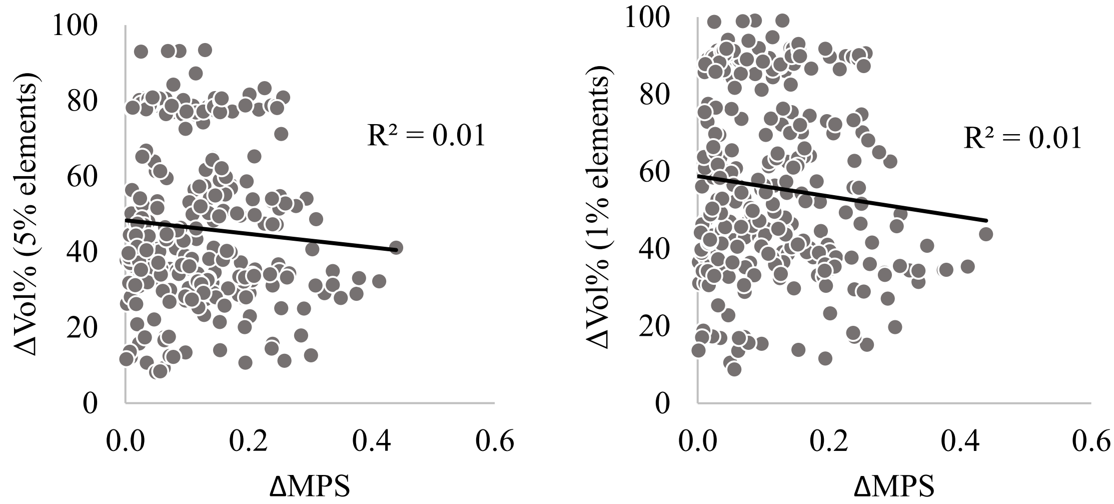

Figure 4.17 Scatter plots comparing ΔMPS with volume error in a) top 5% elements with maximum strain and b) top 1% elements with maximum strain

4.8 Regression of kinematic errors with brain volume error

Regression of kinematic errors against volume error in brain elements suggest that angular velocity errors were the only errors exhibiting positive slope. In regression plots to explore how the volume of error in strain distribution compare with errors in kinematic inputs, a positive R^2 relationship was noticed only with angular velocity errors ($R^2 = 0.42$). In addition to the negative regression relationship of linear acceleration, linear velocity and angular acceleration against volumetric strain errors, the goodness of fit corresponding to these regression analyses was also low (***Figure 4.18***). This further strengthens the earlier findings that the linear kinematics or angular acceleration has less effect on strain errors compared to angular velocity. The regression analysis suggests that the distribution of strain errors may also be related to resultant angular velocity errors. However, the residual errors are compelling which suggests the possibility of factors other than the resultant angular velocity that might influence the distribution of strain. An explanation for the residual errors may be component velocity errors as discussed in the Section 4.5.

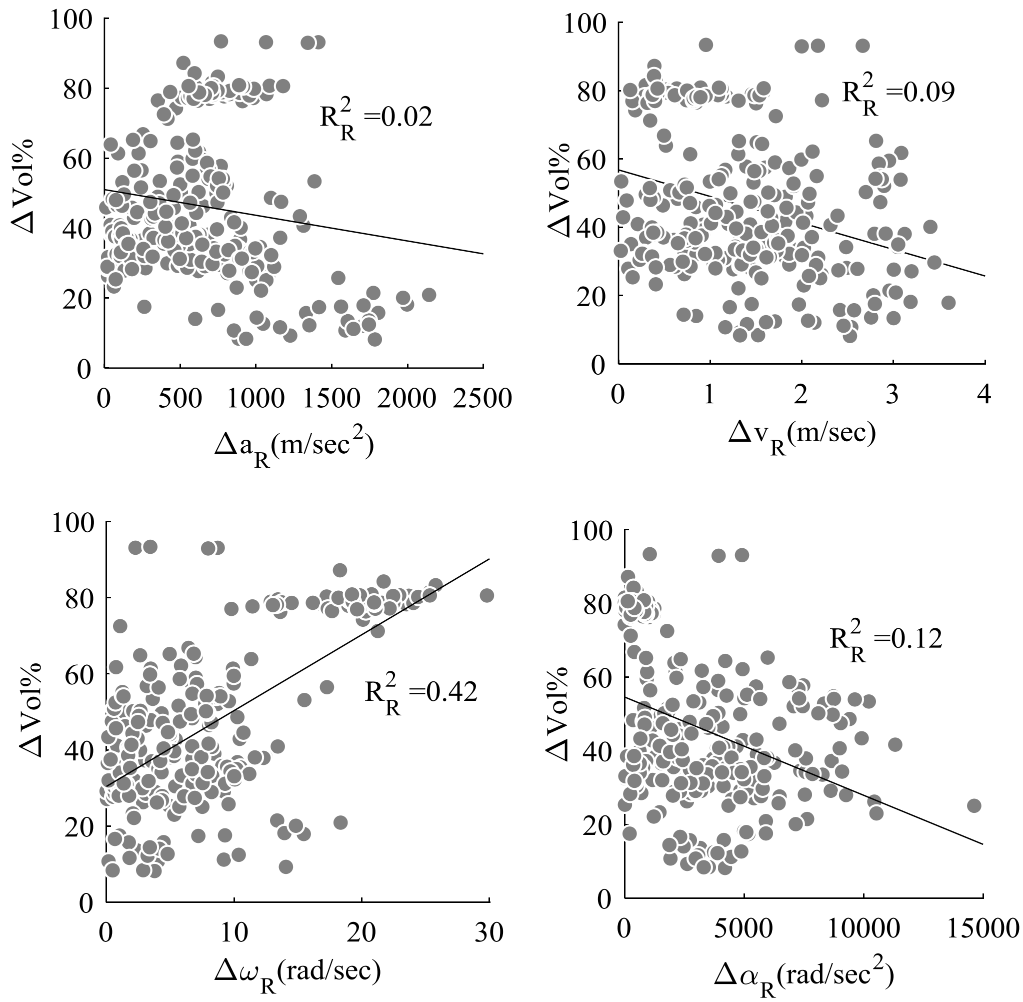

Figure 4.18: Scatter plots comparing input kinematic error with corresponding strain volume error

5. Discussion

The goal of this thesis was to identify the input error sources in wearable sensors that influence errors in FE strain calculation, including element level strain errors. Football helmet impacts were simulated in the laboratory using the Hybrid III head and the GFT wearable sensor. The impact kinematics from both the sensors were collected and used in brain strain simulations. Regression analysis was performed using data collected from both Hybrid III and GFT sensor. The results obtained in this thesis convey,

- The MPS percentile values scale with each other and hence the choice of a specific percentile will not affect the outcome of a simple regression analysis.
- A full transformation of wearable sensor kinematics does not alter the strain magnitude compared to partially transformed kinematics.
- Limiting angular velocity errors in wearable sensor measurement could ultimately reduce brain strain errors.
- Strain magnitudes from FE brain models are sensitive to direction of the head rotation and the axis about which the rotation is greatest.
- High strain distribution errors can still occur in impacts with low MPS error.

The multiple results from the thesis aim to encompass the possible input and output errors in brain strain prediction using a wearable sensor. The initial finding from the regression analysis suggests that resultant angular velocity errors explained the strain errors the best. Further analysis examining the directional sensitivity of SIMon demonstrated the possibility of high strain errors even in the absence of resultant angular velocity error which in turn imply that component angular velocity error has greater influence on strain error. A much-detailed study of brain strain by looking into element level strains showed that low MPS strain errors can still have an error in the distribution of maximum brain strain predicted. Error possibilities at multiple stages of brain strain calculation using FE models are discussed in this thesis along with the research gaps in brain strain prediction with impact kinematics.

5.1 Strain percentiles and their ability to predict MPS

MPS was used in all regression analysis against kinematic errors in this thesis after confirming that MPS scaled with other percentile strains. The FE distribution of strain elements in blunt impacts with football helmet displayed a bimodal trend with a right-skewed curve for all impacts conducted in this thesis. The strain values for 95th, 99th, and 99.9th percentiles scaled proportionally with the MPS and using either of these strain magnitudes will not affect the outcome of the regression analysis. In all impacts conducted in this thesis, the 95th percentile MPS was less than 50% of the MPS value, and 99th percentile MPS was ~50% of the MPS.

A major concern in using the 100th percentile MPS is the possibility of spurious elements [39]. A magnified histogram (top 0.01% elements with high strain) of few impact data reveals a discontinuity in the MPS magnitude of the maximum element (***Figure 5.1***). The discontinuity in the strain magnitude of the element with highest strain is generally noticed above 99.9th percentile. Despite this fact, the maximum strain is always scaled with other percentile strains and generally falls within the top 5% brain strain region (***Figure 5.2***). However, in this thesis MPS (100th percentile strain) is predominantly used in regression analysis since it has been shown that MPS scales with other percentiles in the dataset used.

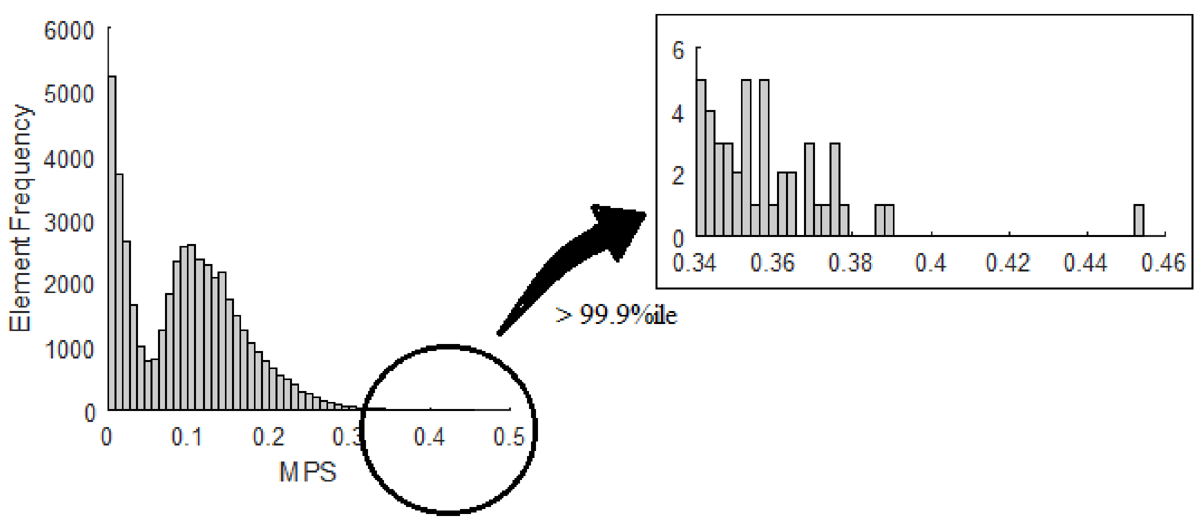

Figure 5.1 Example histogram plot displaying the distribution of strains above 99.9th percentile with a jump in the strain value of 100th percentile MPS

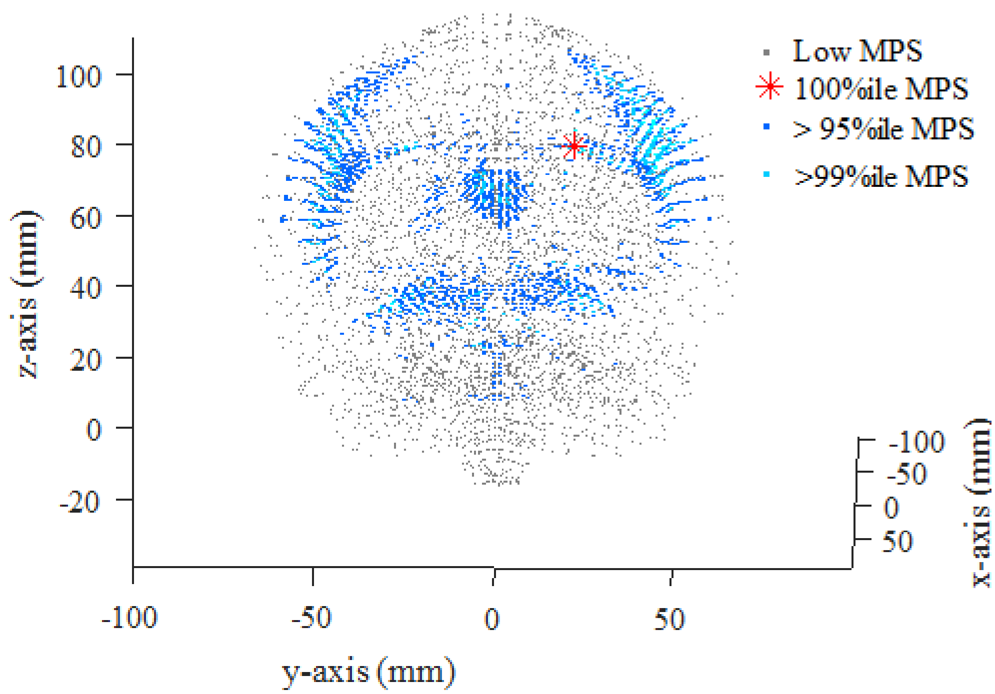

Figure 5.2 3D plot of distribution of strains greater than 95%ile in the impact corresponding to Figure 5.1

5.2 Linear acceleration does not create strains comparable to an angular velocity

Evidence suggests that brain strain magnitudes obtained from both linear acceleration and angular velocity could just be achieved by only using angular velocity. Linear acceleration magnitudes as high as 143g and 249g created strains up to 0.2 (**Figure *4.9***). However, such a high magnitude of linear acceleration is rare in real-world impacts [68], [86], [90]. The sub-study result has shown that a strain of 0.2 could be created by pure angular velocity as low as 10 rad/sec (**Figure *4.12***). Since impacts with linear acceleration above 140g are characterized by angular velocities greater than 10g (**Figure *5.3***) the resulting strain is mostly driven by the angular velocity. For example, comparing the results from sub-study, linear acceleration of 143g to influence strain more, the corresponding angular velocity should be less than 10 rad/sec which was not noticed in any of the 276 impacts conducted in this thesis (**Figure *5.3***). Similar finding was reported by Kleiven [32] using FE brain model by Royal Institute of Technology (Stockholm). In this study the author have shown that angular velocity alone was able to achieve strain created by both linear acceleration and angular velocity. This suggests that the strain is driven by angular velocities including the impacts whose linear acceleration range exceeds 140g. Hence, limiting the angular velocity errors (both directional and magnitude error) is sufficient to limit the corresponding brain strain error magnitude.

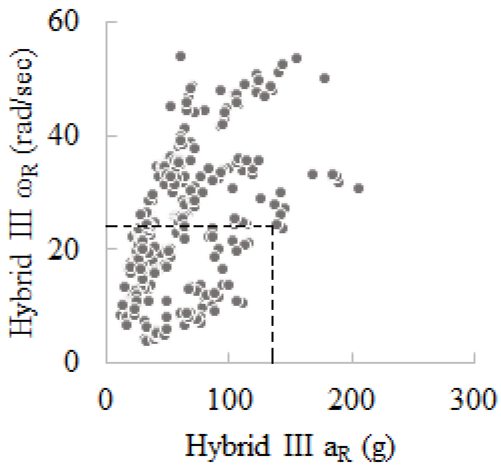

Figure 5.3: Scatter plot comparing peak linear acceleration and corresponding peak angular velocity with dotted lines marking the minimum peak angular velocity recorded by Hybrid III and GFT for a peak linear acceleration of 140g

5.3 Full transformation in wearable sensors

Transformation of GFT kinematics to the Hybrid III head center may not be required for strain calculation with SIMon. On the usage of wearable sensors in brain strain prediction, literature have suggested a linear transformation of kinematics to head COG [21], [22], [70]. By comparing the strain results of partially transformed kinematics and fully transformed kinematics, this study has shown that full transformation to head COG is optional for wearable sensor impact data. Though the accuracy of the direction of the sensor's component angular kinematics is crucial in brain strain prediction, the linear distance of the sensor's axis from the reference axis does not affect the strain magnitude. In the tissue level strain prediction, though the full transformation does show an increase in the agreement of elements with the highest strain predicted by both sensors, the difference is less than 2%. The role of linear acceleration, as well as full transformation on the distribution of element level brain strain is not explored in detail in this research. Though strain magnitude is unaffected by a full transformation of GFT kinematics, outliers in Figure 4.6 suggest that a full transformation might have an effect on strain distribution. Impact samples for which the volumetric strain error changes with full transformation (Figure *4.6*) requires specific research methods focusing on the effect of individual kinematics on strain distribution in FE brain models. However, the preliminary regression analysis suggests that the full transformation of sensor kinematics to head COG has a negligible effect on the strain or strain distribution errors. This is due to the fact the full transformation only affects the linear kinematics and not the rotational kinematics. Since linear kinematics have a negligible effect on brain strain, full transformation also turns to be ineffective in brain strain calculation. Thus wearable sensors can disregard the much complicated full transformation of its kinematics to head COG. Rather, the relatively simpler rotational or partial transformation of the sensor kinematics to the head axis is necessary.

5.4 Peak errors vs. time domain errors

The effort to compare time domain kinematic error with MPS error did not provide sufficient information to determine a predictor for strain errors. In addition to the unsynchronized kinematic data, a time domain difference failed to provide a consistent outcome in multiple categories as the maximum difference between two kinematic curves in time domain was often governed by a valley in the signals at a time period much earlier than the maximum strain occurred as shown in **Figure *5.4***. Though these signals are closely aligned, the difference in the time-domain is driven by the GFT valley at an approximate time of 20 ms. It is to be noticed that the majority of the angular velocity signals that contribute towards the final strain occurs after 20 ms in this example. Also, the strains are unaltered during a valley in the signals, which suggest that a valley may not be the kinematic characteristics that explain the brain strain magnitude. As this method of time-domain comparison fails to capture the characteristics of a signal that contributes to the maximum strain, the corresponding regression analysis did not yield a consistent outcome across different categories. However, a consistent finding was possible with peak kinematics as they are essential characteristics in kinematic curves that contribute to strain. The fact that peak kinematics have been effectively used in brain strain metrics to predict brain strain [25], [38], [39] suggests peak kinematics as a better choice among kinematic curve characteristics in brain strain prediction.

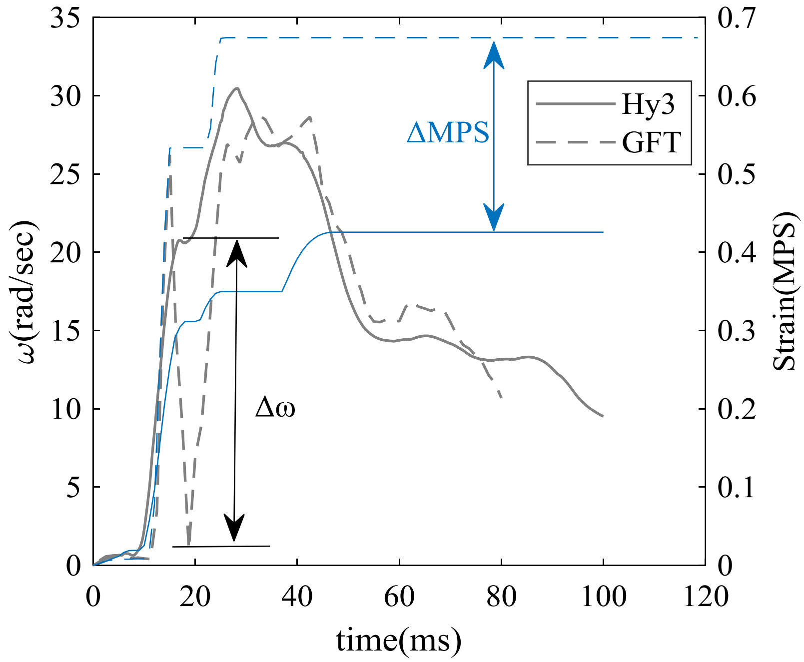

Figure 5.4: Time domain Hybrid III and GFT resultant angular velocities and corresponding strain for a left impact

Hybrid III and GFT peak kinematics in this thesis having R^2 of up to 0.98 with strain (**Figure *5.5***) are believed to be the reason why peak kinematic errors were better predictors for strain errors compared to time-domain errors.

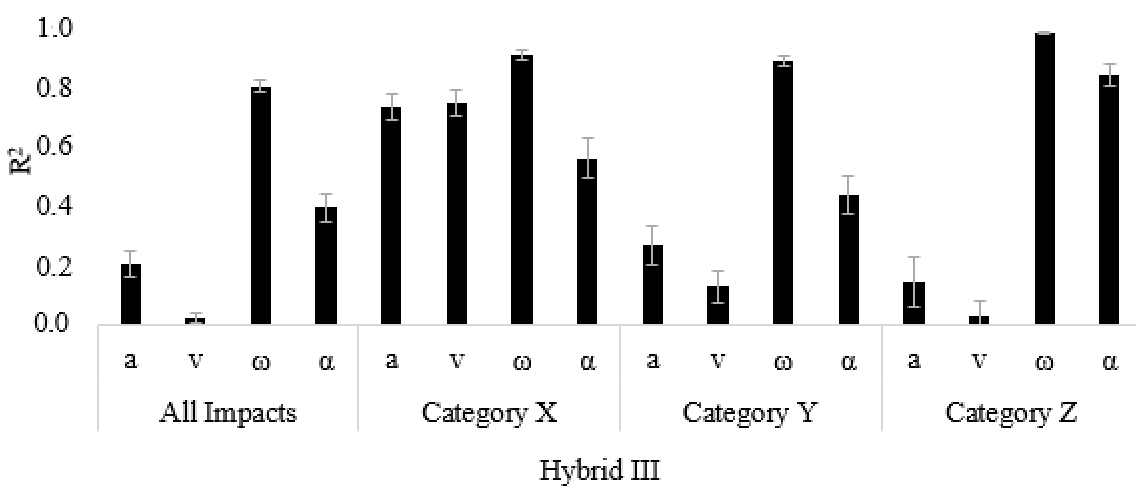

a)

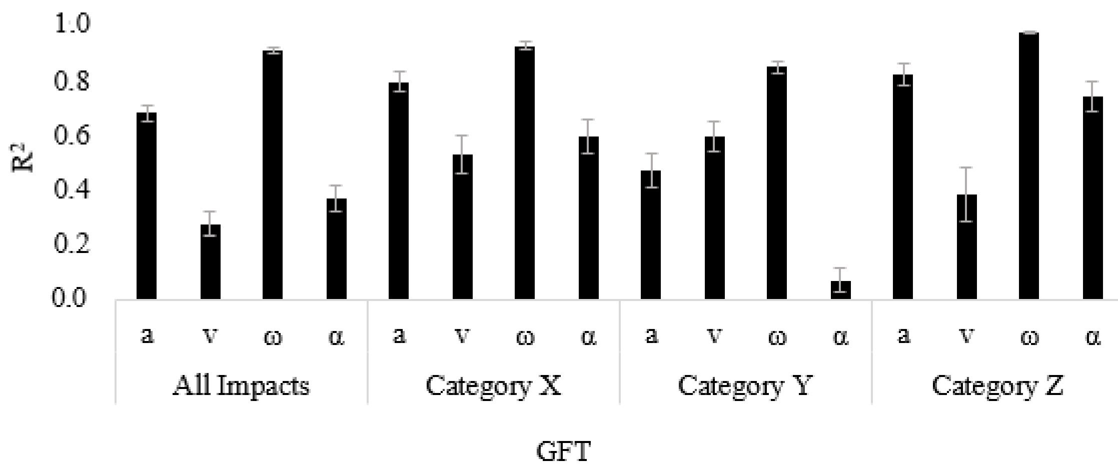

b)

Figure 5.5: Regression result showing the coefficient of determination (R^2) of a) Hybrid III and b) GFT peak resultant kinematics with maximum strain

5.5 Kinematic error predictor for strain error

The regression results of peak kinematic errors with strain errors suggest that peak angular velocity errors are the best predictors for strain errors. The primary goal of the thesis was to determine the kinematic error that best predicts strain error. In a comparison among different kinematics errors (Δa, Δv, Δω and Δα) vs. strain error, the resultant errors were better predictors compared to component errors since resultant kinematics are a function of component kinematics. By an overall comparison and by impact sub-sets stratified based on angular velocity direction, peak resultant angular velocity error predicts the strain errors best compared to the other kinematics outside the bounds of one standard error. Though resultant angular acceleration error exhibited second high R^2 value, the regression result of angular velocity (ω_R) with MPS ($R^2_{\text{Hybrid III}}$ = 0.80±0.02, R^2_{GFT} = 0.90±0.01) was more than twice that of angular acceleration (α_R) with MPS ($R^2_{\text{Hybrid III}}$ = 0.39±0.05, R^2_{GFT} = 0.37±0.05). This agrees with earlier research which states peak angular acceleration alone cannot be used for brain injury prediction whereas peak angular velocity alone is sufficient for brain injury prediction [25], [38]. Hence, evidence suggesting brain strain as a function of peak angular acceleration is poor, which in turn indicates that reducing the errors in peak angular acceleration may not improve strain prediction compared to angular velocity. These findings confirm that, between all the input kinematics, the error in peak angular velocity of GFT best predicts the error in brain strain calculations.

5.6 Resultant vs. component angular velocity errors

Though resultant angular velocity error is the best predictor for strain error, the component angular velocity errors exhibit influence over the error in strain magnitude and distribution of strains. Since the resultant kinematics used in this thesis ignores component direction, it cannot be concluded that limiting the resultant angular velocity error will limit the strain error without considering the effect of directional angular velocity errors on strain error. The component kinematic data (ω_x, ω_y, ω_z) being used as input to SIMon in brain strain calculations, the possibility of directional angular velocity errors, as opposed to resultant angular velocity error influencing the brain strain error is high.

A better insight on the role of component angular velocity on strain distribution was obtained by the comparison of three impacts with the same resultant magnitude. The strain magnitude, as well as the strain distribution of these impacts, were shown to vary, though the resultant angular velocity was similar. The interpretation of this result is that direction of angular velocity influences the distribution of brain strain. Because the distribution of brain strain is relevant in studying potential brain injury, it is important that a wearable accurately measure the components of angular velocity. Also, it is to be emphasized that the resultant angular velocity error is the best standalone predictor for strain error but is not the most useful for eliminating strain error. Strain errors can still occur between identical resultant angular velocities when there is a change in component data. Hence relying only on $\Delta\omega_R$ to predict strain errors can be misleading.

5.7 Direction sensitivity of the SIMon FE model

Evidence suggests that a higher percentage of strain errors can still be observed in impacts with no errors in the amplitude of the resultant angular velocity. In addition to strain errors created by a mismatch of sensor axis direction, strain errors of up to 20% were noticed due to rotational misalignment of the wearable sensor's axis. Rotational misalignment of the sensor axis alters the angular kinematics of x, y and z axes. Redistribution of the axis kinematics, especially in angular velocity about the sensitive z and y axes, lead to high strain errors. Both the direction (+ve and –ve) and the magnitude changes in the component angular velocity were shown to have effects on the output strain. For example, an angular velocity of +5rad/sec and -5rad/sec in z-axis could result in different MPS. All these results confirm that the component angular velocity errors have a causal effect on the strain errors. Research that focuses on validation of the wearable sensors predominantly focus on resultant kinematics [24], [68], [70], [91] and little or no importance is given to directional kinematics. Though resultant angular kinematics can predict the strain errors, it is the underlying component angular kinematics that influences the strain and strain distribution errors. Given the sensitivity of brain strain to directional kinematics, it is essential that wearable sensor manufacturers and sensor validation research address the inaccuracies in directional kinematic measurements. Limiting the component angular velocity errors should be prioritized over limiting resultant angular velocity errors. This will ensure that both the resultant angular velocity errors and the strain errors are corrected.

Though many studies agree that brain strain is influenced by impact direction[42], [67], [70], very few studies have focused on the direction sensitivity of brain strain to impact kinematics [39], [46], [47]. The findings in this thesis convey that the brain strain sensitivity is greater for rotation about z-axis and least for x-axis rotation. This agrees with the weighing factors used in the equation for the brain strain injury metric RVCI. The weighing factors which is the ratio of MPS calculated between different axis used in RVCI (with the x-axis as reference) is given as 1, 1± 0.18, 1.17 ± 0.17 for the x-axis , y-axis and z-axis respectively [47]. A pathophysiological study by Margulies [37] states that the presence of falx-cerebri in the sagittal plane reduces the intracranial deformation in a side to side motion of the head. This may be one reason for the least sensitivity of brain strain to x-axis rotations. Thus, accuracy of component kinematics is important for the prediction of brain strain and strain distribution. Also, many proposed brain injury metrics are equations that require component kinematics. Hence, it is of paramount importance to measure components correctly so that the brain injury metrics we compute are also correct in magnitude. It is essential for wearable sensors to ensure their axis direction complies with SAE J211-1 [75] standard which is followed by standard head models if the sensor measurements are to be used in FE brain strain calculations.

5.8 Limitations

As with other laboratory-based experimental methods, the limitations of this study is the ATD Hybrid III which may not precisely replicate the biomechanics of a human head and neck. The Hybrid III head form which was primarily constructed for automotive crash tests and may not be perfectly suited to be used with helmet compared to the NOCSAE head form. In the presented experiments, however, it was ensured that the helmet fit with the Hybrid III was intact after every impact. Hybrid III is the standardized head form available to date along with NOCSAE head form developed specifically for helmet testing and research have shown that the difference in response between these two head forms tends to be small [63].

The brain strain response from this study was also based on a single FE brain model which could also be considered as a limitation. However, the brain model has been validated by comparing its response with cadaver and animal brain strain responses [48], [54]. Literature comparing multiple FE models including SIMon have concluded that all models show similar trends in brain strain responses [55] and SIMon brain strain response was comparable to high-resolution FE brain models [56]. Also, in the presented study the choice of the ATD or the FE head model may not have a significant impact on the outcome since the study focuses on comparative analysis on two sensors.

Another limitation of this study is that the pulse width of the signals was ignored in the analysis. Research by Gabler et al. which studied impact kinematics along with the duration of the impact suggests that only peak angular velocity is sufficient for predicting brain injuries however longer duration (>50ms) do have minor effects on the strain [38]. An R^2 value of 0.80 (Hybrid III) and 0.90 (GFT) between peak angular velocity and MPS in this study confirms that peak angular velocity data may be sufficient. Though pulse width of the angular velocity does not affect strains compared to peaks [38], future studies could explore the effect of pulse width errors on strain errors.

The unsynchronized kinematic data between the two sensors as discussed in Section 3.3.2 limited the ability to perform appropriate time-domain analysis. Though analysis with peak kinematics in this study was able to yield consistent outcome with the unsynchronized data, future studies could investigate a system design that will ensure the time-synchronization of the two sensors.

Only simple statistical analysis was used in this study since the goal was to determine the kinematic error that was most explanatory of strain error. Complex statistical analysis to study the interactions of impact locations or combination of kinematics were not performed in this study. Though simple linear regression was sufficient in the analysis with peak kinematics and maximum strain, an extensive study is required to better understand the role of directional kinematics in strain distribution where a complex statistical tool could be of importance.

6. Conclusion

The objective of this thesis was to determine the kinematic errors that explain the strain errors in FE brain strain predictions using wearable sensor kinematics. Impact kinematics of real-world head impacts in sports are sought after by researchers for brain injury predictions in sports where there is a high risk of head injury. Though wearable sensors provide the possibility of acquiring real-world impact kinematics, brain strain predictions with wearable sensor data are restricted due to the uncertainty of the sensor's accuracy. Extensive research have thus focused on quantifying the error in wearable sensor kinematics by comparing it with reference sensors. However, there is no research that measured the effect of these kinematic errors on brain strain prediction using FE models. This study thus compared the brain strain errors to kinematic errors which in turn provide insight into the kinematic factors that influence strain.

Peak resultant angular velocity errors regressed with strain errors achieved highest R^2 compared to the other kinematics. However, it was also determined that MPS is sensitive to directions and accuracy of directional component angular velocities and not just resultant is essential for better FE-based brain strain predictions. To achieve better brain injury measurement, it is essential that direction of the component rotational velocities are expressed relative to the head coordinate system prescribed for the brain model. Kinematic measurements by wearable sensors that are rotationally misaligned to reference axis are required to be rotationally transformed. But, a linear transformation of the wearable sensors kinematics to the head COG is not essential, as it does not affect the brain strain predictions. Error in the input kinematics to the FE brain model, in addition to affecting the strain magnitude, created a larger error in the location of the maximum strains predicted. Since FE models use directional component angular velocities as input, limiting errors in the same will lead to better brain strain prediction with wearable sensors.

The distribution of element level strains was studied to fill the gap in the literature on the choice of the 95th percentile strain for regression analysis. The study reveals that the 95th percentile along with 99th and 99.9th percentile strain scaled with MPS and usage of the MPS in regression analysis will not affect the reliability of the outcome.

6.1 Significance of the study

Literature to date on validation of a wearable head impact sensor is limited to resultant kinematics and have widely ignored directional component kinematics. In addition, the ultimate purpose of measuring head impact kinematics being in brain injury prediction, it has not been explored yet how the error in head impact kinematics will affect a brain injury prediction when using FE brain models. This thesis has laid the foundational steps towards using the wearable head impact sensors in FE brain model injury prediction by identifying the error sources in the sensor measurements that lead to errors in the brain injury prediction. The major finding of this study implies the following significance.

1. If a wearable does not measure component rotational kinematics accurately, accurate brain strain distribution cannot be calculated, and this could have implications for the overall utility of a wearable sensor in brain injury research with athletes.

2. Researchers using wearable head impact sensors should validate component kinematics in addition to resultant kinematics if the sensor kinematics are intended to be used in FE brain models for brain injury prediction.

7. Recommendations

Based on the observations made from the thesis, the following recommendations are proposed for wearable sensor kinematics validation.

- Calibration of wearable sensors should focus on accurate measurement of component kinematics, in particular rotational kinematics, and not resultants.

- The direction of the component kinematics from wearable sensors should be aligned with the axes standard outlined by SAE [75] which is followed by standard ATDs and FE brain models. In addition, based on the findings in this study that uses the SIMon model, linear of transformation of kinematics may be unnecessary if the goal of the researcher applying the wearable sensor is to estimate brain strain from a kinematics-driven finite element brain model.

References

[1] H. S. Martland, “Punch drunk,” Journal of the American Medical Association, vol. 91, no. 15, pp. 1103–1107, Oct. 1928.

[2] B. I. Omalu, S. T. DeKosky, R. L. Minster, M. I. Kamboh, R. L. Hamilton, and C. H. Wecht, “Chronic Traumatic Encephalopathy in a National Football League Player,” *Neurosurgery*, vol. 57, no. 1, pp. 128–134, Jul. 2005.

[3] D. J. T. D. M. Sosin J. E. Sniezek, “Incidence of mild and moderate brain injury in the United States, 1991,” *Brain Injury*, vol. 10, no. 1, pp. 47–54, Jan. 1996.

[4] B. E. Gavett, R. A. Stern, and A. C. McKee, “Chronic Traumatic Encephalopathy: A Potential Late Effect of Sport-Related Concussive and Subconcussive Head Trauma,” *Clinics in Sports Medicine*, vol. 30, no. 1, pp. 179–188, Jan. 2011.

[5] J. Mez, D. H. Daneshvar, P. T. Kiernan, B. Abdolmohammadi, V. E. Alvarez, B. R. Huber, M. L. Alosco, T. M. Solomon, C. J. Nowinski, L. McHale, K. A. Cormier, C. A. Kubilus, B. M. Martin, L. Murphy, C. M. Baugh, P. H. Montenigro, C. E. Chaisson, Y. Tripodis, N. W. Kowall, J. Weuve, M. D. McClean, R. C. Cantu, L. E. Goldstein, D. I. Katz, R. A. Stern, T. D. Stein, and A. C. McKee, “Clinicopathological Evaluation of Chronic Traumatic Encephalopathy in Players of American Football,” *JAMA*, vol. 318, no. 4, pp. 360–370, Jul. 2017.

[6] J. C. Maroon, R. Winkelman, J. Bost, A. Amos, C. Mathyssek, and V. Miele, “Chronic Traumatic Encephalopathy in Contact Sports: A Systematic Review of All Reported Pathological Cases,” *PLOS ONE*, vol. 10, no. 2, p. e0117338, Feb. 2015.

[7] R. S. Naunheim, J. Standeven, C. Richter, and L. M. Lewis, “Comparison of Impact Data in Hockey, Football, and Soccer:,” *The Journal of Trauma: Injury, Infection, and Critical Care*, vol. 48, no. 5, pp. 938–941, May 2000.

[8] K. M. Guskiewicz, S. W. Marshall, J. Bailes, M. McCrea, R. C. Cantu, C. Randolph, and B. D. Jordan, “Association between Recurrent Concussion and Late-Life Cognitive Impairment in Retired Professional Football Players,” *Neurosurgery*, vol. 57, no. 4, pp. 719–726, Oct. 2005.

[9] J. J. Crisco, R. Fiore, J. G. Beckwith, J. J. Chu, P. G. Brolinson, S. Duma, T. W. McAllister, A.-C. Duhaime, and R. M. Greenwald, “Frequency and Location of Head Impact Exposures in Individual Collegiate Football Players,” *Journal of Athletic Training*, vol. 45, no. 6, pp. 549–559, Nov. 2010.

[10] S. M. Duma, S. J. Manoogian, W. R. Bussone, P. G. Brolinson, M. W. Goforth, J. J. Donnenwerth, R. M. Greenwald, J. J. Chu, and J. J. Crisco, “Analysis of Real-time Head Accelerations in Collegiate Football Players,” *Clinical Journal of Sport Medicine*, vol. 15, no. 1, p. 3, Jan. 2005.

[11] K. M. Guskiewicz, M. McCrea, S. W. Marshall, R. C. Cantu, C. Randolph, W. Barr, J. A. Onate, and J. P. Kelly, "Cumulative Effects Associated With Recurrent Concussion in Collegiate Football Players: The NCAA Concussion Study," *JAMA*, vol. 290, no. 19, pp. 2549–2555, Nov. 2003.

[12] J. S. Delaney, V. J. Lacroix, S. Leclerc, and K. M. Johnston, "Concussions during the 1997 Canadian Football League season," *Clin J Sport Med*, vol. 10, no. 1, pp. 9–14, Jan. 2000.

[13] F. O. Mueller, "Fatalities from head and cervical spine injuries occurring in tackle football: 50 years' experience," *Clinics in Sports Medicine*, vol. 17, no. 1, pp. 169–182, Jan. 1998.

[14] S. Manoogian, D. McNeely, M. Goforth, G. Brolinson, and S. Duma, "Head acceleration is less than 10 percent of helmet acceleration during a football impact," presented at the ISB XXth Congress - ASB 29th Annual Meeting, Cleveland, Ohio.

[15] N. Cortes, A. E. Lincoln, G. D. Myer, L. Hepburn, M. Higgins, M. Putukian, and S. V. Caswell, "Video Analysis Verification of Head Impact Events Measured by Wearable Sensors," *Am J Sports Med*, vol. 45, no. 10, pp. 2379–2387, Aug. 2017.

[16] E. J. Pellman, J. W. Powell, D. C. Viano, I. R. Casson, A. M. Tucker, H. Feuer, M. Lovell, J. F. Waeckerle, and D. W. Robertson, "Concussion in Professional Football: Epidemiological Features of Game Injuries and Review of the Literature—Part 3," *Neurosurgery*, vol. 54, no. 1, pp. 81–96, Jan. 2004.

[17] E. J. Pellman, D. C. Viano, A. M. Tucker, I. R. Casson, and J. F. Waeckerle, "Concussion in Professional Football: Reconstruction of Game Impacts and Injuries," *Neurosurgery*, vol. 53, no. 4, pp. 799–814, Sep. 2003.

[18] D. Scheer, G. Karami, and M. Ziejewski, "An Evaluation of the Riddell IQ HITS System in Prediction of an Athlete's Head Acceleration," presented at the 7th Asia-Pacific Congress on Sports Technology, 2015.

[19] "HITS™ Technology | Riddell," 17-Apr-2012. [Online]. Available: http://www.riddell.com/innovation/hits-technology/. [Accessed: 17-Apr-2012].

[20] G. P. Siegmund, S. J. Bonin, J. F. Luck, and C. R. D. Bass, "Validation of a skin-mounted sensor for measuring in-vivo head impacts," in *Proceedings of the 2015 International IRCOBI Conference on the Biomechanics of Injury*, Lyon, France, 2015, p. IRC-15-28.

[21] L. C. Wu, V. Nangia, K. Bui, B. Hammoor, M. Kurt, F. Hernandez, C. Kuo, and D. B. Camarillo, "In Vivo Evaluation of Wearable Head Impact Sensors," *Annals of Biomedical Engineering*, vol. 44, no. 4, pp. 1234–1245, Apr. 2016.

[22] D. B. Camarillo, P. B. Shull, J. Mattson, R. Shultz, and D. Garza, "An Instrumented Mouthguard for Measuring Linear and Angular Head Impact Kinematics in American Football," *Ann Biomed Eng*, vol. 41, no. 9, pp. 1939–1949, Sep. 2013.

[23] R. Jadischke, D. C. Viano, N. Dau, A. I. King, and J. McCarthy, "On the accuracy of the Head Impact Telemetry (HIT) System used in football helmets," *Journal of Biomechanics*, vol. 46, no. 13, pp. 2310–2315, Sep. 2013.

[24] B. M. Knowles, H. Yu, and C. R. Dennison, "Accuracy of a Wearable Sensor for Measures of Head Kinematics and Calculation of Brain Tissue Strain," *Journal of Applied Biomechanics*, vol. 33, no. 1, pp. 2–11, Feb. 2017.

[25] E. G. Takhounts, V. Hasija, S. A. Ridella, S. Rowson, and S. M. Duma, "KINEMATIC ROTATIONAL BRAIN INJURY CRITERION (BRIC)," p. 10.

[26] S. Ji, H. Ghadyani, R. P. Bolander, J. G. Beckwith, J. C. Ford, T. W. McAllister, L. A. Flashman, K. D. Paulsen, K. Ernstrom, S. Jain, R. Raman, L. Zhang, and R. M. Greenwald, "Parametric Comparisons of Intracranial Mechanical Responses from Three Validated Finite Element Models of the Human Head," *Ann Biomed Eng*, vol. 42, no. 1, pp. 11–24, Jan. 2014.

[27] T. W. Barber, J. A. Brockway, and L. S. Higgins, "THE DENSITY OF TISSUES IN AND ABOUT THE HEAD," *Acta Neurologica Scandinavica*, vol. 46, no. 1, pp. 85–92, Mar. 1970.

[28] "Anatomy of the Nervous System - Microbiology For Allied Health Students - OpenStax CNX." [Online]. Available: https://cnx.org/contents/b_iEO9W7@1.1:K5Qgugxa@3/Anatomy-of-the-Nervous-System. [Accessed: 24-Sep-2018].

[29] A. H. S. Holbourn, "Mechanics of head injuries," *The Lancet*, vol. 242, no. 6267, pp. 438–441, Oct. 1943.

[30] J. W. Melvin and J. W. Lighthall, "Brain-Injury Biomechanics," in *Accidental Injury: Biomechanics and Prevention*, A. M. Nahum and J. W. Melvin, Eds. New York, NY: Springer New York, 2002, pp. 277–302.

[31] F. Dunning, "Inflatable padding for football helmet or the like," US3761959A, 02-Oct-1973.

[32] S. Kleiven, "Predictors for Traumatic Brain Injuries Evaluated through Accident Reconstructions," *Stapp Car Crash Journal; Ann Arbor*, vol. 51, pp. 81–114, Oct. 2007.

[33] A. K. Ommaya, R. L. Grubb, and R. A. Naumann, "Coup and contre-coup injury: observations on the mechanics of visible brain injuries in the rhesus monkey," *Journal of Neurosurgery*, vol. 35, no. 5, pp. 503–516, Nov. 1971.

[34] A. K. Ommaya, A. E. Hirsch, E. S. Flamm, and R. H. Mahon, "Cerebral Concussion in the Monkey: An Experimental Model," *Science*, vol. 153, pp. 211–212, May 1966.

[35] T. A. Gennarelli, J. H. Adams, and D. I. Graham, “Acceleration Induced Head Injury in the Monkey. I. The Model, Its Mechanical and Physiological Correlates,” in *Experimental and Clinical Neuropathology*, 1981, pp. 23–25.

[36] D. Denny-Brown and W. R. Russell, “Experimental cerebral concussion,” *The Journal of Physiology*, vol. 99, no. 1, pp. 153–153, Dec. 1940.

[37] S. S. Margulies, L. E. Thibault, and T. A. Gennarelli, “Physical model simulations of brain injury in the primate,” *Journal of Biomechanics*, vol. 23, no. 8, pp. 823–836, Jan. 1990.

[38] L. F. Gabler, J. R. Crandall, and M. B. Panzer, “Investigating Brain Injury Tolerance in the Sagittal Plane Using a Finite Element Model of the Human Head,” p. 8, 2016.

[39] L. F. Gabler, J. R. Crandall, and M. B. Panzer, “Development of a Metric for Predicting Brain Strain Responses Using Head Kinematics,” *Annals of Biomedical Engineering*, vol. 46, no. 7, pp. 972–985, Jul. 2018.

[40] B. M. Knowles and C. R. Dennison, “Predicting Cumulative and Maximum Brain Strain Measures From HybridIII Head Kinematics: A Combined Laboratory Study and Post-Hoc Regression Analysis,” *Annals of Biomedical Engineering*, vol. 45, no. 9, pp. 2146–2158, Sep. 2017.

[41] L. F. Gabler, J. R. Crandall, and M. B. Panzer, “Assessment of Kinematic Brain Injury Metrics for Predicting Strain Responses in Diverse Automotive Impact Conditions,” *Ann Biomed Eng*, vol. 44, no. 12, pp. 3705–3718, Dec. 2016.

[42] W. N. Hardy, T. B. Khalil, and A. I. King, “Literature review of head injury biomechanics,” *International Journal of Impact Engineering*, vol. 15, no. 4, pp. 561–586, Aug. 1994.

[43] N. Yoganandan, F. A. Pintar, J. Zhang, T. A. Gennarelli, and N. Beuse, “Biomechanical Aspects of Blunt and Penentrating Head Injuries,” in *IUTAM Symposium on Impact Biomechanics: From Fundamental Insights to Applications*, 2005, pp. 173–184.

[44] J. Versace, “A Review of the Severity Index,” SAE International, Warrendale, PA, 710881, Feb. 1971.

[45] L. F. Gabler, J. R. Crandall, and M. B. Panzer, “Assessment of Kinematic Brain Injury Metrics for Predicting Strain Responses in Diverse Automotive Impact Conditions,” *Annals of Biomedical Engineering*, vol. 44, no. 12, pp. 3705–3718, Dec. 2016.

[46] E. G. Takhounts, M. J. Craig, K. Moorhouse, J. McFadden, and V. Hasija, “Development of Brain Injury Criteria (BrIC),” *Stapp Car Crash J*, vol. 57, pp. 243–266, 2013.

[47] T. Yanaoka, Y. Dokko, and Y. Takahashi, “Investigation on an Injury Criterion Related to Traumatic Brain Injury Primarily Induced by Head Rotation,” presented at the SAE 2015 World Congress & Exhibition, 2015.

[48] A. Post and T. Blaine Hoshizaki, "Rotational Acceleration, Brain Tissue Strain, and the Relationship to Concussion," *J Biomech Eng*, vol. 137, no. 3, pp. 030801-030801–8, Mar. 2015.

[49] B. Morrison, B. S. Elkin, J.-P. Dollé, and M. L. Yarmush, "In Vitro Models of Traumatic Brain Injury," *Annual Review of Biomedical Engineering*, vol. 13, no. 1, pp. 91–126, 2011.

[50] E. G. Takhounts, R. H. Eppinger, J. Q. Campbell, R. E. Tannous, E. D. Power, and L. S. Shook, "On the Development of the SIMon Finite Element Head Model," *Stapp Car Crash Journal*, p. 27, 2003.

[51] W. N. Hardy, C. D. Foster, M. J. Mason, K. H. Yang, A. I. King, and S. Tashman, "Investigation of Head Injury Mechanisms Using Neutral Density Technology and High-Speed Biplanar X-ray," *Stapp Car Crash J*, vol. 45, pp. 337–368, Nov. 2001.

[52] L. Zhang, K. H. Yang, R. Dwarampudi, K. Omori, T. Li, K. Chang, W. N. Hardy, T. B. Khalil, and A. I. King, "Recent Advances in Brain Injury Research: A New Human Head Model Development and Validation," p. 28.

[53] L. E. Miller, J. E. Urban, and J. D. Stitzel, "Development and validation of an atlas-based finite element brain model," *Biomech Model Mechanobiol*, vol. 15, no. 5, pp. 1201–1214, Oct. 2016.

[54] H. Mao, L. Zhang, B. Jiang, V. V. Genthikatti, X. Jin, F. Zhu, R. Makwana, A. Gill, G. Jandir, A. Singh, and K. H. Yang, "Development of a Finite Element Human Head Model Partially Validated with Thirty Five Experimental Cases," *Journal of Biomechanical Engineering*, vol. 135, no. 11, 2013.

[55] S. Kleiven and W. N. Hardy, "Correlation of an FE Model of the Human Head with Local Brain Motion : Consequences for Injury Prediction," *Stapp Car Crash journal*, vol. 46, pp. 123–144, 2002.

[56] E. G. Takhounts, S. A. Ridella, V. Hasija, R. E. Tannous, J. Q. Campbell, D. Malone, K. Danelson, J. Stitzel, S. Rowson, and S. Duma, "Investigation of Traumatic Brain Injuries Using the Next Generation of Simulated Injury Monitor (SIMon) Finite Element Head Model," *Stapp Car Crash Journal*, vol. 52, pp. 1–31, Nov. 2008.

[57] A. Talebanpour and L. Smith, "A Comparison between Simulated and Measured Human Brain Response under Mild Acceleration," p. 11, 2017.

[58] L. E. Miller, J. E. Urban, and J. D. Stitzel, "Validation performance comparison for finite element models of the human brain," *Computer Methods in Biomechanics and Biomedical Engineering*, vol. 20, no. 12, pp. 1273–1288, Sep. 2017.

[59] A. C. Bain and D. F. Meaney, "Tissue-Level Thresholds for Axonal Damage in an Experimental Model of Central Nervous System White Matter Injury," *J Biomech Eng*, vol. 122, no. 6, pp. 615–622, Dec. 2000.

[60] S. S. Margulies and L. E. Thibault, “A proposed tolerance criterion for diffuse axonal injury in man,” *Journal of biomechanics*, vol. 25, no. 8, pp. 917–923, 1992.

[61] H. J. Mertz and A. L. Irwin, “Anthropomorphic Test Devices and Injury Risk Assessments,” in *Accidental Injury: Biomechanics and Prevention*, N. Yoganandan, A. M. Nahum, and J. W. Melvin, Eds. New York, NY: Springer New York, 2015, pp. 83–112.

[62] V. R. Hodgson, M. W. Mason, and L. M. Thomas, “Head Model for Impact,” presented at the 16th Stapp Car Crash Conference (1972), 1972.

[63] B. R. Cobb, A. M. Zadnik, and S. Rowson, “Comparative analysis of helmeted impact response of Hybrid III and National Operating Committee on Standards for Athletic Equipment headforms,” *Proceedings of the IMechE*, vol. 230, no. 1, pp. 50–60, Mar. 2016.

[64] M. Kendall, E. S. Walsh, and T. B. Hoshizaki, “Comparison between Hybrid III and Hodgson–WSU headforms by linear and angular dynamic impact response,” *Proceedings of the IMechE*, vol. 226, no. 3–4, pp. 260–265, Sep. 2012.

[65] J. A. Newman and B. M. Gallup, “Biofidelity Improvements to the Hybrid III Headform,” presented at the 28th Stapp Car Crash Conference (1984), 1984.

[66] B. R. Cobb, A. MacAlister, T. J. Young, A. R. Kemper, S. Rowson, and S. M. Duma, “Quantitative comparison of Hybrid III and National Operating Committee on Standards for Athletic Equipment headform shape characteristics and implications on football helmet fit,” *Proceedings of the IMechE*, vol. 229, no. 1, pp. 39–46, Mar. 2015.

[67] G. P. Siegmund, K. M. Guskiewicz, S. W. Marshall, A. L. DeMarco, and S. J. Bonin, “Laboratory Validation of Two Wearable Sensor Systems for Measuring Head Impact Severity in Football Players,” *Annals of Biomedical Engineering*, vol. 44, no. 4, pp. 1257–1274, Apr. 2016.

[68] J. G. Beckwith, R. M. Greenwald, and J. J. Chu, “Measuring Head Kinematics in Football: Correlation Between the Head Impact Telemetry System and Hybrid III Headform,” *Ann Biomed Eng*, vol. 40, no. 1, pp. 237–248, Jan. 2012.

[69] K. R. Campbell, M. J. Warnica, I. C. Levine, J. S. Brooks, A. C. Laing, T. A. Burkhart, and J. P. Dickey, “Laboratory Evaluation of the gForce Tracker™, a Head Impact Kinematic Measuring Device for Use in Football Helmets,” *Annals of Biomedical Engineering*, vol. 44, pp. 1246–1256, Apr. 2016.

[70] M. A. Allison, Y. S. Kang, M. R. Maltese, J. H. Bolte, and K. B. Arbogast, “Measurement of Hybrid III Head Impact Kinematics Using an Accelerometer and Gyroscope System in Ice Hockey Helmets,” *Ann Biomed Eng*, vol. 43, no. 8, pp. 1896–1906, Aug. 2015.

[71] M. B. Panzer, B. S. Myers, B. P. Capehart, and C. R. Bass, “Development of a Finite Element Model for Blast Brain Injury and the Effects of CSF Cavitation,” *Ann Biomed Eng*, vol. 40, no. 7, pp. 1530–1544, Jul. 2012.

[72] H. Y. Yu, B. M. Knowles, and C. R. Dennison, “A Test Bed to Examine Helmet Fit and Retention and Biomechanical Measures of Head and Neck Injury in Simulated Impact,” *JoVE (Journal of Visualized Experiments)*, no. 127, pp. e56288–e56288, Sep. 2017.

[73] I. Ebrahimi, F. Golnaraghi, and G. G. Wang, “Factors Influencing the Oblique Impact Test of Motorcycle Helmets.” [Online]. Available: http://www.tandfonline.com/doi/pdf/10.1080/15389588.2014.937804?needAccess=true. [Accessed: 22-Feb-2018].

[74] N. J. Mills, S. Wilkes, S. Derler, and A. Flisch, “FEA of oblique impact tests on a motorcycle helmet,” *International Journal of Impact Engineering*, vol. 36, no. 7, pp. 913–925, Jul. 2009.

[75] “SAE J211 Instrumentation for Impact Test - Part 1: Electronic Instrumentation.” SAE International, 2007.

[76] H. Kimpara, Y. Nakahira, M. Iwamoto, S. Rowson, and S. Duma, “Head Injury Prediction Methods Based on 6 Degree of Freedom Head Acceleration Measurements during Impact,” *IJAE*, vol. 2, no. 2, pp. 13–19, 2011.

[77] J. G. Beckwith, J. J. Chu, and R. M. Greenwald, “Validation of a Noninvasive System for Measuring Head Acceleration for Use during Boxing Competition,” *Journal of Applied Biomechanics*, vol. 23, no. 3, pp. 238–244, Aug. 2007.

[78] N. Yoganandan, J. Zhang, and F. A. Pintar, “Force and Acceleration Corridors from Lateral Head Impact,” *Traffic Injury Prevention*, vol. 5, no. 4, pp. 368–373, Dec. 2004.

[79] L. C. Wu, K. Laksari, C. Kuo, J. F. Luck, S. Kleiven, C. R. ‘Dale’ Bass, and D. B. Camarillo, “Bandwidth and sample rate requirements for wearable head impact sensors,” *Journal of Biomechanics*, vol. 49, no. 13, pp. 2918–2924, Sep. 2016.

[80] A. Padgaonkar, K. W. Krieger, and A. King, “Measurement of Angular Acceleration of a Rigid Body Using Linear Accelerometers,” *Journal of Applied Mechanics*, vol. 42, Sep. 1975.

[81] “GFT3S User Manual (GForce Tracker Sensor) by Artaflex.” [Online]. Available: https://www.cleancss.com/user-manuals/UP2/GFT3S. [Accessed: 24-Nov-2018].

[82] G. P. Siegmund, K. M. Guskiewicz, S. W. Marshall, A. L. DeMarco, and S. J. Bonin, “Laboratory Validation of Two Wearable Sensor Systems for Measuring Head Impact Severity in Football Players,” *Ann Biomed Eng*, vol. 44, no. 4, pp. 1257–1274, Apr. 2016.

[83] “HIII_50th_Male_Drawings.pdf.” National Highway Traffic Safety Administration, Apr-1997.

[84] R. C. Hibbeler, *Engineering mechanics. Statics and dynamics. 8th*. Upper Saddle River, NJ: Pearson/Prentice-Hall. xvi, 1997.

[85] T. Sauer, *Numerical Analysis*, 2nd ed. Pearson, 2012.

[86] E. J. Pellman, D. C. Viano, A. M. Tucker, and I. R. Casson, "Concussion in Professional Football: Location and Direction of Helmet Impacts—Part 2," *Neurosurgery*, vol. 53, no. 6, pp. 1328–1341, Dec. 2003.

[87] W. N. Hardy, M. J. Mason, C. D. Foster, C. S. Shah, J. M. Kopacz, K. H. Yang, A. I. King, J. Bishop, M. Bey, W. Anderst, and S. Tashman, "A Study of the Response of the Human Cadaver Head to Impact," *Stapp Car Crash J*, vol. 51, pp. 17–80, Oct. 2007.

[88] S. Milton, "A Sample Size formula for Multiple Regression Studies." 1986.

[89] P. Cohen, S. G. West, L. S. Aiken, S. G. West, and L. S. Aiken, *Applied Multiple Regression/Correlation Analysis for the Behavioral Sciences*. Psychology Press, 2014.

[90] D. C. Viano, E. J. Pellman, C. Withnall, and N. Shewchenko, "Concussion in Professional FootballPerformance of Newer Helmets in Reconstructed Game Impacts—Part 13," *Neurosurgery*, vol. 59, no. 3, pp. 591–606, Sep. 2006.

[91] D. Nevins, L. Smith, and J. Kensrud, "Laboratory Evaluation of Wireless Head Impact Sensor," *Procedia Engineering*, vol. 112, pp. 175–179, Jan. 2015.